MAGNETIC MOMENTS AND LOW-LYING ENERGY LEVELS IN ^{142}Pr

MAGNETIC MOMENTS AND LOW-LYING ENERGY LEVELS IN ^{142}Pr

by

SHERALI GULAMALI HUSSEIN, B.Sc.

A Thesis

Submitted to the School of Graduate Studies

in Partial Fulfilment of the Requirements

for the Degree

Doctor of Philosophy

McMaster University

March 1973

DOCTOR OF PHILOSOPHY (1973) McMASTER UNIVERSITY
(Physics) Hamilton, Ontario

TITLE: Magnetic Moments and Low-lying Energy Levels in ^{142}Pr

AUTHOR: Sherali Gulamali Hussein, B.Sc. (Wales)

SUPERVISOR: Dr. R. G. Summers-Gill

NUMBER OF PAGES: ix, 115

SCOPE AND CONTENTS:

Atomic beam magnetic resonance has been used to study the 14.6 min isomer and the 19.2 hr ground state in ^{142}Pr. For the isomeric state the results are:

$$I = 5$$

$$J = 9/2: A = 245(10) \text{ MHz},$$

$$B = 100(450) \text{ MHz},$$

$$\mu = 2.2(1) \text{ nuclear magnetons.}$$

Re-interpretation of previous results for the ground state hyperfine structure, together with some new data, yield the following interaction constants:

$$J = 9/2: A = 65.6(2) \text{ MHz},$$

$$B = 22(2) \text{ MHz}.$$

The effect on μ is of minor consequence but the quadrupole moment is tripled in value. With the sign of the moment determined to be positive, the results are:

$$\mu = 0.234(1) \text{ nuclear magnetons},$$

$$Q = 0.110(25) \text{ barns}.$$

In addition, the combination of a high-resolution

^{141}Pr(d,p) experiment and the analysis of singles and coincidence gamma ray data has been used to reveal two new states at 89.7 and 358.1 KeV; these are tentatively assigned spins 6^- and 7^- respectively.

The results have been interpreted in terms of configuration-mixing between $\pi 2d_{5/2}\nu 2f_{7/2}$ and $\pi 1g_{7/2}\nu 2f_{7/2}$. The resulting wave functions for both the ground state and the isomeric state, as determined from the (d,p) spectroscopic factors, are quite different from those required to fit the measured magnetic moments. In view of this discrepancy, a possible mixing of higher configurations into the low-lying states cannot be ruled out.

Finally, a mixed-configuration shell model calculation using Surface Delta Interaction has been carried out, and its predictions are compared with the experimental results.

ACKNOWLEDGEMENTS

I am happy to have an opportunity to express my appreciation to all those who have helped make my stay at McMaster a pleasant one, and this research work possible. In particular, I would like to sincerely thank the following:

Dr. R. G. Summers-Gill, my Supervisor, for suggesting this project and for his patience and understanding.

The other members of my Supervisory Committee, Drs. J. A. Cameron and R. H. Tomlinson, for their guidance and interest.

Past and present members of the group: Hamish Robertson and Tony Pierce, for their help in carrying out the atomic beam experiments; Malcolm Macphail and Neil Sanderson, for their friendship and approach to physics; Don Dohan and Terry Taylor, for many a helpful discussion; and Aquila Islam and Konrad Aniol for their assistance during the experimental runs.

The staffs of the Reactor and Tandem Accelerator, for their cooperation.

Mrs. H. Kennelly, for expertly typing this manuscript.

This work was supported by grants to the group from the National Research Council of Canada. Financial assistance to the author from the Ontario Graduate Fellowship Programme and McMaster University is gratefully acknowledged.

To Isobel

TABLE OF CONTENTS

LIST OF FIGURES

LIST OF TABLES

INTRODUCTION

Recently Kern et al. (1968) have carried out an extensive study of the nuclear levels in ^{142}Pr, using a combination of (d,p) reaction and thermal-neutron capture γ-ray spectroscopy . The low-lying states, up to ∿ 200 keV, are interpreted in terms of mixing between the two configurations: $\pi 2d_{5/2}\nu 2f_{7/2}$ and $\pi 1g_{7/2}\nu 2f_{7/2}$. In this way, not only were the spins of the states deduced but also their wave functions. In particular, the 14.6 min isomeric state at 3.683 keV is predicted to have spin and parity 5^-. More recently, Mellema et al. (1970) have also studied the nuclear level spins of ^{142}Pr by means of nuclear orientation.

A similar study of the levels in ^{140}La (which has only two fewer protons than ^{142}Pr) has also been carried out (Kern et al., 1967; Jurney et al., 1970). All the fourteen states expected from the two configurations have been observed, and their spins and parities assigned. Moreover, the (d,p) spectroscopic factors, M1 branching ratios and the ground state magnetic moment can all be explained in a consistent manner. Nevertheless, it is obviously desirable to test the model further. Since the knowledge of magnetic moments offers a

critical test for the nuclear wave functions, the main object of the present research project was to obtain that information, for the case of ^{142}Pr.

Using atomic beam magnetic resonance, the nuclear spin and the magnetic dipole moment of the 14.6 min isomeric state have been determined; the result for the spin is I=5, in agreement with the prediction of Kern et al.

Some years ago, Cabezas et al. (1962) made an atomic beam investigation of ^{142}Pr ground state, and reported the magnitude of the nuclear magnetic moment. Although the sign of the moment was undetermined, neither sign fits the prediction of Kern et al. for the ground state wave function. Using two radio-frequency loops in a "flop-out on flop-in" atomic beam experiment, the sign of the magnetic moment has been determined. In the process, it was found that the original resonances of Cabezas et al. had been misinterpreted; additional experimental data to substantiate this claim have been obtained. The effect of the new interpretation on the magnetic moment is of minor consequence, but the quadrupole moment is tripled in value.

In an attempt to understand the magnetic moment results, a search for the four missing states in ^{142}Pr was initiated. A combination of high resolution (d,p) reaction and the analysis of singles and coincidence γ-ray data has been used to locate two additional states in the low-energy level scheme of ^{142}Pr. Tentative spin assignments for these states have been made.

Finally, a mixed-configuration shell model calculation

for ^{142}Pr has been attempted, and its predictions are compared with the experimental results.

CHAPTER I

NUCLEAR THEORY

1.1 The Shell Model

It is now apparent that the understanding of nuclear structure is a complex and formidable task. Nevertheless, physicists have approached the problem by resorting to rather simple models and successive approximations, always aiming to keep track of the physics involved. The historical development of the nuclear shell model (see for example, Elliot and Lane, 1957) provides an excellent example of such an approach. The present-day shell model calculations have come a long way from the extreme single-particle model proposed in the late forties (M. Goeppert Mayer, 1948,1949; Haxel, Jensen and Suess, 1948, 1949).

The description of a nucleus in terms of individual particles moving independently in an effective central field formed by all other particles is called a shell model. In contrast to the atomic case, however, there is no a priori reason to believe that the shell model can be applied to the nuclear case. In the first place, it is difficult to justify independent motion in the presence of strong nuclear forces. Secondly, there is no physical object in the nucleus that can serve as the source

for a strong central potential. Historically, therefore, it was the remarkable success of explaining a large body of experimental results that generated the initial faith and interest in the model.

1.1a Shell Model Hamiltonian

In the simplest form of the shell model, the single-particle model, the effect of the internucleon interactions is approximated by an average central potential, $U_i(r_i)$, in which the orbital angular momentum of a nucleon is a constant of motion. The individual nucleons move in independent stationary orbits but it is assumed that like nucleons pair off in such a way that many of the nuclear properties are determined solely by the last unpaired nucleon. The model takes no other account of correlations among the nucleons (except through the Pauli exclusion principle) and has no explicit reference to two-body forces. Such a simple potential of any shape, however, fails to reproduce the experimentally observed single-particle spectrum. A spin-dependent term, $\xi(r_i)\vec{\ell}_i\cdot\vec{s}_i$, is therefore included in the Hamiltonian which has the form

$$H_N = \sum_{i=1}^{A} T_i + U_i(r_i) + \xi(r_i)\vec{\ell}_i\cdot\vec{s}_i \ .$$

The orbital angular momentum is, then, no longer a constant of motion, and only J_i ($\vec{J}_i = \vec{\ell}_i + \vec{s}_i$) and its z-component m_i, are good quantum numbers. A particle state is thus characterized by four quantum numbers: n,ℓ,J and m. By adjusting the strength of the spin-orbit force, it is possible to reproduce the energy

gaps in the single-particle spectrum at the observed "magic numbers".

Experimentally, it is found that when a system consists of entirely filled shells plus a single nucleon, the single-particle model succeeds reasonably well in predicting the spins and parities of nuclear ground states. The spin of an odd-odd nucleus, however, cannot be predicted since there is no way of telling which of the various possible resultants of the two angular momenta lies lowest in the energy. More specifically, the various J-values in the absence of internucleon interactions are degenerate. In a more sophisticated model, therefore, all the "loose" particles outside closed shells (forming an inert core) are treated on an equal footing. In addition, a two-body force between the "active" nucleons is postulated, so that the Hamiltonian has the form:

$$H_N = \sum_{i=1}^{N} T_i + U_i(r_i) + \xi(r_i)\vec{l}_i \cdot \vec{s}_i + \sum_{i<j}^{N} V_{ij}(r_{ij}) \qquad (1.1)$$

where the summation extends only over the particles outside the inert core. The two-body force, $V(r_{ij})$, has been introduced to take into account the effect of internucleon interactions. However, it will be noted that it only represents the interaction between the extra-core nucleons. Moreover, it is not the same as that for two free nucleons. Hence, it is usually referred to as effective residual interaction.

1.1b Shell Model Techniques

Any shell model calculation aims at diagonalizing the Hamiltonian given by equation 1.1, in order to obtain its eigenfunctions and eigenvalues. Once the resulting total wave functions are known, a host of the other nuclear properties may be predicted.

In order to carry out such a procedure it is first necessary to construct a properly antisymmetrized N-particle wave function. If the basis states are chosen in $|n\ell jm\rangle$ representation so that they are diagonal in $\vec{\ell}\cdot\vec{s}$, then

$$\langle JM \left| \sum_{i=1}^{N} [T_i + U_i(r_i) + \xi(r_i)\vec{\ell}_i\cdot\vec{s}_i] \right| JM\rangle = \sum_{i=1}^{N} E_i$$

where E_i are simply the single-particle energies. A nuclear state is now characterised by the total angular momentum J and its projection M, obtained by coupling together the individual single-particle states. Most of the physics, however, is contained in the interaction matrix element:

$$\langle JM \left| \sum_{i<j}^{N} V(r_{ij}) \right| JM\rangle .$$

Shell model calculations are fraught with two basic difficulties. First, the exact form of the residual interaction is not known. In fact, one of the main objectives of nuclear structure studies is to elucidate the nature of this interaction. For many purposes, therefore, it is sufficient to choose a simple

analytic form with a few adjustable parameters. One such interaction, which has been frequently used in recent years both in the s-d shell and for odd-A nuclei with 82 neutrons, is the so called Surface Delta Interaction (SDI). It has the form:

$$V_{ij} = -4\pi A_T \delta(\Omega_{ij}) \delta(\vec{r}_i - \vec{R}) \delta(\vec{r}_j - \vec{R}) \qquad (1.2)$$

where Ω_{ij} is the angle between the radius vectors $\vec{r}_i$, $\vec{r}_j$ of the interacting pair of nucleons. The basic assumption of SDI is that the interaction takes place only at the surface of the nucleus. The kinetic energy of the nucleons in a nucleus is smallest at the surface, and it is known from nucleon-nucleon scattering that the interaction diminishes rapidly for large kinetic energies, so that the above assumption is a plausible one. The short-range nuclear force is approximated (only for mathematical simplification) by a δ-force. Physically, this means that the interaction is non-zero only if the two nucleons are at the same place (on the surface). The assumption is now made that the one-particle radial wave functions all have approximately the same amplitude at the surface. If these were exactly the same, the different radial integrals would be equal. (This is also obtained if the two-body force is a function of Ω_{ij} only). The only adjustable parameters of SDI are, therefore, the interaction strengths, A_T, which depend on the total isospin quantum number, T^* (=0 or 1).

*In the isospin formalism, an additional quantum number, the isospin t, is assigned to each nucleon. The isospin projection (or the z-component) $t_z = +1/2$ denotes a neutron and $t_z = -1/2$ denotes a proton.

Another source of difficulty in shell model calculations is the problem of deciding upon an appropriate configuration space. In principle, the "active" nucleons should be allowed to occupy all of the unfilled shell model states. In practice, however, it is necessary to truncate the basis states, guided by the energy-level systematics from adjoining nuclei. After one has chosen the form of the residual interaction and decided upon a configuration space, the problem reduces to a straight-forward if somewhat long and tedious, mathematical computation. Recently, J. B. French, E. C. Halbert, J. B. McGrory and S. S. M. Wong at Oak Ridge have generated a powerful shell model programme called Mixed-Configuration Shell Model Code (MCSMC). Based on the tensorial ideas of J. B. French (French et al.,1969), the programme can handle as many as six "active" shells and can treat matrices of order $N \leq 190$. For a specified configuration, the programme constructs the basis multi-particle states by appropriate coupling of single-shell wave functions. Using the two-body matrix elements (input data), it then calculates and diagonalizes the multi-nucleon Hamiltonian matrices to yield nuclear energy levels and nuclear wave functions. The shell model calculations for ^{142}Pr, to be described later, have been made possible due to the tremendous efforts by D. A. Dohan who not only modified MCSMC to run on CDC 6400 at McMaster but also provided assistance and enthusiasm in initiating these calculations.

1.2 Nuclear Moments

The electromagnetic properties of the nucleus arise from the charge and current distributions due to the individual nucleons. The nucleus will, therefore, interact with an external electromagnetic system, e.g. the orbital electrons. It is possible to express the energy of this interaction in terms of multipole moments of increasing orders. The electric and magnetic multipole operators of order λ are:

$$O^{\mu}_{\lambda}(E\lambda) = e\sum_{i=1}^{A} g_{\ell_i} r_i^{\lambda} Y^{\mu}_{\lambda}(\theta_i,\phi_i) \qquad (1.3)$$

$$O^{\mu}_{\lambda}(M\lambda) = \mu_N \sum_{i=1}^{A} \text{grad}[r_i^{\lambda} Y^{\mu}_{\lambda}(\theta_i,\phi_i)]\cdot[g_{\ell_i} \frac{2}{\lambda+1} \vec{\ell}_i + g_{s_i} \vec{s}_i] \qquad (1.4)$$

where (r_i,θ_i,ϕ_i) are the coordinates of i^{th} particle, and g_{ℓ_i} and g_{s_i} are its orbital and spin g-factors respectively. g_{ℓ_i}=+1 for protons and 0 for neutrons. $g_{s_i} = 2\mu_i/\mu_N$, where μ_i denotes the magnetic moment of the i^{th} particle and μ_N is the nuclear magneton.

The static moments may now be defined as the expectation values of the appropriate multipole operators in which the z-component of $\vec{J}$ has its maximum value J. The magnetic dipole and electric quadrupole moments are then given by

$$\mu = \mu_N \langle JM | \sum_i (g_{\ell_i} \vec{\ell}_i + g_{s_i} \vec{s}_i) | JM \rangle_{M=J} \qquad (1.5)$$

$$Q = [\tfrac{4\pi}{5}]^{1/2} \langle JM | \sum_i g_{\ell_i} r_i^2 Y^0_2(\theta_i,\phi_i) | JM \rangle_{M=J} . \qquad (1.6)$$

It should be noticed that the quantity Q has an additional numerical factor in front, introduced purely for conventional reasons.

If the nucleus is assumed to be in a state of definite parity, then non-vanishing matrix elements exist only for even-λ in the electric and odd-λ in the magnetic case. Also, the highest order of an observable static moment is $\lambda = 2J$.

1.2a Magnetic Moments

According to the single-particle shell model, the magnetic moment of a nucleus is simply that of the last odd nucleon. By writing

$$g_\ell \vec{\ell} + g_s \vec{s} = g_\ell \vec{J} + (g_s - g_\ell)\vec{s}$$

in equation 1.5, the magnetic moment (in nuclear magnetons) of an odd-A nucleus can easily be shown to be:

$$\mu = \frac{1}{2}[g_\ell + g_s)J + (g_\ell - g_s)\frac{\ell(\ell+1) - \frac{3}{4}}{J+1}].$$

When the free-nucleon g-factors are used in the above expression, one obtains the so-called Schmidt values. Experimentally, it is found that, for most odd-A nuclei, the magnitudes of the magnetic moments are smaller than the Schmidt values. These systematic deviations may be explained by invoking the "quenching" of the free-nucleon g-factors or by postulating configuration mixing.

For odd-odd nuclei, if the angular momenta $\vec{J}_p$ and $\vec{J}_n$, of a proton and a neutron, couple to a total $\vec{J} = \vec{J}_p + \vec{J}_n$, the magnetic moment, again in nuclear magnetons, becomes:

$$\mu_{\text{odd-odd}} = \frac{1}{2}[(g_p + g_n)J + (g_p - g_n)\frac{J_p(J_p+1) - J_n(J_n+1)}{J+1}]$$

where g_p and g_n are the g-factors derived from the Schmidt values.

That is, $g_p = \mu_{Schmidt}/J_p\mu_N$. Alternatively, the proton and neutron g-factors can be taken from the measured magnetic moments of the adjoining odd-A nuclei. This latter procedure allows for any configuration mixing in the odd-A nucleus, and therefore, produces better agreement with the experimental results.

1.3 The (d,p) Reaction

The (d,p) reaction falls into a class of nuclear reactions referred to as direct reactions: so called, because they proceed on a very short time scale without formation of a compound nucleus. The incoming particle, the deuteron in this case, is simply split into two fragments; the neutron is absorbed into the target nucleus while the proton continues more or less undisturbed. The process can be regarded essentially as a nuclear-surface phenomenon, and hence, should be well described by the shell model in which a few nucleons at the Fermi surface are considered to be "active".

According to the semi-classical description of (d,p) reaction, the momentum imparted to the residual nucleus is simply:

$$\vec{K}\hbar = (\vec{K}_d - \vec{K}_p)\hbar$$

where $\vec{K}_d$ and $\vec{K}_p$ refer to the deuteron and the proton momenta respectively. The assumption is now made that the proton is not significantly deflected by the Coulomb forces from the nucleus. The linear momentum $K\hbar$ imparted to the nucleus is then the momentum that the neutron brings with it. If the impact parameter $\approx R$, the nuclear radius, then the corresponding orbital angular momentum

is given by

$$KR = \sqrt{\ell(\ell+1)}\,\pi. \qquad (1.6)$$

The model outlined so far is, no doubt, a very crude one. However, it predicts an important property of direct reactions, namely that it is possible to determine the orbital angular momentum quantum number of the neutron by determining K. It also suggests a maximum in the differential cross section for an angle that satisfies equation 1.6. Both these features are also borne out by the more refined distorted wave treatment.

1.3a Differential Cross Section

It is the purpose of this section to outline the important features and approximations in the derivation of the expression for the differential cross section for direct reactions. For a complete mathematical treatment, the reader is referred to the publications by G. R. Satchler (1964,1965).

For generality, let the notation A(a,b)B represent the reaction. A standard result of the general theory of scattering gives the differential cross section as:

$$\frac{d\sigma}{d\Omega} = \frac{M_a M_b}{(2\pi\hbar^2)^2} \cdot \frac{K_b}{K_a} \cdot \left|T_{fi}\right|^2$$

where M and K are the reduced masses and wave vectors respectively. The transition amplitude, T_{fi}, is given by the matrix element of the direct interaction with respect to the initial and final state wave functions. That is

$$T_{fi} = \langle \psi_b \psi_B e^{i\vec{K}_b \cdot \vec{r}_b} | V_{aB} | \psi_{aA}^{(+)} \rangle \qquad (1.7)$$

The incoming waves are, of course, in the aA entrance channel but the outgoing waves can be in all open exit channels, so that equation 1.7 is exact. At this point, however, some approximations have to be made in order to replace $\psi_{aA}^{(+)}$ by a computable quantity, and hence, evaluate the transition matrix element.

The distorted-wave Born approximation (DWBA) considers only the elastic scattering part of $\psi_{aA}^{(+)}$, and the transition is described as taking place between elastic scattering states. This is a reasonable approximation since, in direct reactions, the interaction simply scatters particles without re-arranging them. The so-called optical model potentials are introduced in the entrance and exit channels to describe the scattering of particles a and b; the interaction responsible for the actual reaction can then be treated as a perturbation. With these assumptions, the expression for the transition matrix becomes:

$$T_{fi} = \int d\vec{r}_a \int d\vec{r}_b \chi_b^{(-)}(\vec{K}_b, \vec{r}_b) \langle \psi_{bB} | V_{bc} | \chi_{aA} \rangle \chi_a^{(+)}(\vec{K}_a, \vec{r}_a) \qquad (1.8)$$

The subscript c refers to the transferred particle. χ_a, χ_b are now distorted waves in the entrance and exit channels respectively. These wave functions are obtained by solving the appropriate Schrödinger equation using an optical model potential. The explicit form for such a potential, in common use for the (d,p) reaction described in this work, may be written as

$$U(r) = U_c(r) - [V_R f_R(r) + i\, W_D f_I(r)] \qquad (1.9)$$

where $U_c(r)$ represents the long-range Coulomb force - the interaction of a point charge (Ze) with a uniformly charged sphere

(Z'e) of radius R_c. The second term describes the strong nuclear force; it contains an imaginary part which mathematically simulates the surface absorption (loss of flux). The potential function, $f_R(r)$, has the Woods-Saxon form:

$$f_R(r) = [1 + \exp(\frac{r-R_c}{a})]^{-1} \quad . \qquad (1.10)$$

R_c is defined as the radius where the nuclear potential has decreased to half its maximum value, and the diffuseness parameter, a, is a measure of the surface thickness of the nucleus. It is customary to use for the shape of the imaginary potential a mixture of a volume term (dominant at high bombarding energies) and a surface term (dominant at low bombarding energies). The volume imaginary term is simply the Woods-Saxon potential given by equation 1.10. The surface imaginary term, $f_I(r)$ in equation 1.9, is taken of the form of the derivative of the Woods-Saxon shape. Sometimes it is necessary to include in U(r) a force which is sensitive to the spin direction of the incoming particle, such as a spin-orbit force, thus introducing further potential parameters. These parameters are adjusted to obtain a fit to the experimental elastic scattering results.

The nuclear matrix element $\langle\psi_{bB}|V_{bc}|\psi_{aA}\rangle$ in equation 1.8 acts as an effective interaction producing the transition between the elastic scattering states. It contains all the important nuclear structure information. It should be noticed that V_{bc} represents the interaction between the outgoing particle and the transferred nucleon. For a (d,p) reaction, for

example, $V_{bc} \equiv V_{pn}$. Assuming that the internal coordinates of "a" are independent of those of "A", ψ_{aA} may be written as

$$\psi_{aA} = \psi_a \psi_A \cdot$$

Similarly,

$$\psi_{bB} = \psi_b \psi_B \cdot$$

The interaction V_{bc} is independent of internal coordinates of the target nucleus, A, so that

$$\langle \psi_{bB} | V_{bc} | \psi_{aA} \rangle = \int dx_b \, dx_c \psi_b \langle \psi_B | \psi_A \rangle V_{bc} \psi_a \cdot$$

The overlap of the target with the residual nucleus defines the wave function for the transferred particle c:

$$\langle \psi_B | \psi_A \rangle = \sum_{j\mu} \langle J_A j M_A \mu | J_B M_B \rangle \phi^{BA^*}_{j\mu} (x_c, \vec{r}_{cA})$$

where x_c represents the spin coordinates (and any other possible internal coordinates). $\phi^{BA}_{j\mu}$ depends on initial and final states of A and B, and may be separated into its radial, orbital and spin parts:

$$\phi_{j\mu}(x_c, \vec{r}_{cA}) = \sum_m \langle \ell s \; m, \mu - m | j\mu \rangle R_{\ell j}(r_{cA}) Y^m_\ell (\theta_{cA}, \phi_{cA}) \cdot \phi_{s, \mu - m}(x_c)$$

where s is the intrinsic spin of particle c. The spherical harmonic in the above expression (and hence, in the nuclear matrix element) exhibits an important feature of direct reactions, namely that the reaction cross sections will have pronounced angular dependence. An angular distribution of the outgoing particles, therefore, determines the ℓ-value of the transferred particle and the parity change $(-)^\ell$ in the transition.

The expression for the nuclear matrix element, thus,

involves a six-dimensional integral which is difficult to evaluate. In the commonly used zero-range approximation, the assumption is made that the outgoing particle appears at the same point at which the transferred particle is absorbed. This, in effect, implies that $\vec{r}_a$ is equal to $\vec{r}_b$. The integral now reduces to a three-dimensional one, and is easier to compute. To obtain the reaction cross section, the transition amplitude must be squared, and summed over the final and averaged over the initial magnetic sub-states. It is customary to write down the reaction cross section as:

$$\sigma_{exp}(\theta) = N\left[\frac{\sigma_{DWBA}}{2j+1}\right] \frac{2J_f+1}{2J_i+1} S_{\ell j} \qquad (1.11)$$

where $(\sigma_{DWBA}/2j+1)$ is the theoretical cross section calculated in the distorted wave Born approximation, and the normalization constant N = 1.53 for a (d,p) reaction (Bassel 1966). The spectroscopic factor $S_{\ell j}$ is the overlap between the appropriately anti-symmetrized initial and final states:

$$S_{\ell j} = \langle \psi_i \otimes \psi_{\substack{\text{transferred} \\ \text{particle}}} | \psi_f \rangle^2 \qquad (1.12)$$

where the cross denotes vector coupling.

1.3b Mixed Configurations

In a nuclear reaction both the target and the final state nuclei are invariably in given states of definite spin and parity. Let

$$\psi_{J_i M_i} = \sum_p a_p \phi^p_{J_i M_i}$$

$$\psi_{J_f M_f} = \sum_q b_q \phi^q_{J_f M_f}$$

represent the initial and final mixed-configuration wave functions, where a_p and b_q are the corresponding mixing amplitudes. One of the crucial assumptions of direct reaction theory is that, whatever the configuration of the target nucleus may be, it remains unaltered during the reaction. The transferred particle is simply (weakly) coupled to the target ground state to form the final states. According to equation 1.12 the spectroscopic factor is then given by:

$$S = \left\langle \left(\sum_p a_p \phi^p_{J_i M_i}\right) \otimes \phi_{j\mu} \middle| \sum_q b_q \phi^q_{J_f M_f} \right\rangle^2$$

where $\phi_{j\mu}$ denotes the wave function of the transferred particle.

More specifically, consider the case of a (d,p) reaction in which the "active" shell, ρ, of the target nucleus has (n-1) particles. As a result of the stripping reaction, the final nucleus will have n particles (neutrons) in the ρ-shell. One can construct the n-particle (final-state) wave function by coupling the transferred particle to the (n-1)-particle target wave function, by making use of appropriate expansion coefficients and ensuring antisymmetry. The expression for the spectroscopic factor then reduces to:

$$S_{\ell j} = n\left[\sum_\alpha \langle \rho^n J_f | \rho^{n-1} \alpha \rangle \delta_{J_i \alpha}\right]^2 \left[\sum_{pq} a_p b_q\right]^2$$

where the factor n is a result of the fact that the stripped

particle can be placed in n equivalent positions in the ρ-shell. The expansion coefficient $\langle \rho^n J_f | \rho^{n-1} \alpha \rangle$ is called a "coefficient of fractional parentage".

For example, in the $^{141}Pr(d,p)^{142}Pr$ reaction, of interest in this work, the "active" neutron shells in the target nucleus are empty. For a neutron transfer, then

$$n\left[\sum_{\alpha} \langle \rho^n J_f | \rho^{n-1} \alpha \rangle \delta_{J_i \alpha}\right]^2 = 1,$$

and

$$S_{\ell j} = \left[\sum_{pq} a_p b_q\right]^2 . \qquad (1.13)$$

CHAPTER II

THE ODD-ODD NUCLEUS PRASEODYMIUM-142

The odd-odd nuclei beyond the doubly magic $^{132}_{50}Sn_{82}$ form an interesting region in the mass table. The energy-level systematics of the neighbouring odd-A nuclei suggest that the 83^{rd} neutron is undoubtedly in the $2f_{7/2}$ shell-model state. Thus, the ground states of ^{141}Ce and ^{143}Nd have spin and parity $7/2^-$. Also, the first excited state (spin and parity $3/2^-$) occurs at $\sim$ 660 keV in ^{141}Ce and $\sim$ 740 keV in ^{143}Nd. On the other hand, the protons beyond the shell closure at Z=50 occupy the $1g_{7/2}$ and $2d_{5/2}$ orbitals. In fact, the two low-lying states arising from these configurations lie very close in energy. For example, in ^{141}Pr which has 82 neutrons and 59 protons, the ground state has spin and parity $5/2^+$ and the $7/2^+$ first excited state occurs at 145 keV. The next available proton state, $1h_{11/2}$, is observed at $\sim$ 1100 keV. In the corresponding odd-odd ^{142}Pr nucleus, therefore, one can expect the low-lying states to be formed from two different configurations:

$$\pi 2d_{5/2}\nu 2f_{7/2} : J^\pi = 1^-, 2^-, \ldots, 6^-$$

$$\pi 1g_{7/2}\nu 2f_{7/2} : J^\pi = 0^-, 1^-, \ldots, 7^-.$$

Due to the residual neutron-proton interaction the states in each group will not be degenerate. Due also to this interaction

one can expect configuration mixing, so that the actual eigenstates of ^{142}Pr will contain components of both configurations. Of course, the total angular momentum is a good quantum number, so one can write:

$$|\psi>_{1J} = \alpha_{1J}|\pi 2d_{5/2}\nu 2f_{7/2}:J> \pm \beta_{1J}|\pi 1g_{7/2}\nu 2f_{7/2}:J> \quad (2.1a)$$

$$|\psi>_{2J} = \alpha_{2J}|\pi 2d_{5/2}\nu 2f_{7/2}:J> \pm \beta_{2J}|\pi 1g_{7/2}\nu 2f_{7/2}:J> \quad (2.1b)$$

where a necessary condition for the orthornormality of the state vectors, α and β, requires that:

$$|\beta_{1J}| = [1 - \alpha_{1J}^2]^{1/2} = \alpha_{2J}$$

$$|\beta_{2J}| = \alpha_{1J} .$$

Thus, the low-lying energy spectrum of the odd-odd ^{142}Pr should consist of fourteen negative parity states. The ordering of the levels resulting from a specific neutron-proton configuration is sensitive to the nature of the residual interaction. It is this feature which makes the study of these odd-odd nuclei so important, since a detailed study of their level structure can reveal the nature of the interaction.

2.1 The Low-lying States

Kern et al. (1968) have carried out a detailed study of the nuclear levels in ^{142}Pr by a combination of (d,p) reaction and thermal-neutron capture gamma ray spectroscopy. In what follows, a review of their published work will be presented.

If the wave function of a state populated in a direct

(d,p) reaction has the form of equation 2.1, then the (d,p) intensity of that state is given by

$$I_J = N(2J+1)\alpha_{iJ}^2 , \quad i = 1,2 \quad . \qquad (2.2)$$

Since the ground state of the target nucleus, ^{141}Pr, has $J^\pi = 5/2^+$ and the transferred neutron is stripped into the $f_{7/2}$ orbital, states with spins 0^- and 7^- will not be populated in a $^{141}Pr(d,p)^{142}Pr$ reaction. If the sum of the strengths of the remaining twelve states, arising from $\ell_n=3$ neutron transfer, is normalized to 100, then

$$N \sum_{J=1}^{6} (2J+1) = 100$$

and the normalization factor N = 2.08. The expected summed intensity of the pair of states, each with spin J, is given below:

Spin J:	1	2	3	4	5	6
Intensity:	6.3	10.4	14.6	18.7	22.9	27.1

In the (d,p) experiment of Kern et al, eight low-lying states were explicitly observed and resolved. Although the presence of several unresolved multiplets did not permit angular distributions of individual peaks to be determined, the group of levels from the ground state to 200 keV showed the expected $\ell_n=3$ transfer. In addition, the energies of the gamma ray transitions, following thermal-neutron capture, have been

measured to a high precision. Combining their (d,p) intensities and the results of high- and low-energy (n,γ) data, the level-energies, spins and wave functions of ten low-lying states were deduced. The analysis was based on the following assumptions:

(i) The low-lying negative parity states arise from the mixing of two configurations: $\pi d_{5/2}\nu f_{7/2}$ and $\pi g_{7/2}\nu f_{7/2}$, so that the (d,p) spectroscopic factors, as given by equation 2.2, determine the spins and the state vectors.

(ii) Since the target nucleus in the reaction $^{141}Pr(n,\gamma)^{142}Pr$, has $J^{\pi} = 5/2^{+}$, the slow-neutron capture states will have spins 2^{+} and/or 3^{+}. Primary E1 transitions can, therefore, populate low-lying levels with spins 1^{-},2^{-},3^{-} or 4^{-} only.

(iii) The low-energy transitions, following the decay of the negative parity states up to 200 keV, were assumed to have a predominantly M1 character. These transitions should, therefore, involve a spin change of one or zero, unless such a mode of de-excitation is impossible.

The results of their analysis are summarized in Table 2.1, where the level-energies, spins, (d,p) intensities and the mixing amplitudes of the low-lying states are shown. The ground state peak in the (d,p) experiment was unresolved, so that only the sum intensity of the doublet has been experimentally determined. In order to allow for this unresolved doublet, the (d,p) energies were shifted upwards by 1.6 keV. Also, by assuming that the two members of the doublet are approximately equally intense, their separation was estimated as twice the energy shift, that is 3.2±1.5 keV. The last column

Table 2.1

A Summary of results for the low-lying states in ^{142}Pr, obtained by Kern et al.

Level Energy (KeV)		Spin	Normalized (d,p) Intensity	Mixing Amplitudes			
				(d,p)		γ-ray branching fit	
(d,p)	(n,γ)			α	|β|	α	β
0.0 } ±1.5	0.0	2 }	16.7(8)	0.87	0.49	0.96	-0.28
3.2 }	3.683(4)	5 }		0.64	0.77	0.63	-0.78
17.8(6)	17.740(4)	3	5.0(5)	0.59	0.81	0.60	-0.80
63.7(2)	63.746(4)	6 }	30.5(15)	1.00	0	0.997	0.07
	72.294(4)	4 }		0.34	0.94	0.22	-0.975
86.2(7)	84.998(3)	1	5.5(3)	0.93	0.37	0.995	0.10
128.0(4)	128.251(5)	5	12.8(6)	0.77	0.64	0.78	0.63
144.6(4)	144.587(4)	4	17.4(9)	0.94	0.34	0.975	0.22
176.8(3)	176.863(3)	3	9.9(5)	0.81	0.59	0.80	0.60
200.8(5)	200.525(4)	2	2.3(2)	0.49	0.87	0.28	0.96

in Table 2.1 shows the state vectors obtained from the γ-ray branching ratios. The theoretical values depend on three parameters: (i) the mixing parameters α and $|\beta|$, (ii) the relative phases in the wave function and (iii) the g-factors for the neighbouring odd-A nuclei. Starting from the values predicted by the (d,p) amplitudes, the phases were adjusted to obtain a fit to the observed branching ratios. The state vectors were then varied to arrive at the final results. It is pointed out that if the (d,p) amplitudes are not kept as a guide, it is possible to arrive at a completely different set of state vectors. It can be seen from the results given in Table 2.1 that, on the whole, the agreement between the α's obtained from the (d,p) spectroscopic factors and those that fit the branching ratios is remarkable. The two missing states (with $J^{\pi} = 1^{-}$ and 6^{-}) are precisely those for which the admixture is predicted to be small; these states should, therefore, be very weakly populated in a (d,p) reaction. Unfortunately, the γ-ray data failed to reveal the positions of these two states, and also those with spins 0^{-} and 7^{-} not populated by a (d,p) reaction.

CHAPTER III

THEORY OF ATOMIC BEAM MAGNETIC RESONANCE

In the absence of any external magnetic fields, the total Hamiltonian for a free atom is:

$$H = H_N + H_e + H_{hfs}$$

where H_N and H_e represent the nuclear and electronic contributions respectively, and H_{hfs} represents the interaction between the atomic and nuclear electromagnetic fields. The nuclear part of the Hamiltonian has already been discussed in Chapter I. Since the nuclear energy levels are widely spaced compared to the electronic levels, the nucleus may be assumed to be in a single eigenstate, usually the ground state or a metastable isomeric state, with definite spin and parity. In the following discussion, therefore, the effect of the first term in the Hamiltonian will be neglected.

3.1 Electronic Hamiltonian

The Hamiltonian for a system of N interacting electrons is given by

$$H_e = \sum_{i=1}^{N} \left(\frac{p_i^2}{2m} - \frac{Ze^2}{r_i} + \xi(r_i)\vec{\ell}_i\cdot\vec{s}_i\right) + \sum_{i>j} \frac{e^2}{r_{ij}} \qquad (3.1)$$

where r_i is the radial coordinate of the i^{th} electron, $\vec{\ell}_i$ and $\vec{s}_i$ are its orbital and spin angular momenta, and $r_{ij} = |\vec{r}_i - \vec{r}_j|$.

Terms in $\vec{\ell}_i \cdot \vec{\ell}_j$, $\vec{\ell}_i \cdot \vec{s}_j$ and $\vec{s}_i \cdot \vec{s}_j$ are usually neglected.

The state of an electron may be uniquely defined by a set of four quantum numbers*. According to the atomic shell model, electrons may be grouped into shells characterised by the value of n. These may be subdivided into sub-shells, each with the same n but different values for ℓ. The arrangement of atomic electrons with shells and sub-shells is called a configuration. Due to the restriction imposed by the Pauli principle, the maximum number of electrons in a given sub-shell is $2(2\ell+1)$. Moreover, since the electrons in the filled shells have the same radial distribution, they give rise to a spherically symmetric potential. This property is made use of in obtaining the eigenvalues of the Hamiltonian of equation 3.1.

The electronic Hamiltonian as given by equation 3.1 may be diagonalised by first considering an approximate Hamiltonian:

$$H_c = \sum_i \frac{p_i^2}{2m} + V(r_i)$$

where the first term is simply the kinetic energy of all the electrons, and $V(r_i)$ is a spherically symmetric central potential which arises from the $-\sum_i \frac{Ze^2}{r_i}$ term and the spherically

---

*The four quantum numbers are: n, ℓ, m_ℓ and m_s. n and ℓ are called principal and orbital quantum numbers, respectively. m_ℓ is the z-component of ℓ and may have $(2\ell+1)$ different values: $-\ell$, $-\ell+1$, ..., ℓ. m_s is the z-component of the spin quantum number s, and may be 1/2 or - 1/2.

symmetric part of $\sum_{i>j} \frac{e^2}{r_{ij}}$.

In the central field approximation, therefore, H_c is taken as the zeroth-order Hamiltonian. Because V(r) does not simply depend on 1/r, the zeroth-order energy solution, E_c, is both a function of n and ℓ. This is called the configuration energy. The complete solution may then be obtained by treating the remainder of the terms in 3.1 as a perturbation. Thus,

$$H_{pert} = \sum_{i>j} \frac{e^2}{r_{ij}} + \sum_i \xi(r_i)\vec{\ell}_i \cdot \vec{s}_i. \qquad (3.2)$$

The first term represents the non-spherical part of the mutual repulsion between the electrons, and the second term is the spin-orbit interaction due to relativistic effects. The summation is carried only over the electrons outside the closed shells, since the rest of the first term has already been included in the H_c, and for electrons in closed shells, $\sum_i \vec{\ell}_i \cdot \vec{s}_i = 0$.

For more than a single electron outside closed shells, one must couple the angular momenta of the individual electrons. For the low-lying states of all but the heavier atoms, the mutual repulsion (the first term of equation 3.2) is dominant, and one uses Russell-Saunders or L-S coupling. According to this coupling scheme the total orbital and total spin angular momenta are given by:

$$\vec{L} = \sum_i \vec{\ell}_i$$

$$\vec{S} = \sum_i \vec{s}_i.$$

Again, since for a closed shell, $\sum_i \vec{\ell}_i = \sum_i \vec{s}_i = 0$, the summation need only be carried over unfilled shells. The total angular momentum of the system is then

$$\vec{J} = \vec{L}+\vec{S}.$$

In order to carry out the perturbation calculations one may, therefore, choose basis states characterised by the quantum numbers: L, S, J and M_J where M_J is the z-component of the total angular momentum of the system.

To first order, the mutual repulsion term raises the L,S degeneracy, so that each configuration splits into terms with given values of L and S, and denoted ^{2S+1}L. Each term, in turn, is (2L+1)(2S+1)-fold degenerate. This degeneracy is partially lifted by the first-order correction due to the spin-orbit force which causes J-dependence. The lowest member of the L-S multiplet may be deduced from Hund's rules, provided all the unfilled electrons are equivalent (that is, electrons having the same values of n and ℓ). More generally, one can study the Zeeman effect of the fine structure to deduce atomic ground states.

For praseodymium, which has 59 electrons, the ground state configuration is: $4f^3 6s^2$ and Hund's rules predict the lowest member of this configuration to be $^4I_{9/2}$. The J-value has been confirmed experimentally, and the measured value for the electronic gyromagnetic ratio is $g_J = -0.731055(1)$ (Lew, 1953,1970). Corrections to the theoretically calculated values of g_J arise from relativistic and diamagnetic effects, breakdown

of Russell-Saunders coupling and configuration interaction. The last two effects are due to the second-order correction terms in the perturbation calculation. The calculated value, $g_J = -0.7307$ for praseodymium, however, indicates that configuration mixing is negligible (Judd and Lindgren, 1961).

3.2 Hyperfine Structure

The last term, H_{hfs}, in the atomic Hamiltonian may be expressed as:

$$H_{hfs} = \sum_{\lambda,\mu} (-1)^{\mu} O_{\lambda}^{\mu}(\vec{r}_e) O_{\lambda}^{-\mu}(\vec{r}_N)$$

where O_{λ}^{μ} is the electric or magnetic multipole operator of order λ, and $\vec{r}_e$ and $\vec{r}_N$ refer to the electronic and nuclear coordinates respectively. The only terms in the above expansion that lead to non-vanishing static moments are the odd-λ magnetic and even-λ electric operators. Since the magnitude of the interaction decreases rapidly with increasing λ, only the magnetic dipole and electric quadrupole terms will be considered. Thus,

$$H_{hfs} = H_{M1} + H_{E2}.$$

The terms are (Kopfermann, 1958):

$$H_{M1} = hA\, \vec{I}\cdot\vec{J}$$

$$H_{E2} = hB\, \frac{3(\vec{I}\cdot\vec{J})^2 + \frac{3}{2}(\vec{I}\cdot\vec{J}) - I(I+1)J(J+1)}{2I(2I-1)J(2J-1)}.$$

I^* and J are the nuclear and electronic spins respectively.

*Here and elsewhere, when both the nuclear and electronic spins enter the discussion, the usual notation J for the nuclear spin will be relaced by I.

A and B are called the hyperfine interaction constants and are related to μ_I and Q, the nuclear magnetic dipole and electric quadrupole moments. The exact relationships between A, B and μ_I,Q involve electronic wave functions. For the present work, however, it is sufficient to note that, for two isotopes in the same electronic state,

$$\frac{A_1}{A_2} = \frac{(\mu_I/I)_1}{(\mu_I/I)_2}$$

$$\frac{B_1}{B_2} = Q_1/Q_2.$$

These two expressions, the so-called Fermi-Segrè formula, may be used to deduce μ_I and Q from measured A and B, if all these quantities are known for another isotope. Deviations from this rule are caused by the finite size of the nucleus. The so-called hyperfine anomalies, however, are typically less than 1% and are important only for atoms with unpaired s electrons.

The hyperfine interaction couples the nuclear and atomic angular momenta, so that the total angular momentum of the system is

$$\vec{F} = \vec{I}+\vec{J}.$$

Each fine structure level, therefore, splits into (2I+1) (if $I \leq J$) hyperfine levels, each characterised by the quantum number, F. The hyperfine Hamiltonian may be diagonalized in the $|FM_F\rangle$ representation, where M_F is the z-component of F. Thus, the energy of a hyperfine level is given by

$$W(F) = \langle FM_F|H_{M1}|FM_F\rangle + \langle FM_F|H_{E2}|FM_F\rangle.$$

By noting that

$$\vec{I}\cdot\vec{J} = \frac{1}{2}[F(F+1)-I(I+1)-J(J+1)] \equiv \frac{1}{2}K$$

it can be easily shown that

$$W(F) = hA\,\frac{K}{2}+hB\,\frac{\frac{3}{4}K(K+1)-I(I+1)J(J+1)}{2I(2I-1)J(2J-1)}\,.$$

It is worthwhile to note that the ordering of the F-states depends both on the ratio B/A and the sign of A. Moreover, the hyperfine interaction constants may be determined by measuring the splittings between the different F-states. In order to do this by the atomic beam magnetic resonance method, however, the atom must be subjected to an external magnetic field.

3.2 a The Effect of External Magnetic Field

For an atom in an external field, $\vec{H}$, the Hamiltonian should include an additional term

$$\mathcal{H}_M = -\vec{\mu}_J\cdot\vec{H} - \vec{\mu}_I\cdot\vec{H}$$

to represent the interaction of atomic and nuclear dipole moments, μ_J and μ_I respectively, with the external field. Since

$$\vec{\mu}_J = g_J\mu_o\vec{J} \quad \text{and} \quad \vec{\mu}_I = g_I\mu_o\vec{I},$$

where g_J and g_I are the atomic and nuclear g-factors respectively, and μ_o is the Bohr magneton, $\mathcal{H}_M$ may be re-written as:

$$\mathcal{H}_M = -g_J\mu_o J_z H - g_I\mu_o I_z H$$

where the direction of the field is along the z-axis. Because of the negative charge of the electron, μ_J is negative and hence, $g_J < 0$.

If the strength of the field is such that $H_{hfs} >> H_M$, H_M may be treated as a perturbation to the hyperfine states. To first-order in the perturbation, only the matrix elements of J_z and I_z, diagonal in F, need be considered. Thus,

$$W(F,M_F) = W(F) + \langle IJFM_F|H_M|IJFM_F\rangle$$

$$= W(F) - \mu_o M_F H[g_J \frac{F(F+1)+J(J+1)-I(I+1)}{2F(F+1)}$$

$$+ g_I \frac{F(F+1)-J(J+1)+I(I+1)}{2F(F+1)}] .$$

The effect of the magnetic field is, thus, to split each hyperfine state into 2F+1 Zeeman levels. If the g_I term, which is small compared to the g_J term, is neglected for the present, then the splitting of the adjacent Zeeman levels is (remembering that $g_J < o$):

$$W(FM_F)-W(F,M_F-1) = -g_J\mu_o H[\frac{F(F+1)+J(J+1)-I(I+1)}{2F(F+1)}] . \quad (3.3)$$

At higher magnetic fields, it is necessary to evaluate the second-order terms in the perturbation theory. These involve off-diagonal matrix elements, and are given by:

$$\sum_{F\neq F'} \frac{\langle FM_F|H_M|F'M_F\rangle^2}{W_F-W_{F'}} .$$

H_M can only connect states having the same value of M_F and for which $F' = F\pm1$. Moreover, the matrix is symmetric so that:

$$\langle FM_F|H_M|F-1,M_F\rangle = \langle F-1,M_F|H_M|FM_F\rangle$$

$$= -g_J\mu_o H[\frac{(F+J-1)(F-J+1)(F+J+I+1)(J+I+1-F)(F^2-M_F^2)}{4F^2(2F-1)(2F+1)}]^{1/2} . \quad (3.4)$$

It should be noted that the second-order terms involve the square of the magnetic field, causing a departure of $W(F,M_F)$ from linear field dependence, and also depend on the hyperfine interaction constants.

At much higher fields, it becomes more appropriate to treat the field dependent terms exactly and H_{hfs} as the perturbation, in an $|IM_IJM_J\rangle$ representation. The expression for the Zeeman energies then becomes

$$W(M_IM_J) = hAM_IM_J + hB \frac{[3M_J^2-J(J+1)][3M_I^2-I(I+1)]}{2J(2J-1)2I(2I-1)}$$

$$-g_J\mu_oM_JH - g_I\mu_oM_IH.$$

It will be noticed that, at these higher fields, the levels once more approach a linear field dependence.

CHAPTER IV

EXPERIMENTAL APPARATUS AND TECHNIQUE

4.1 The Atomic Beam Machine

The atomic beam apparatus used to carry out this work has been described in detail by King (1960) and Cameron et al. (1962). In this section, therefore, only the essential features of the machine and the relevant modifications will be presented.

Fig. 4.1 shows a schematic diagram of the apparatus. The sample under study is contained in an oven with a narrow slit, which is heated by electron bombardment. At a temperature sufficiently high to produce a vapour pressure of the source material of between 0.1 and 1.0 millimetre of mercury, a steady beam of atoms emerges from the oven slit and enters the main chamber of the machine. The main chamber is maintained under a high vacuum ($\sim 10^{-6}$ mm Hg). This allows the beam to traverse the length of the apparatus with minimal scattering from residual gas atoms.

An atom in an inhomogeneous magnetic field experiences a force which, if the field is sufficiently strong, is given by

$$F_z = \mu_o g_J M_J \frac{\partial H}{\partial z} = \mu_{eff} \frac{\partial H}{\partial z} .$$

In an atomic beam apparatus, such a strong, inhomogenous magnetic

Figure 4.1

Schematic diagram showing the main features of the atomic beam apparatus. The trajectory of the atoms which have undergone a transition is shown by a solid line. The stop-wire,S, prevents the undeflected atoms from reaching the detector. The second RF loop and the moveable beam stop are used in the sign of the moment determination (see section 5.2b).

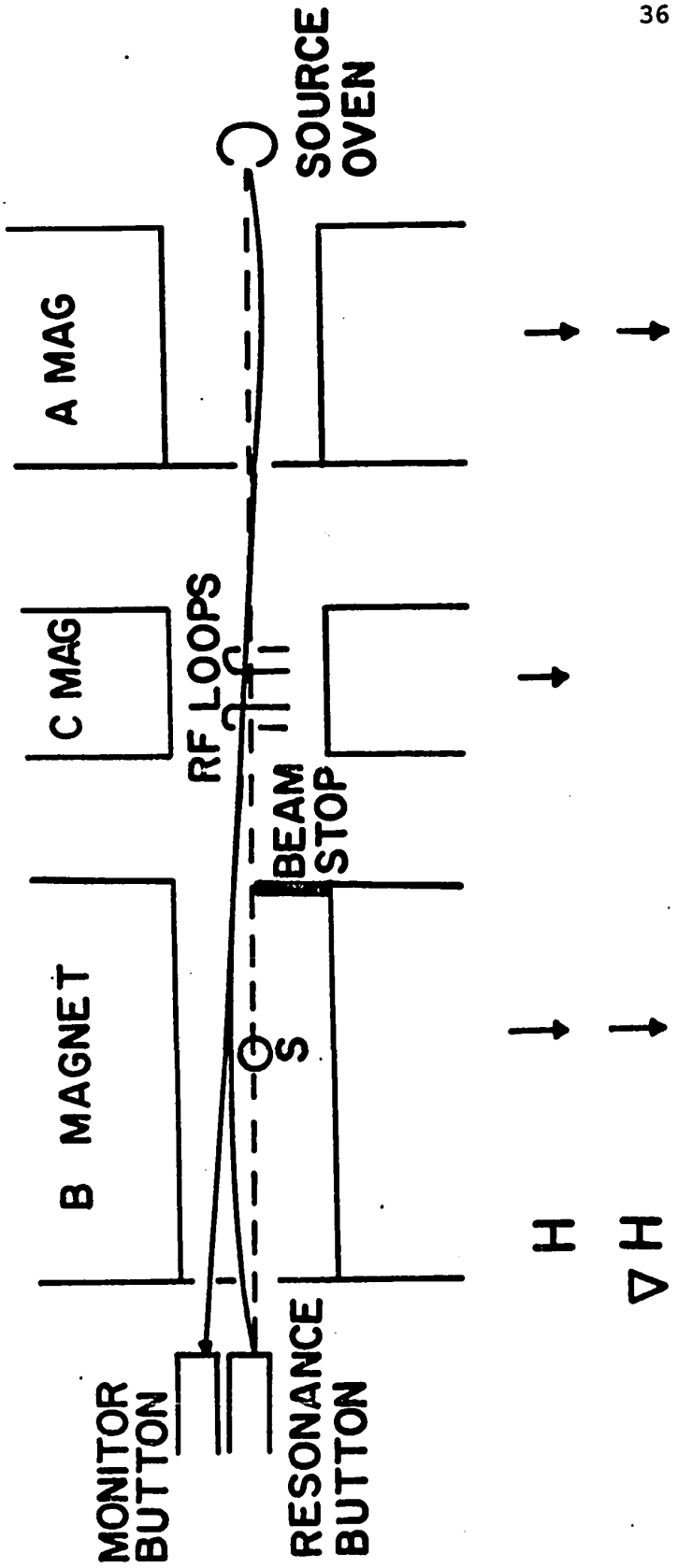
SOURCE OVEN
A MAG
C MAG
RF LOOPS
BEAM STOP
B MAGNET
S
MONITOR BUTTON
RESONANCE BUTTON
H
ΔH

field is provided by a set of magnets A and B, known as deflecting or focusing magnets. Atoms emerging from the source oven in a forward direction at a slight angle can be deflected back to the axis by the A magnet provided their velocities and M_J are appropriate. The trajectory of the atoms depends on the magnitude and sign of their M_J. Both A and B magnets have their field gradients in the same direction, so that all atoms passing through the A magnet are deflected away from the axis by the B magnet and, hence, are not detected. However, if in the region between the A and B magnets, an atom undergoes a change of state such that the M_J of the atom changes its sign, then the B magnet will refocus it on to the detector. This is the so called "flop-in" geometry. In addition, the ratio of the strengths of the A and B magnets is such that only those atoms with M_J unaltered in magnitude are refocused. Slits placed across the beam path select atoms of appropriate M_J and velocity, while a stop wire, S, prevents the fast moving atoms or those with $M_J=0$ from reaching the detector.

In the intermediate region between the two deflecting magnets, the atoms pass through a low but highly homogenous magnetic field provided by the C magnet. Transitions between the atomic energy levels are induced by a weak radiofrequency oscillating magnetic field.

The purpose of the second radiofrequency loop and the moveable slit (beam-stop) installed in the B magnet gap, shown in the diagram, will be discussed in a later section.

4.1a Beam Detection

If the isotope under study is not radioactive, the stable beam is detected in the machine itself by means of a surface ionization detector. For a radioactive sample, however, the beam is allowed to land on a pair of stainless steel surfaces called "buttons". Fluctuations in the beam intensity are monitored by a double collection technique (Stinson et al., 1967). In this method, in addition to collecting the atoms that have undergone a transition, on a resonance "button", the "thrown-out" beam which undergoes no transition in the C-magnet is allowed to land on a monitor "button". The ratio of the activities on the two "buttons" provides the necessary normalisation for the changes in the beam intensity.

After an exposure to a radioactive beam both the monitor and resonance "buttons" are removed from the machine through a vacuum interlock and taken to the adjacent counting room, where the activity is detected and recorded. Two different types of counters were used in the present experiments. The 19.2 hr ground state activity of praseodymium was detected using thin-window Geiger counters, which are shielded and provided with anti-coincidence circuits to discriminate against cosmic ray background. The background count rate is typically 2 counts per min. The detection of the 14.6 min activity of the isomeric state, on the other hand, required the construction of windowless, continuous-flow gas counters. This is discussed below in some detail.

The decay of the 14.6 min isomeric state and the 19.2 hr ground state in ^{142}Pr are shown in Fig. 4.2. The ground state activity may be recorded by detecting the 1.51 MeV transition in ^{142}Nd. Due to the decay of the 14.6 min activity there is an initial "growing-in" of the ground state activity; this offers a method of detecting the short-lived activity, which has been used to measure the half-life of the isomeric state (Kern et al., 1967). Unfortunately, in the atomic beam experiments carried out to study the isomeric state, the presence of the ground state activity in the beam, with our poor counting statistics, is sufficiently high so as to obscure the "growing-in" due to the short-lived activity. It was, therefore, essential to detect the 14.6 min activity directly. The total conversion coefficient for the 3.7 keV transition in ^{142}Pr has been estimated to be $\sim 3.10^9$ (Kern et al., 1967). A possible method of identifying the 14.6 min activity in an atomic beam study is, then, to detect the conversion electrons and/or the associated x-rays.

Since the energy of the transitions is so low, conversion will take place in the M and higher shells. The emission of a conversion electron from an atomic subshell will create a vacancy in that shell, which will subsequently be filled by an electron from a higher shell. The binding energy associated with this process is either given up by the emission of a characteristic x-ray, or used up to eject another electron, the so-called Auger electron. One may define the fluorescence yield of the i^{th} subshell of an atom, ω_i, as the probability that a vacancy in that

Figure 4.2

The decay of the 14.6 min isomeric state in ^{142}Pr.

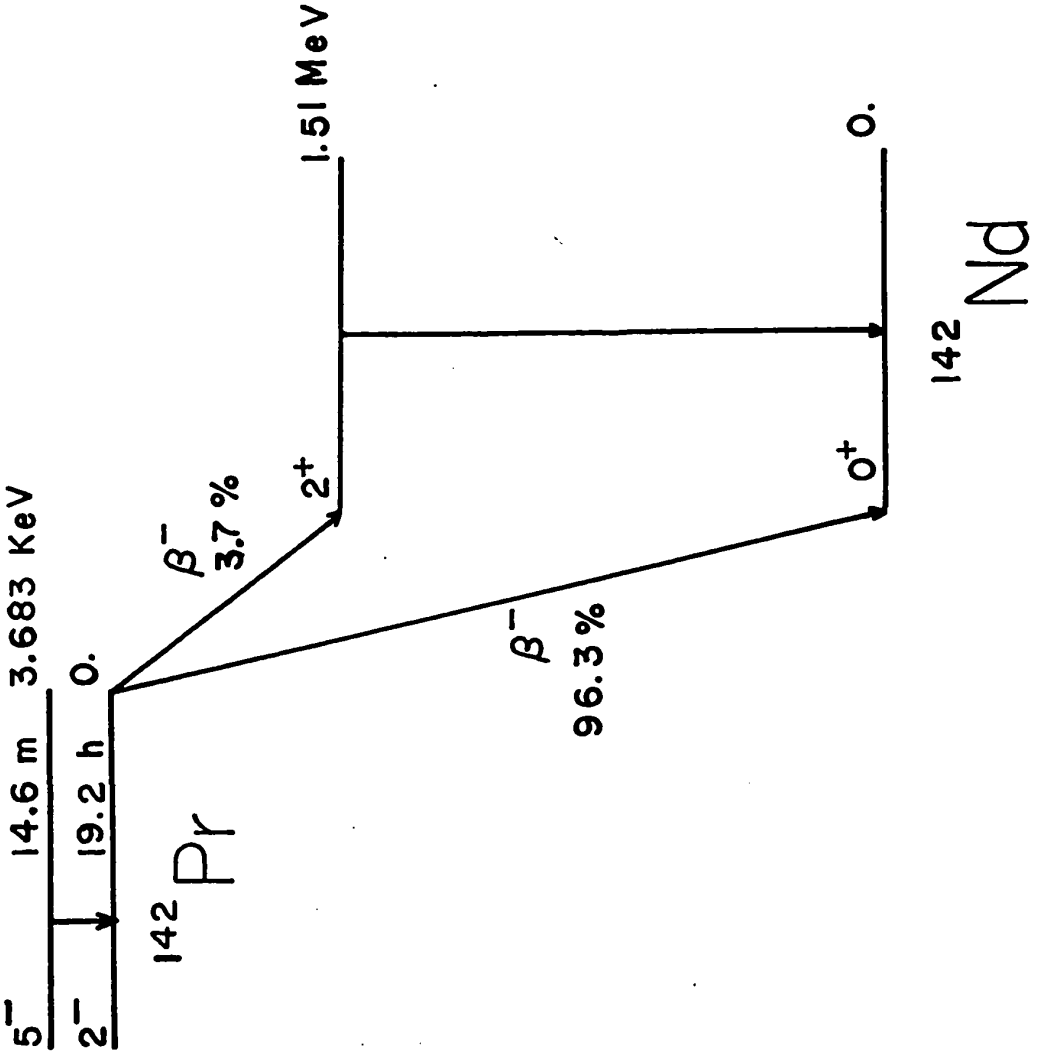
5⁻
2⁻
14.6 m
19.2 h
3.683 KeV
0.
142 Pr
β⁻ 3.7 %
β⁻ 96.3 %
2⁺
0⁺
1.51 MeV
0.
142 Nd

subshell is filled by a radiative transition (x-ray emission). Similarly, the Auger yield of the same subshell may be defined as the probability that an electron is emitted as the result of filling the vacancy. The K- and L-shell fluorescence yields have been measured over quite an extensive region of the periodic table (Fink et al., 1966). However, the information for the fluorescence yields for M- and higher shells is very scarce. Measurements for eight elements between Z=76 and Z=97 have been reported in the literature (Fink et al., 1966 and Karttunen et al., 1971). The experimental results indicate that the M-shell fluorescence yields are quite small and tend to decrease with lower Z. If these measurements are extrapolated to Z=59, one may estimate ω_M for ^{142}Pr to be $\sim$ 0.003. Theoretical calculations of McGuire (1972) also predict a similar result. This means that the probability for X-ray emission would be very small indeed, and that the emission of conversion electrons should be followed almost solely by Auger electrons. As discussed later, this appears to be true experimentally for the case of ^{142}Pr.

4.1b The Gas Counters

In order to detect the 14.6 min activity, an array of ten windowless, continuous-flow gas counters were machined out of a single 2.5 ft long brass bar. The radioactive sample which is collected on a stainless steel "button" may be inserted in any one of the counters through a slot, and thus, forms an integral part of the counter wall. The "button" is held $\sim$ 2 mm from the high voltage element which is a 0.0025 cm O.D. platinum wire

loop about 0.5 cm in diameter. The details of the design and operation of the counters are summarized below.

In an attempt to detect x-rays following the emission of conversion electrons a formvar (polyvinyl butyral) window of thickness $\lesssim$ 5 $\mu gm/cm^2$ was installed. The thickness was such as to stop completely the conversion electrons but allow the x-rays through without any significant absorption. With such an arrangement, however, no 14.6 min activity could be detected. It was mentioned earlier that the M-shell fluorescence yield for ^{142}Pr is expected to be extremely small. The failure to detect any x-rays indicates that this is indeed the case. This also implies that the gas counters had to be necessarily windowless in order to detect the short lived activity.

The M-shell electron binding energies range from 1.51 to 0.965 keV so that the electrons associated with the conversion process have an energy of 2.2 to 2.7 keV. The range of 2 keV electrons in argon at atmospheric pressure is $\sim$ 0.5 mm; this limits the sensitive volume of the counters to a region extending to only $\sim$ 0.5 mm from the sample. The operational voltage of the counters had to be such as to produce a sufficiently large electric field to allow gas multiplication to ensue very near the sample. A plot of count rate against voltage is shown in Fig. 4.3. Besides the appearance of a "plateau" near 1.45 kV, it was found that, at this voltage, the relative efficiencies of the different counters were nominally the same. The counters were, therefore, operated at 1.45 kV.

Figure 4.3

Count rate vs. voltage. The operational voltage for the counters was chosen to be 1.45 KV.

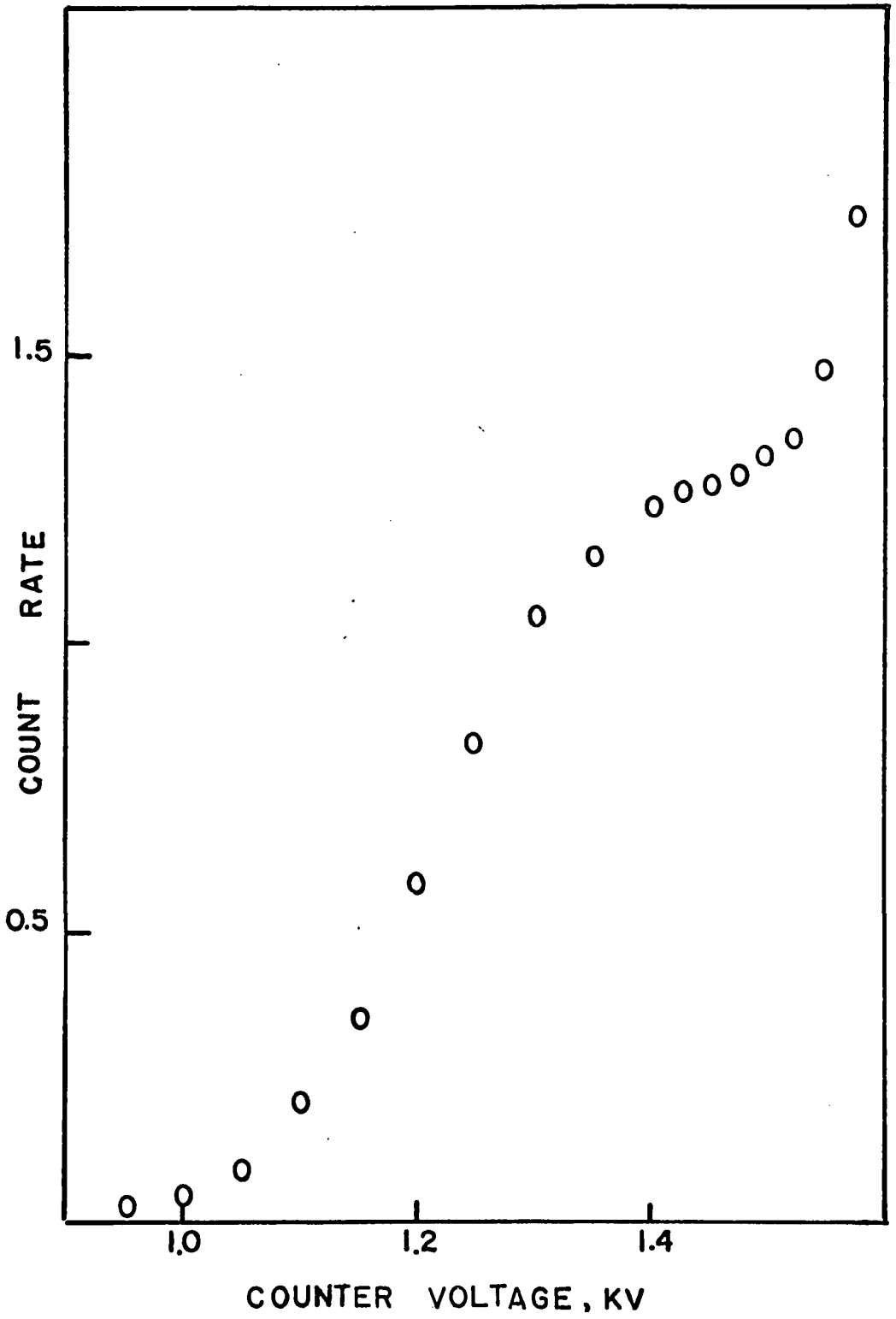
1.5
0.5
COUNT RATE
1.0
1.2
1.4
COUNTER VOLTAGE, KV

The commercially available mixture of 90% argon-10% methane was used as the counting gas. The variation of the counter efficiency with gas delivery pressure is shown in Fig. 4.4, for two radioactive samples: ^{3}H and ^{137}Cs. It will be noticed that at low flow-rates the count rate drops drastically. It was, therefore, ensured that the counters were always operated at flow-rates where the efficiency was maximum and constant.

Since the counters were windowless, during each "button" change, they were exposed to air with a consequent decrease in counting efficiency. This effect is due to air contamination of the counting gas (Quaranta et al., 1967). It was found that $\sim$ 2 min had to elapse after each "button" change, for the counters to regain their normal efficiency.

The presence of any insulating material on the counter walls will allow a layer of positive charge to build up with a consequent degradation of the electric field strength. The so-called space-charge effect will therefore lead to a decrease in counting efficiency. For this reason, the insulator between the high voltage element and ground had to be remotely placed so as not to "see" the sensitive volume of the counter. For the same precautionary reason, the "buttons" were thoroughly cleaned and polished to remove any insulating films from their surfaces.

For the detection of the low-energy, 14.6 min activity, the radioactive sample has to be sufficiently thin to avoid any self-absorption in the sample. This, however, was no problem, since in an atomic beam experiment, one is dealing with samples which are at the most only a few atomic layers thick.

Figure 4.4

Counter efficiency as function of delivery pressure. The solid points are for ^{3}H and the open circles are for ^{137}Cs.

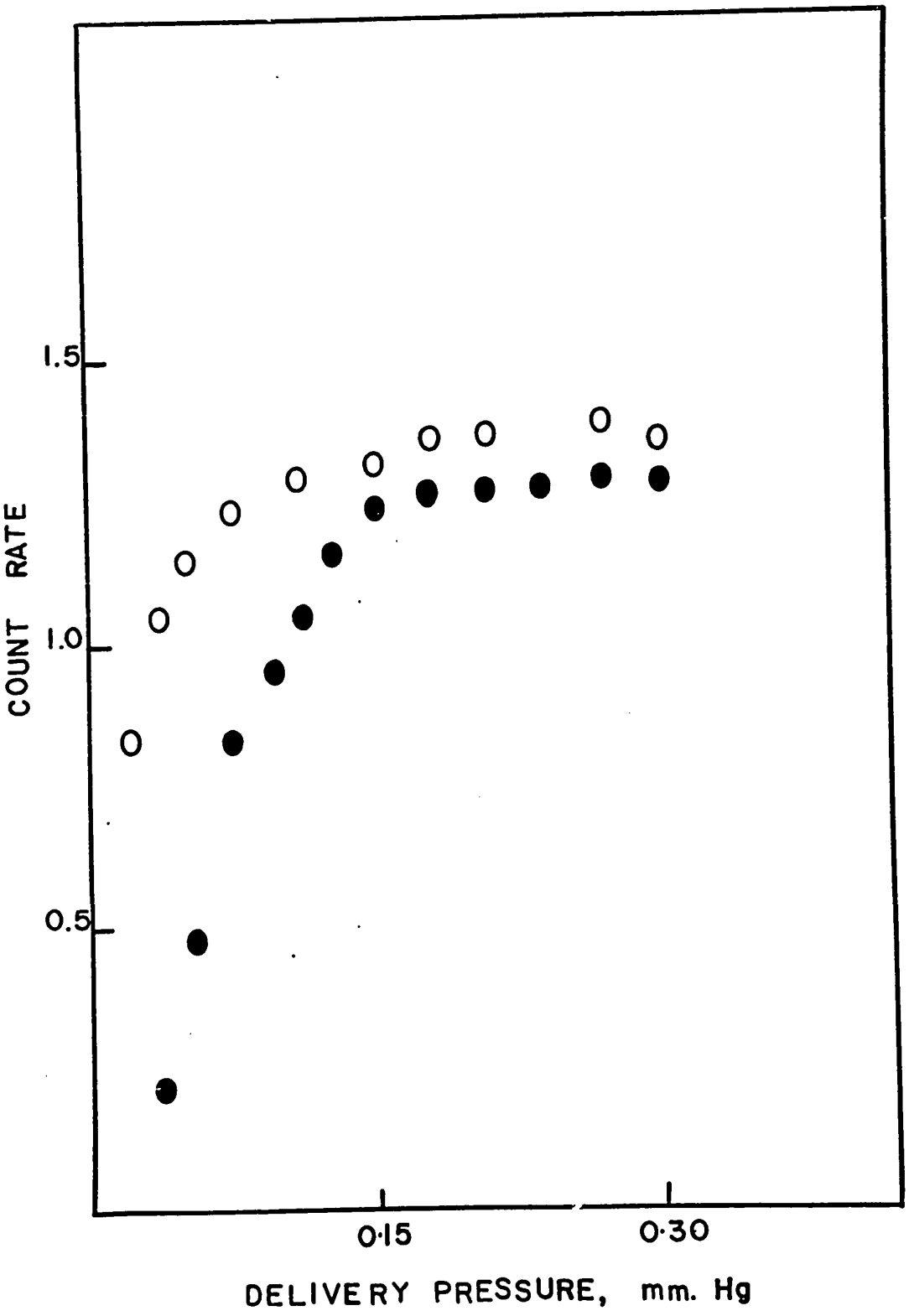
1.5
1.0
0.5
COUNT RATE
0·15
0·30
DELIVERY PRESSURE, mm. Hg

The counter background was typically 2-5 counts per min. The counter walls and the high voltage elements had to be periodically cleaned in order to maintain low enough background. On the whole, the stability of such counters is poor, especially for the type of activity one is dealing with in these experiments.

4.2 Measurement of Nuclear Spins and Moments: A General Description of the Method

A variety of electronic and nuclear properties of an atom may be determined by a detailed study of its hyperfine structure, using the method of atomic beams. Since the present work only concerns the nuclear properties of praseodymium-142, a general description of the method of measuring nuclear spins and magnetic moments will be given.

The basic principle of the technique is to measure the spacing between the hyperfine levels by inducing magnetic dipole transitions between them. The transitions are induced by a weak radiofrequency oscillating magnetic field set up in the region of the C-magnet. With the direction of the RF field perpendicular to the static field, the selection rules for the transitions are

$$\Delta F = 0, \pm 1 \; ; \; \Delta M_F = \pm 1.$$

If the RF amplitude is sufficiently large, it is possible to induce several successive transitions between the adjacent, approximately equally spaced Zeeman levels. These so-called multiple quantum transitions (MQT) are of great importance in atomic beam studies. The selection rules for a n-quantum transition

are

$$\Delta F = 0 \quad \Delta M_F = \pm n.$$

A detailed account of both the theoretical and practical aspects of MQT has been given by Pierce (1966).

At a low magnetic field, the frequency of a $\Delta F=0$ Zeeman transition is given by (see equation 3.3)

$$\nu_{nom} = \frac{W(FM_F) - W(FM_F-1)}{h} = - \frac{g_J \mu_o H}{h} f(J,F,I) \qquad (4.1)$$

where f is a function of J,F and the nuclear spin I. If the electronic angular momentum, J, and the gyromagnetic ratio, g_J, are known for an atomic state, the nuclear spin can be determined by simply observing these transitions.

At higher magnetic fields, the frequency of a $\Delta F=0$ transition becomes

$$\nu = \nu_{nom} + \frac{C_1 H^2}{C_2 A + C_3 B} \qquad (4.2)$$

where C_1, C_2 and C_3 are functions of J, g_J, g_I, F and I. Since the denominator of the second term involves the hyperfine interaction constants, A and B, these may be determined by following the low-field transitions to increasingly higher magnetic fields. Of course, in order to determine both A and B uniquely, it is necessary to make the measurements in at least two different F-states. A more direct method of measuring the hyperfine constants is to detect low-field hyperfine transitions. However, with no previous knowledge of A and B, the search range for these transitions is too large, and the experiments laborious, especially for a radioactive sample.

Once a set of resonances has been obtained, a computer programme (the one used for the present work is called LOWFIT) can be used to calculate the values of A and B which best fit the experimental data. For different combinations of A and B, the programme computes (by an exact diagonalization of the magnetic hyperfine Hamiltonian) the residuals between the experimentally observed frequencies and those predicted at appropriate fields for the particular transition assumed. The values of A and B which minimize

$$\chi^2 = \sum_{i=1}^{N} \frac{(\nu_{cal}-\nu_{obs})_i^2}{(\Delta\nu_{tot})_i^2}$$

are adopted as the experimentally determined values. The total error assigned to the observed transition frequency is taken to be

$$\Delta\nu_{tot} = \{(\Delta\nu_{obs})^2 + (\Delta H \frac{\partial\nu}{\partial H})^2\}^{1/2}$$

where $\Delta\nu_{obs}$ is some fraction of the resonance width and ΔH is the uncertainty in the magnetic field.

With A and B determined to a desired accuracy, the magnetic and quadrupole moments may be deduced from the Fermi-Segrè formula. In the method outlined so far, however, there is no way of actually identifying the M_F values of the Zeeman levels involved. The level ordering of F-states depends both on the ratio B/A and the sign of A, and therefore, if A and B are both reversed in sign, the same Zeeman frequencies result. Thus, the method yields information only about the magnitude of μ_I and Q, and the relative sign between them.

In writing down equations 3.3 and 3.4, the effect due to the interaction of the magnetic dipole moment, μ_I, with the external magnetic field was neglected. This is a valid procedure at low magnetic fields, since $\mu_I \sim 10^{-3} \mu_J$. However, at sufficiently large magnetic fields, it is possible to experimentally detect the effect of the $\vec{\mu}_I \cdot \vec{H}$ term. For a reasonably large value of the magnetic moment, this offers a feasible experimental method of determining the sign of the dipole moment. For the ground state of ^{142}Pr, however, $\mu_I \sim 0.2$ n.m. The resulting contribution due to the $\vec{\mu}_I \cdot \vec{H}$ term at 500 Gauss (the limit at which the C magnet in the McMaster machine can be operated) is only of the order of 10 Kc/s, and cannot be detected because of the experimental errors. An alternative approach is, therefore, necessary. The method consists of inferring the level ordering of F-states (which depends on the sign of μ_I) by preferentially focussing atoms in a given M_J state. The details of this method which is, in principle, similar to the "flop-out on flop-in" technique used by King and Jaccarino (1954) and Childs et al. (1960), will be described in the next chapter.

CHAPTER V

ATOMIC BEAM EXPERIMENTS AND RESULTS

The main purpose of this research project was to measure the nuclear spin and magnetic dipole moment of the 14.6 min isomeric state of ^{142}Pr. The determination of the sign of the ground state magnetic moment followed as a logical extension. This, in turn, necessitated some additional experiments in order to re-interpret the previously published results for the ground state hyperfine structure. In this chapter, the details and results of these experiments will be presented.

5.1 ^{142m}Pr Experiments

An initial requirement of any atomic beam experiment is the production of a steady atomic beam of the sample under study. The short-lived, 14.6 min activity was produced in the McMaster reactor by thermal-neutron irradiation of $\sim$ 60 mg of natural praseodymium metal. A sufficiently strong source of ^{142m}Pr, with a comparatively smaller amount of the 19 hr ground state activity, is formed during a $\sim$ 20 min irradiation in a neutron flux of 10^{13} neutrons per cm^2 per sec. The sample, after irradiation, is conveyed via a pneumatic tube to the isotope laboratory adjoining the atomic beam machine room, from where it can be loaded into the machine with a minimum loss of time. The sample itself is contained in a small, sharp-lipped tantalum crucible which, in turn, is placed in a tantalum oven with a narrow slit. This is necessary in order to reduce the chances of praseodymium

metal creeping up the oven walls and clogging the slit. The oven is heated by electron bombardment; at an oven input power corresponding to a temperature of ∿ 2000°K, a satisfactory beam of praseodymium atoms is obtained, which can be used over a period of two to three half lives. Due to the short half-life of the isotope, it was necessary to produce an intense beam in as short a time as possible. As a consequence, high and fluctuating machine background presented a formidable problem, and many experimental runs were rendered useless as a result.

In order to test the performance of the counters and identify the 14.6 min activity in the beam, a pair of "buttons" was exposed to an atomic beam of ^{142m}Pr. After a 10 min exposure, the "buttons" were inserted in one of the counters and their decay followed for a period of several hours. Fig. 5.1 shows the decay of the activity. A straight line corresponding to a half-life of 14.6 min has been drawn through the points obtained after peeling off the long-lived 19.2 hr background. This shows that sufficient amounts of the 14.6 min activity can be produced and detected so as to make an atomic beam study of the isomeric state feasible.

The C-field is calibrated using resonances in ^{39}K, both before and after the actual experiment, to ensure that it did not change during the run. This,however, does not rule out any short-term fluctuations which can smear out a resonance or distort its line shape. As a rule, the first exposure is always carried out with the RF power turned off; this provides a measure of the machine background. If necessary, this may be repeated either

Figure 5.1

Decay of ^{142m}Pr activity. The horizontal scale is time in minutes. Note the change in scale at the 65-minute mark.

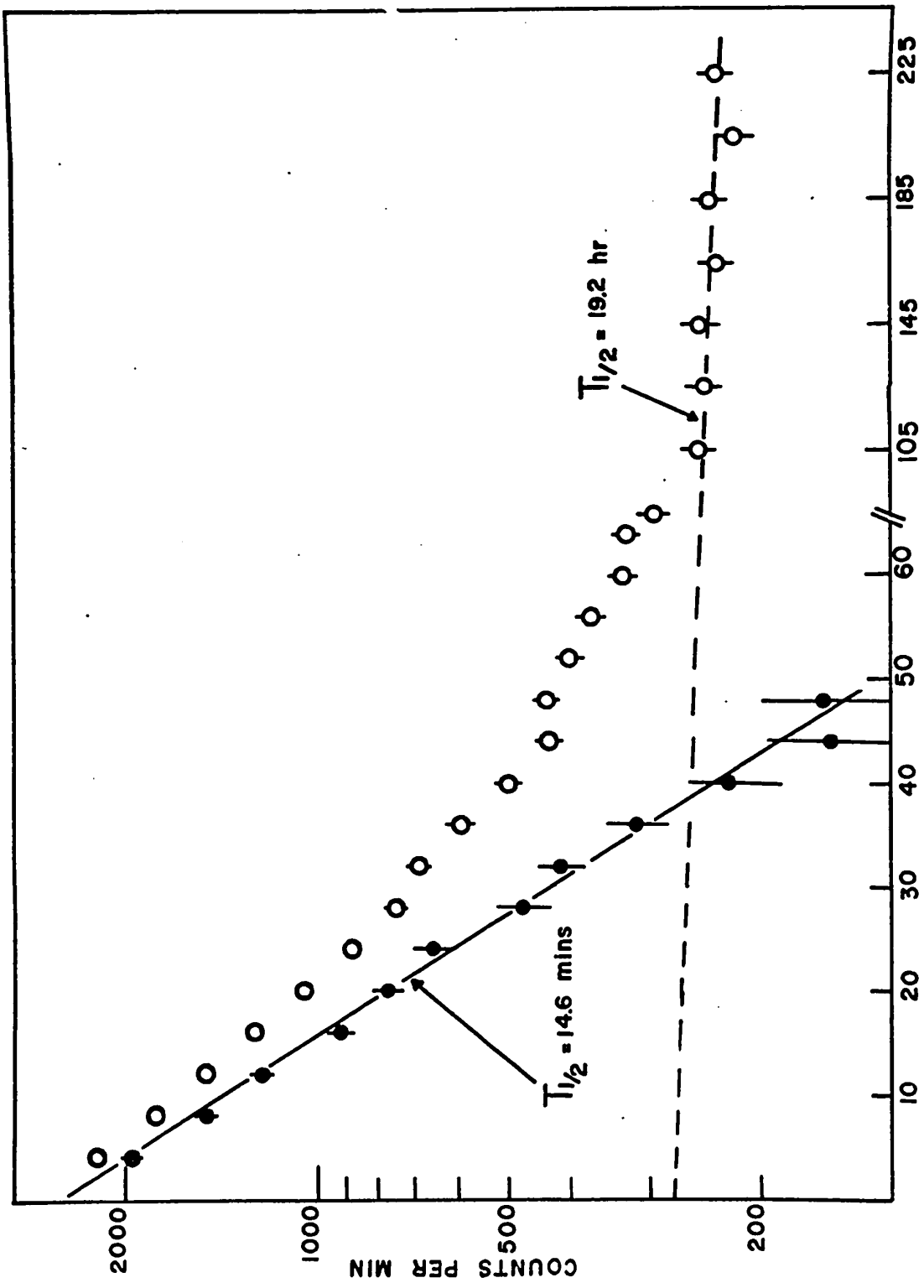
COUNTS PER MIN
2000
1000
500
200
10
20
30
40
50
60
105
145
185
225
$T_{1/2}$ = 19.2 hr
$T_{1/2}$ = 14.6 mins

during or at the end of a run, to check for the stability of the background. Again, one cannot guarantee absolute stability throughout the experiment, and the consistency of data must provide the ultimate test.

With the C-field calibrated and the RF generator set at a predetermined frequency, a pair of stainless steel surfaces ("buttons") is exposed to the radioactive beam for a period of 2-3 mins. At the end of an exposure, the "buttons" are withdrawn from the machine through a vacuum interlock and replaced with a fresh pair for the next frequency exposure. Meanwhile, the exposed pair is taken to an adjoining room where its activity is detected and recorded. In order to eliminate any effect from different counter efficiencies, both "buttons" are counted in the same counter. As explained earlier, the double-collection technique provides the necessary normalization for beam fluctuations and different exposure times. The output from the counters are fed to scalers which can accumulate counts for some predetermined time interval chosen to give a statistically significant number of counts. The activity on each "button" is followed for a period of several half-lives, and the results are entered into a computer programme which extracts the 14.6 min activity. The ratio of the activities on the two "buttons", resonance-to-monitor, is taken as a measure of resonance signal. By repeating this procedure for a series of frequencies, it is possible to trace out the resonance line-shape.

The electronic structure of praseodymium is well known

(Lew, 1953, 1970; Cabezas et al., 1962). The measured electronic angular momentum, J, confirms that the lowest-lying member of the ground state configuration $4f^3 6s^2$ is $^4I_{9/2}$. Also, the measured value of the electronic gyromagnetic ratio, g_J=-0.731055(1), is in good agreement with the L-S coupling value.

Since J and g_J are known, the method of determining the nuclear spin, I, consisted of exposing a series of "buttons" at resonance frequencies predicted by equation 3.3 for various values of I ranging from 0 to 7. An increase in the signal for a certain value of I indicates a resonance, and thus, determines the nuclear spin. Care must be taken in choosing a low enough magnetic field so that equation 3.3 applies. In any case, once the nuclear spin has been determined, the magnetic field can be changed and the resonance observed again in order to verify that the "linear field-dependence" was indeed applicable. For a given value of I there are 2I+1 (J>I) or 2J+1 (I>J) F-states. Of these, only those F-states, in which transitions of the type $M_J \longleftrightarrow -M_J$ exist, need be considered. These are:

F = I+9/2, I+7/2,.....,I+1/2 for I=7,6,...3,2.

F = 11/2, 9/2, 7/2 for I=1, and

F = 9/2 for I=0.

Also, because of the linear field dependence of energy at low fields, all the focussable multiple quantum transitions in a given F-state are superimposed, so that for a given value of I the number of possible transitions is, at the most, five. From

among these, those transitions which determine the nuclear spin uniquely are examined (see Fig. 5.2).

In order to measure the nuclear spin of the isomeric state two experimental runs were carried out at a C-field of 3.08(3) Gauss. In each case, the activity on the resonance "button" was followed in time to ensure that it was indeed decaying with the appropriate half-life. The combined results of the two runs are shown in Fig. 5.2. An increase in the signal is observed at a frequency corresponding to the value I=5, and the radioactive decay of the state involved has a half-life of 14.6 min. These results, considered along with the method of isotope production, unambiguously determine the nuclear spin of the 3.68 keV state of ^{142}Pr to be 5.

With the nuclear spin measured, the method of determining the hyperfine interaction constants A and B consists of following up the Zeeman ($\Delta F=0$) transitions at higher magnetic fields.

Since the ground state electronic angular momentum J=9/2 and the nuclear spin I=5, there are a large number of possible F-states, ranging from F=19/2 to 1/2. Fig. 5.3 shows a schematic energy level diagram, drawn for the case of A>0 (normal level ordering). Since in the present work, resonances were observed only in F=19/2 and F=17/2 states, the splitting of these states is shown in detail. The focussable $\Delta F=0$ transitions are shown by arrows and labelled by their multiplicity (number of quanta). It will be noticed that there are no focussable transitions (of the type $+M_J \longleftrightarrow -M_J$) in $F \leq 9/2$ states, and that the only obser-

Figure 5.2

The upper diagram shows the frequencies of all the possible resonances for various values of the nuclear spin I, at a magnetic field of 3.08 Gauss. The solid points represent the transitions examined for the spin search.

The lower diagram shows the results of the spin search. Two sets of experimental data points are shown by open circles and solid points respectively. It is concluded that the nuclear spin of ^{142m}Pr is I = 5.

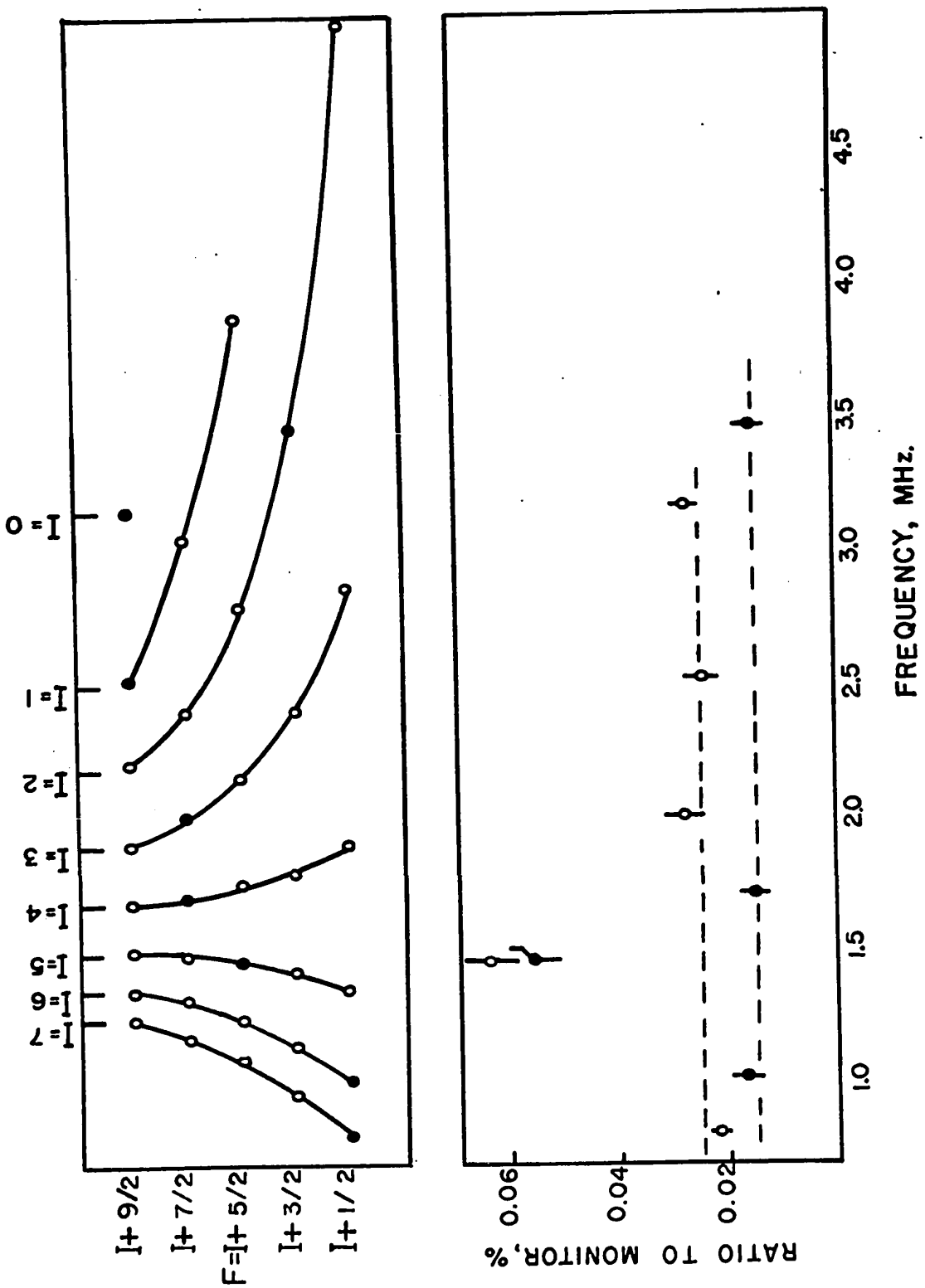
I = 0
I = 1
I = 2
I = 3
I = 4
I = 5
I = 6
I = 7
I+ 9/2
I+ 7/2
F=I+ 5/2
I+ 3/2
I+ 1/2
0.06
0.04
0.02
RATIO TO MONITOR, %
1.0
1.5
2.0
2.5
3.0
3.5
4.0
4.5
FREQUENCY, MHz.

Figure 5.3

A schematic diagram of the hyperfine structure of ^{142m}Pr, assuming A>0. Resonances were observed in the F = 19/2 and F = 17/2 states. The multiple quantum transitions (MQT) are indicated by arrows and labelled by their multiplicity. Upto the highest fields used (100 Gauss) all MQT in a given F-state are superimposed in frequency.

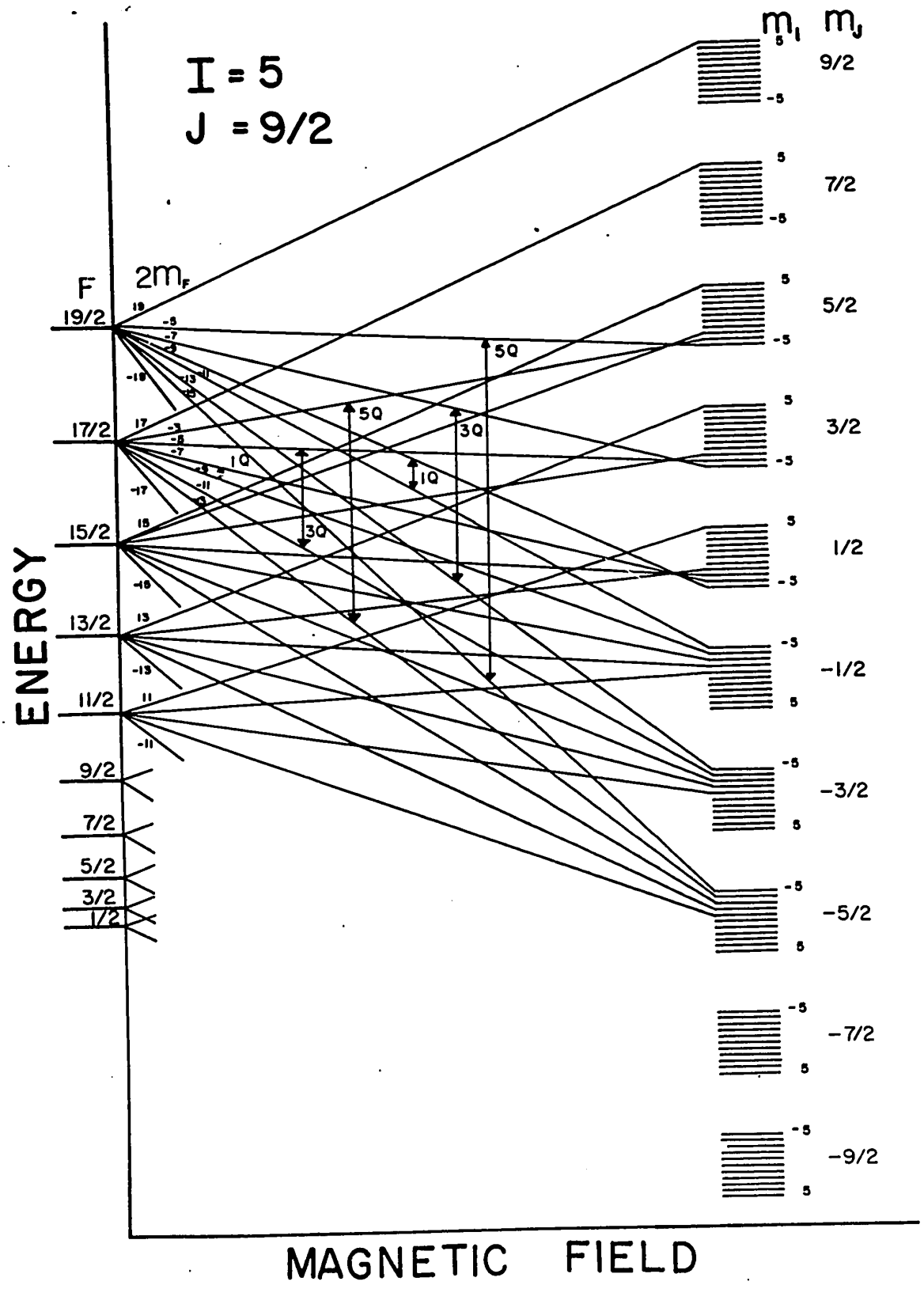
I = 5
J = 9/2
F
2m_F
19/2
17/2
15/2
13/2
11/2
9/2
7/2
5/2
3/2
1/2
1Q
3Q
5Q
m_I
m_J
9/2
7/2
5/2
3/2
1/2
-1/2
-3/2
-5/2
-7/2
-9/2
ENERGY
MAGNETIC FIELD

vable transition in F=11/2 state is a 1-quantum one.

The major source of experimental difficulty was the detection of the 14.6 min activity. Not only is the activity quite short-lived but also its decay involves two components. Moreover, in order to observe the decay of the short-lived component it was necessary to detect 2.2 keV conversion electrons. The windowless gas counters designed for this purpose proved to be quite unstable. As a result, the chances of obtaining a set of useful data points in a given experiment, sufficient to trace out a resonance line-shape, were very small. In view of these facts, the experiments were terminated at 100 Gauss; the experimental results yield a sufficiently accurate value of magnetic moment to make its interpretation meaningful.

A set of eight $\Delta F=0$ resonances observed in F=19/2 and F=17/2 states are shown in Fig. 5.4. Several of these resonances were repeated in order to gain confidence in the data. In some cases, a sufficient number of points could not be obtained from a single experimental run, and the results of two different experiments had to be combined in order to trace out a resonance line-shape. The experimental resonance frequencies and the magnetic fields at which resonances were observed were fed into the computer programme LOWFIT which fits the values of the hyperfine constants A and B to the experimental data. For given values of A and B, the programme computes the theoretical transition frequencies, compares them with the experimental ones and prints out the residuals (difference between experimental and calculated frequencies)

Figure 5.4

$\Delta F = 0$ resonances in ^{142m}Pr. The verical scale is ratio-to-monitor, two percent per division. The points marked RFO represent machine background. Where applicable, the open circles denote data from a separate experiment at the same field. The positions of the resonances calculated using the final values of A and B are shown by arrows.

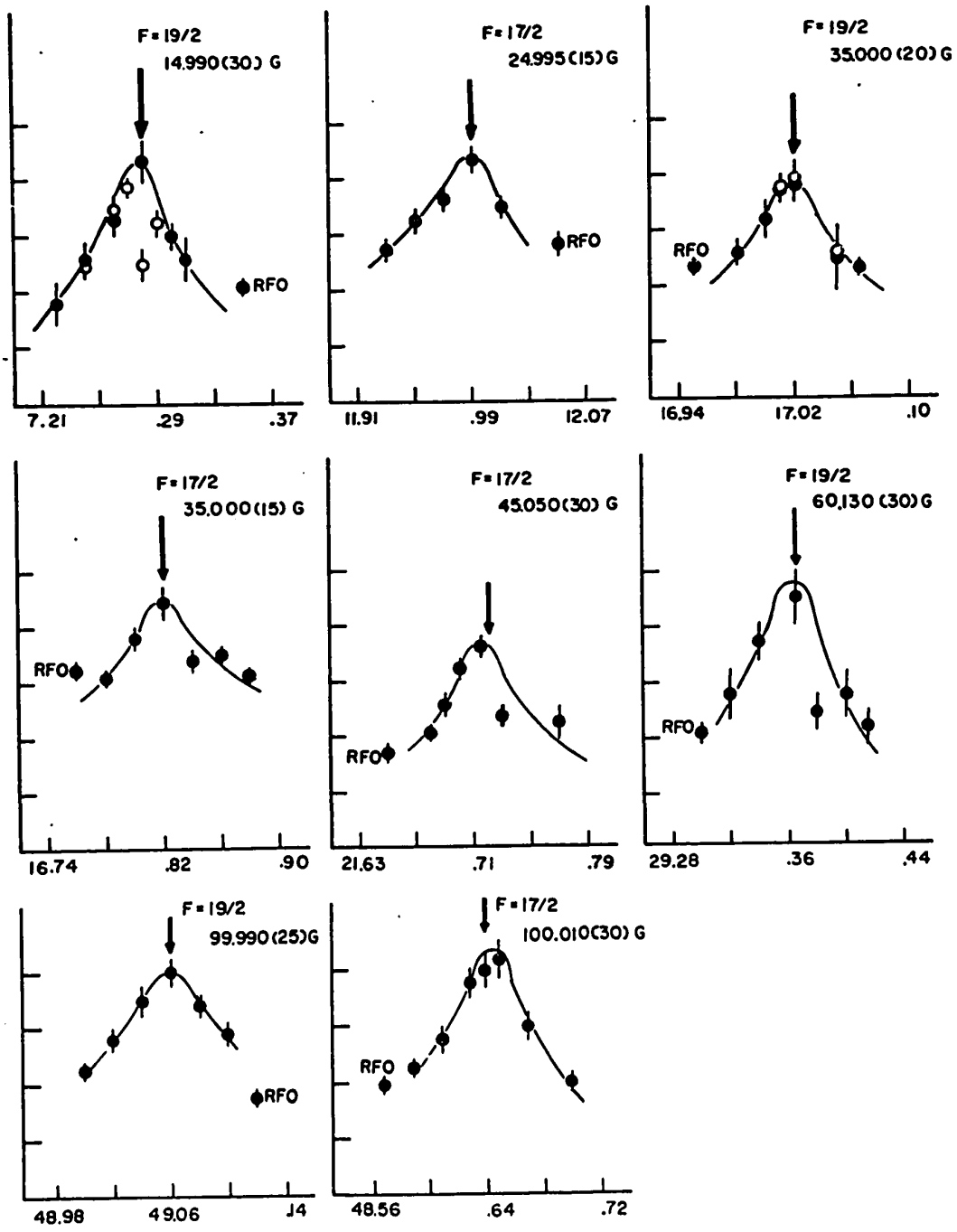
F=19/2
14.990(30) G
RFO
7.21
.29
.37
F=17/2
24.995(15) G
RFO
11.91
.99
12.07
F=19/2
35.000(20) G
RFO
16.94
17.02
.10
F=17/2
35.000(15) G
RFO
16.74
.82
.90
F=17/2
45.050(30) G
RFO
21.63
.71
.79
F=19/2
60.130(30) G
RFO
29.28
.36
.44
F=19/2
99.990(25) G
RFO
48.98
49.06
.14
F=17/2
100.010(30) G
RFO
48.56
.64
.72

and the corresponding chi-squares. Both A and B are then independently incremented by a predetermined amount, and the procedure repeated. A set of A and B which correspond to minimum chi-square is then adopted as final results. It should be pointed out that up to the highest fields used (100 Gauss), the multiple quantum transitions in agiven F-state are superimposed so that the multiplicity of a transition has no bearing on the interpretation of the data. The experimental results are summarized in Table 5.1. The resulting values of the hyperfine constants are:

$$A = 245(10)\ \text{MHz}, \qquad B = 100(450)\ \text{MHz},$$

or

$$A = -260(15)\ \text{MHz}, \qquad B = -100(450)\ \text{MHz},$$

where the errors quoted correspond to a change of one standard deviation. A fit with $A < 0$ yields a minimum chi-square which is two times larger than that obtained with $A > 0$, thus slightly favouring the positive result.

The hyperfine structure of stable ^{141}Pr (I=5/2) has been studied before (Lew, 1970) by the atomic beam method. The results are:

$$A = 926.2087(1)\ \text{MHz}, \qquad B = -11.878(2)\ \text{MHz}.$$

The magnetic moment, extracted directly from the $\vec{\mu}\cdot\vec{H}$ term of the hyperfine Hamiltonian, is

$$\mu = 4.136(2)\ \text{n.m.}$$

Using Fermi-Segrè formula, therefore, the magnetic dipole moment for the 14.6 min isomeric state is found to be:

$$\mu = 2.2(1)\ \text{n.m.},$$

where the positive result for the hyperfine constant has been adopted.

Table 5.1

A summary of $\Delta F=0$ resonances observed in ^{142m}Pr.

F	ν_{obs} (MHz)	H (Gauss)	$\nu_{obs}-\nu_{cal}$ (MHz)
19/2	7.280(15)	14.990(30)	0.004
	17.020(15)	35.000(20)	-0.013
	29.365(15)	60.130(30)	0.010
	49.060(15)	99.990(25)	0.001
17/2	11.990(15)	24.995(15)	-0.013
	16.820(15)	35.000(15)	-0.016
	21.720(15)	45.050(30)	0.012
	48.640(15)	100.010(30)	-0.002

5.2 $^{142}g_{Pr}$ Experiments

5.2a Re-interpretation of Previous Data

In 1962 the atomic beam group at Berkeley reported a study of the hyperfine structure of the ^{142}Pr ground state (Cabezas et al., 1962). A summary of their observations is given in Table 5.2. Fifteen $\Delta F=0$, $\Delta M_F = \pm 1$ resonances in three different F-states were observed at magnetic fields ranging from 8 to 280 Gauss. Treating A, B and g_J as parameters to fit the experimental data, the following results were obtained:

$$|A| = 67.5(5) \text{ MHz},$$

$$|B| = 7.0(2.0) \text{ MHz}, \; B/A > 0$$

$$g_J = -0.7311(3), \text{ for } J=9/2 \text{ state.}$$

Fig. 5.5 shows a schematic diagram of the hyperfine structure of ^{142}Pr for I=2 and A>0. It can be seen that in each of the F-states there are focusable transitions of the type $\Delta F=0$ $\Delta M_F = \pm n$, where $n \geq 1$. Since the 2F+1 magnetic substates at intermediate magnetic fields are not equally spaced, the various multiple quantum transitions (n>1) in a given F-state are quite separated in frequency. In such a case, therefore, in addition to measuring the frequencies of the transitions, one has to identify their multiplicity in order to obtain a unique set of values for A and B. The Berkeley group assumed, without discussion, that all the resonances they saw were one-quantum transitions. Since their apparatus utilizes high deflecting fields ($\sim$ 2-4 times higher than those in the McMaster apparatus), this has been borne out in most, if not all, of their work among the rare earths.

Table 5.2

A re-interpretation of $\Delta F=0$ resonances in ^{142g}Pr observed by Cabezas et al. (1962).

F	ν_{obs} (MHz)	H (Gauss)	$\nu_{obs} - \nu_{cal}$ (MHz)	
			Cabezas et al. (1962)	New interpretation
	5.837(25)	8.246(66)	-0.018	-0.017
	11.320(30)	15.920(62)	-0.002	0.0
	21.300(50)	29.836(54)	0.006	0.010
13/2	38.375(50)	53.423(44)	0.016	0.020
	65.475(50)	90.364(34)	-0.063	-0.059
	110.525(50)	149.713(50)	0.040	0.047
	214.360(20)	279.798(29)	-0.001	-0.003
	6.450(25)	8.246(66)	0.005	0.006
11/2	12.450(50)	15.920(62)	-0.012	-0.011
	23.460(30)	29.836(54)	0.025	0.024
	42.260(25)	53.423(44)	0.020	0.012
	72.360(50)	90.364(34)	0.035	0.003
	48.412(30)	53.423(44)	-0.052	-0.037
9/2	83.240(60)	90.364(34)	0.004	0.041
	142.630(50)	149.713(50)	-0.003	-0.051

Figure 5.5

A schematic diagram showing the hyperfine structure of ^{142g}Pr, drawn for the case A>0. The 1-quantum transitions denoted by Greek letters are those that Cabezas et al. (1962) claim to have observed. The transitions examined in this work are indicated by arrows and labelled by their multiplicity.

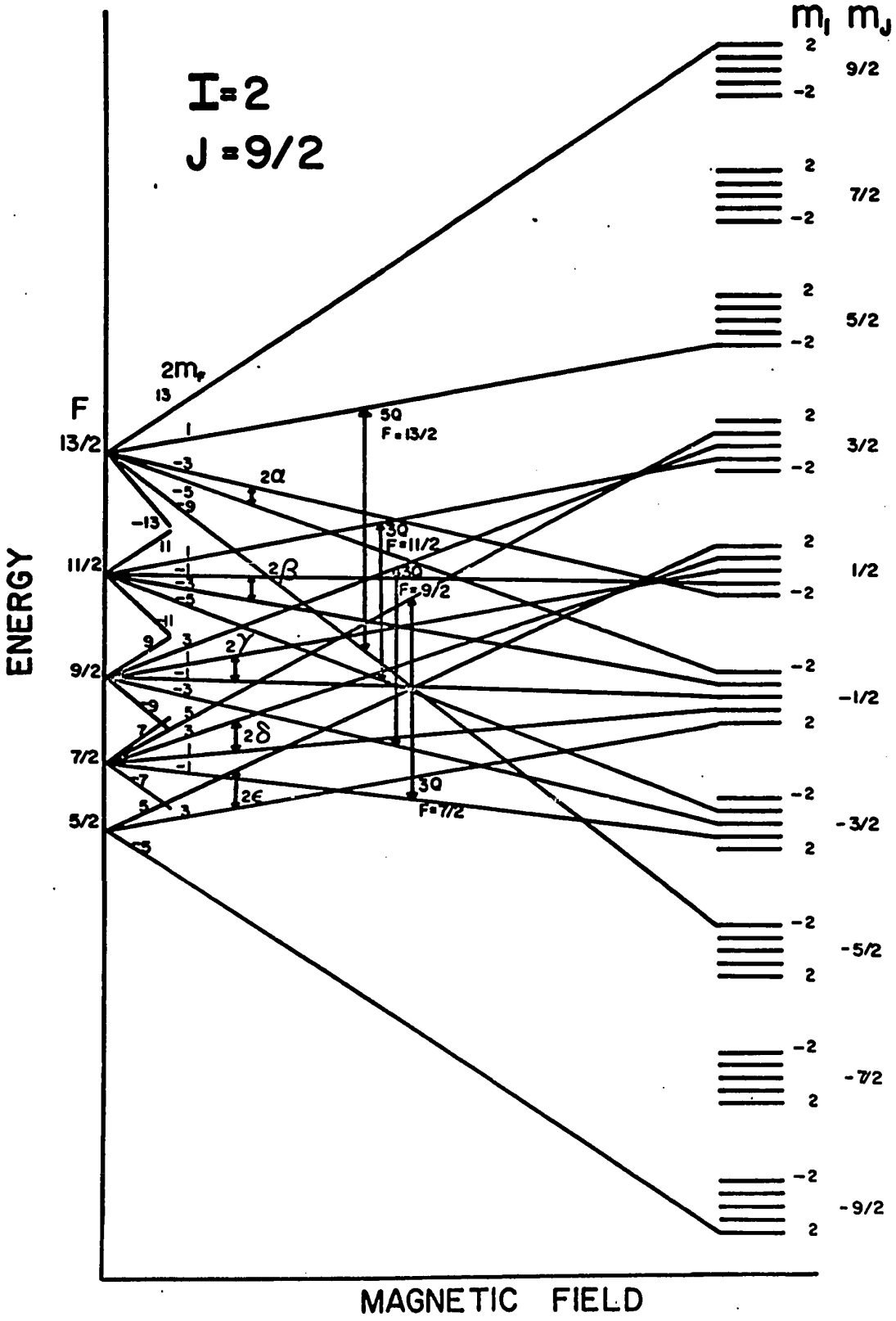
I=2
J=9/2
m_I m_J
F
13/2
11/2
9/2
7/2
5/2
$2m_F$
13
11
9
7
5
3
1
-1
-3
-5
-7
-9
-11
-13
2α
2β
2γ
2δ
2ε
3Q
F=13/2
3Q
F=11/2
3Q
F=9/2
3Q
F=7/2
2
-2
9/2
7/2
5/2
3/2
1/2
-1/2
-3/2
-5/2
-7/2
-9/2
ENERGY
MAGNETIC FIELD

In the experiments initiated at McMaster to determine the sign of the ground state magnetic moment, it was essential to observe multiple quantum transitions. Several initial attempts to do this, using the values of A and B given by Cabezas et al., failed to show the expected behaviour even though the apparatus seemed to be correctly aligned and adequate RF fields were being used. One conceivable explanation was that the high-field resonances interpreted as one-quantum transitions by Cabezas et al. could have been of higher multiplicity. Some evidence for this is borne out by the results of the spin search at 4.2 Gauss, shown (by Fig. 1) in their paper. Fig. 5.6 is a reproduction of that diagram. It can be seen that in the F=5/2 state the intensity of the transition (depicted as '2ε'), which is necessarily a 1-quantum jump, is scarcely above machine background. This seems to suggest that the higher intensities of the spin resonances in the other F-states are due to the overlap of multiple quantum transitions, and that the contributions from 1-quantum transitions are minimal. This is not unexpected since praseodymium has a small g_J, and therefore, the deflection of atoms in the $|M_J| = 1/2$ states will be small - maybe too small even with the large field gradients in the Berkeley apparatus. At any rate, as discussed below the 1-quantum transitions in ^{142}Pr cannot be detected with the McMaster apparatus.

A computer programme MONTE written by R.G.H. Robertson (1970), which examines the transmission of atoms and focussability of various transitions for given sizes of aperture slits and

Figure 5.6

A reproduction of Fig. 1 from the paper by Cabezas et al. (1962), showing the results of the spin search for the ground state of ^{142}Pr. The Greek letters denote the transitions corresponding to I = 2 in different F-states (see Fig. 5.5).

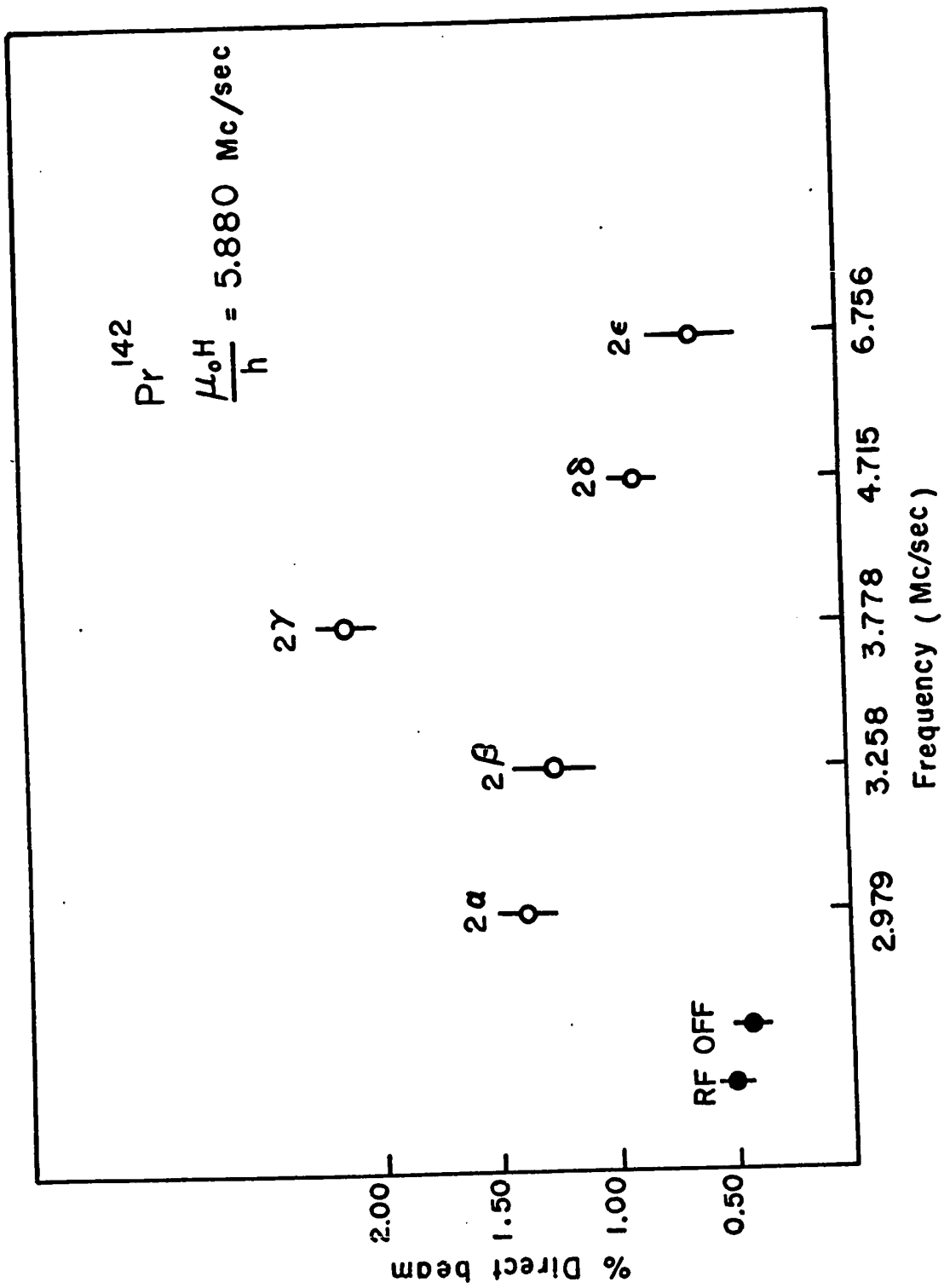
Pr^{142}
$\frac{\mu_o H}{h}$ = 5.880 Mc/sec
2γ
2α
2β
2δ
2ε
RF OFF
2.00
1.50
1.00
0.50
% Direct beam
2.979
3.258
3.778
4.715
6.756
Frequency (Mc/sec)

geometry (of the McMaster apparatus), predicts that the 1-quantum transitions should be a factor of $\sim$ 10 less intense than the 3-quantum transitions. In order to verify this experimentally a search for two low-field transitions was carried out. The results are shown in Fig. 5.7. At a magnetic field of $\sim$ 8 Gauss, the various MQT in the F=13/2 state overlap in frequency, resulting in an intense resonance. On the other hand, the focussable transition in the F=5/2 state, which is a 1-quantum jump, is not seen at all.

Assuming that the resonances observed by Cabezas et.al. were also due to MQT, an alternative interpretation of their data was attempted. Only A and B were treated as adjustable parameters and g_J was fixed at the value -0.731055 since reported by Lew (1970). A fit as good as the original one is obtained assuming all the transitions to be 3-quantum in nature. Of course, the values of A and B were altered from the published ones. To verify the new interpretation, a C-field was selected such that the resonances predicted by the two different sets of hyperfine constants were quite separated in frequency, and a search for these was carried out. Fig. 5.8 shows the four additional resonances observed in four different F-states. The experimental data and analysis, summarized in Table 5.3, clearly shows that the new interpretation must be adopted. The values of the hyperfine constants consistent with the experimental results are:

$$|A| = 65.6(2) \text{ MHz}$$

$$|B| = 22.0(2.0) \text{ MHz}, \quad B/A>0.$$

Figure 5.7

$\Delta F=0$ resonances in ^{142g}Pr at a low magnetic field, showing that the 1-quantum transition (in $F=5/2$) has no detectable intensity. The vertical scale is ratio-to-monitor, two percent per division.

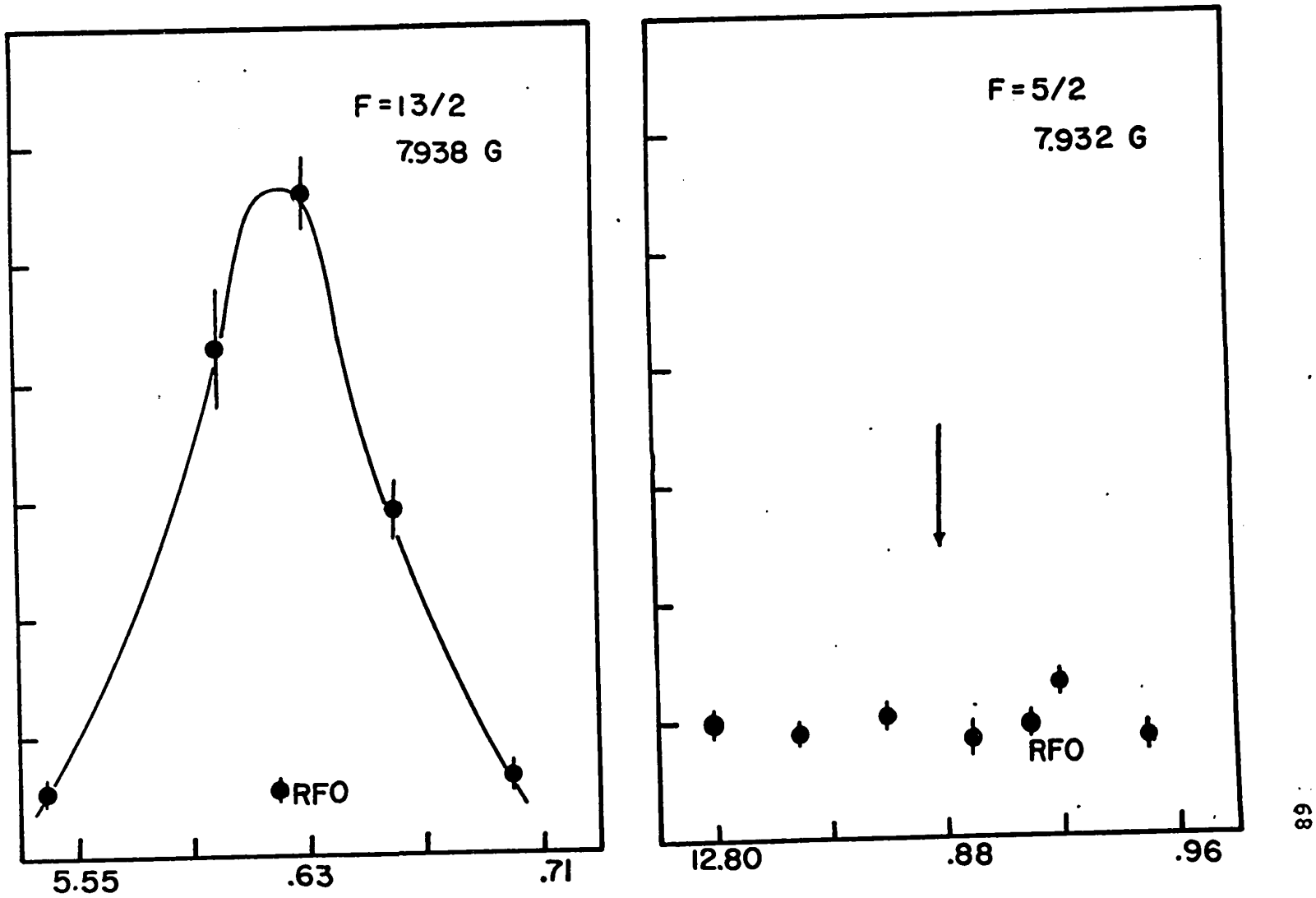
F=13/2
7.938 G
RFO
5.55
.63
.71
F=5/2
7.932 G
RFO
12.80
.88
.96

Table 5.3

$\Delta F=0$ resonances in ^{142g}Pr observed in this work.

F	ν_{obs} (MHz)	H (Gauss)	$\nu_{obs}-\nu_{cal}$ (MHz)
13/2	87.850(10)	120.171(10)	-0.001
11/2	88.710(15)	109.955(15)	0.013
9/2	49.920(10)	55.024(26)	-0.007
7/2	78.750(10)	70.020(23)	-0.005

Figure 5.8

Resonances in ^{142g}Pr observed in this work. The vertical scale is ratio-to-monitor, two percent per division. The positions of the resonces calculated using $|A| = 65.6$ MHz, $|B| = 22.0$ MHz, $B/A>0$ are indicated by solid arrows, while the dashed arrows indicate the expected resonance frequencies with the parameters (A and B) of Cabezas et al.

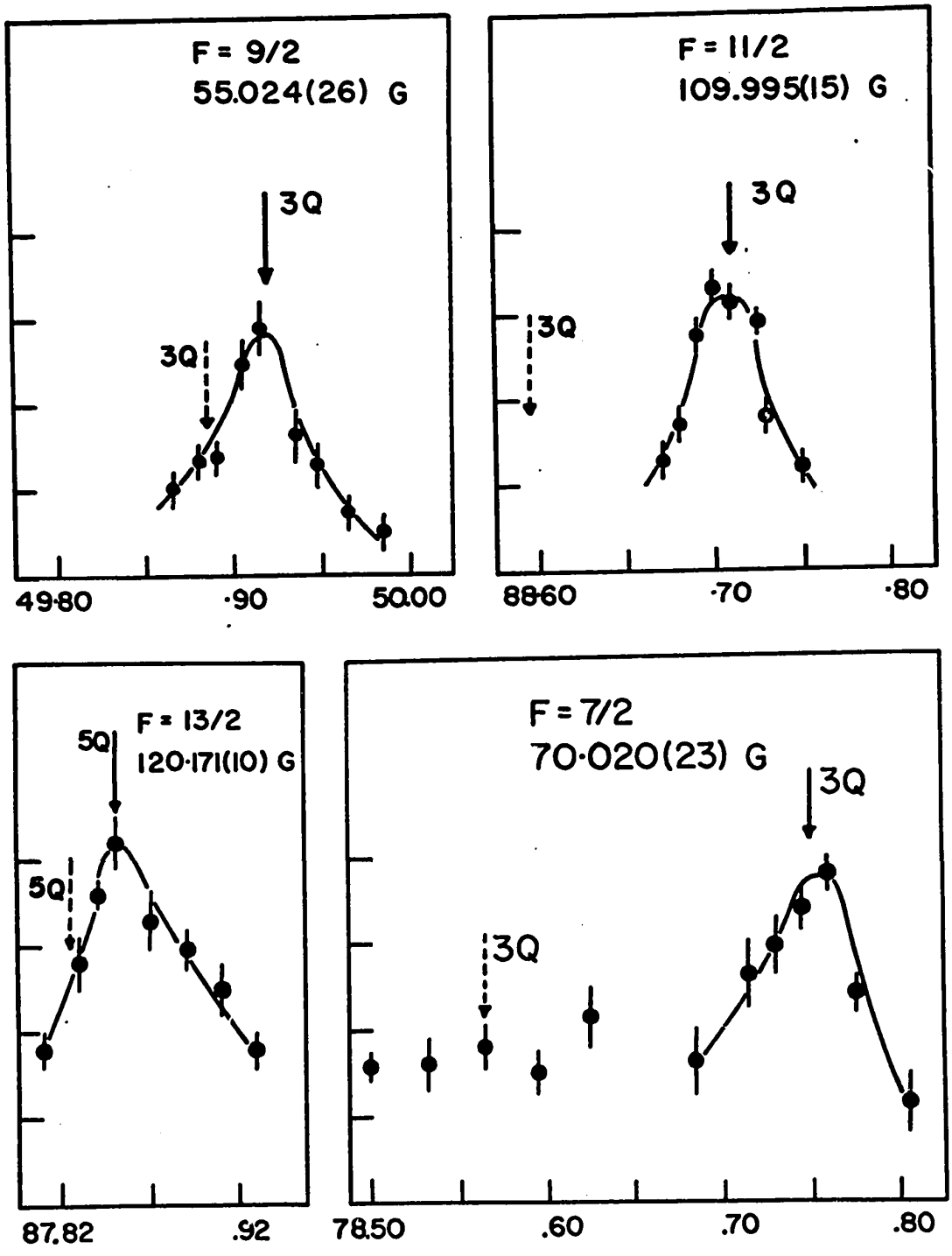
F = 9/2
55.024(26) G
3Q
3Q
49·80
·90
50.00
F = 11/2
109.995(15) G
3Q
3Q
88·60
·70
·80
F = 13/2
120·171(10) G
5Q
5Q
87.82
.92
F = 7/2
70·020(23) G
3Q
3Q
78.50
.60
.70
.80

Using Fermi-Segrè formula, in comparison with the results for ^{141}Pr given in section 5.1, the magnetic moment of ^{142g}Pr is

$$|\mu_I| = 0.234(1) \text{ n.m.}$$

In order to infer the nuclear quadrupole moment Q from the hyperfine constant B, it is necessary to evaluate the electric-quadrupole field (q_J) at the nucleus:

$$B = -e^2 q_J Q \ .$$

Using their value, $|B| = 7.0(2.0)$ MHz, Cabezas et al. have calculated the quadrupole moment for the ground state as $|Q| = 0.035(15)$ barns. With the correct $|B|$, the quadrupole moment becomes

$$Q = \pm 0.110(25) \text{ barns.}$$

The change in μ_I is small indeed, but the quadrupole moment is tripled in value.

5.2b Sign of the Ground State Magnetic Moment

The method used to determine the sign of the ground state magnetic moment of ^{142}Pr is based on the fact that at intermediate magnetic fields, the four levels of a 3-quantum transition are not equally spaced. Fig. 5.9 shows the relevant magnetic substates in F=11/2 for the case of positive and negative magnetic moments. In an atomic beam experiment one normally excites a 3-quantum transition (e.g. F=11/2: M_J=+3/2 $\longleftrightarrow$ M_J=-3/2) with the RF oscillator set at the mean of the three 1-quantum frequencies; all the atoms undergoing such a transition between M_J=+3/2 and M_J=-3/2 states (in either direction) are focussed and detected. However, if an obstacle is placed in the path of

Figure 5.9

Zeeman levels of 3-quantum transition in F = 11/2 state. The transitions examined in the sign of the moment experiment are indicated by arrows.

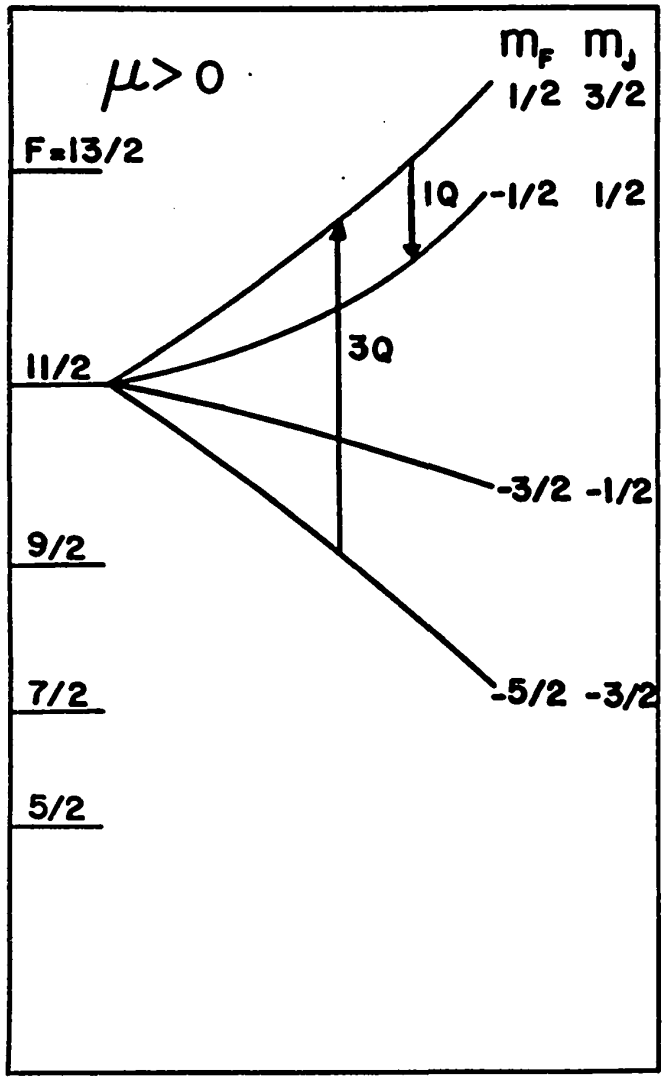
μ>0
m_F m_J
1/2 3/2
F=13/2
1Q
-1/2 1/2
3Q
11/2
-3/2 -1/2
9/2
-5/2 -3/2
7/2
5/2

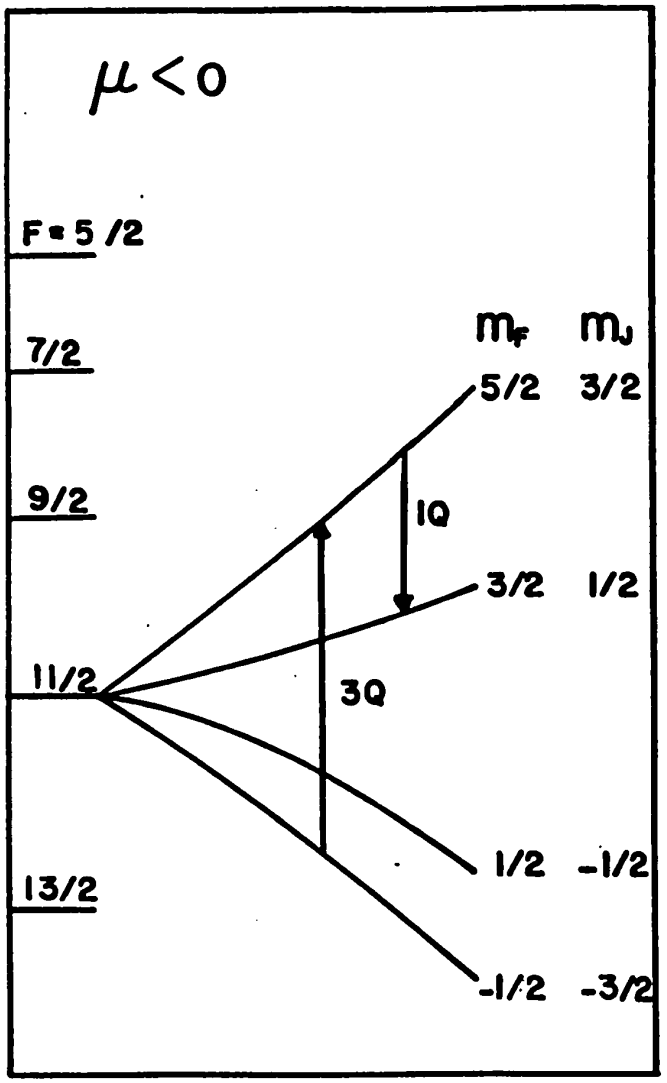
μ<0
F=5/2
m_F m_J
7/2
5/2 3/2
9/2
1Q
3/2 1/2
11/2
3Q
1/2 -1/2
13/2
-1/2 -3/2

the deflected beam on one side of the stop-wire (see Fig. 2.1), it will act as a state-selector allowing only atoms with $M_J>0$ in the B-magnet to be focussed. Then, only the atoms making transitions from an initial state $M_J=-3/2$ to a final state $M_J=+3/2$ can contribute to the 3-quantum intensity. It can be seen from Fig. 5.9 that, for the case $\mu_I>0$, if a second RF loop is used to induce the 1-quantum transition ($M_F=+1/2 \longleftrightarrow M_F=-1/2$), this will cause the 3-quantum resonance to "flop-out". On the other hand, if the magnetic moment is negative, the 1-quantum transition between $M_F=+5/2$ and $M_F=+3/2$ will cause the "flop-out". Thus, by using two RF loops, the first set at the 3-quantum frequency and the other at each of the two 1-quantum frequencies alternately, one can determine the sign of the magnetic moment.

For the actual experiment, it is necessary to select a magnetic field such that all the transitions to be examined are quite separated in frequency. The experiment was carried out at a C-field of $\sim$108 Gauss. The first RF loop was set at the 3-quantum frequency. The second RF loop was set at the 1-quantum frequency appropriate for the case of $\mu_I>0$; this was varied to scan the resonance and provide a "flop-out" line-shape. Next, using the 1-quantum frequency appropriate for the case of $\mu_I<0$, the experiment was repeated. At regular intervals throughout both the experiments the 3-quantum focussable transition alone was examined to ensure its presence.

The results of the two experiments are shown in Fig. 5.10. The 1-quantum frequency applicable to the case $\mu_I>0$ causes the

Figure 5.10

Results of the sign-of-the-moment experiment. The solid points show the data obtained in the two-oscillator experiment, while the open circles represent the 3-quantum intensity alone.

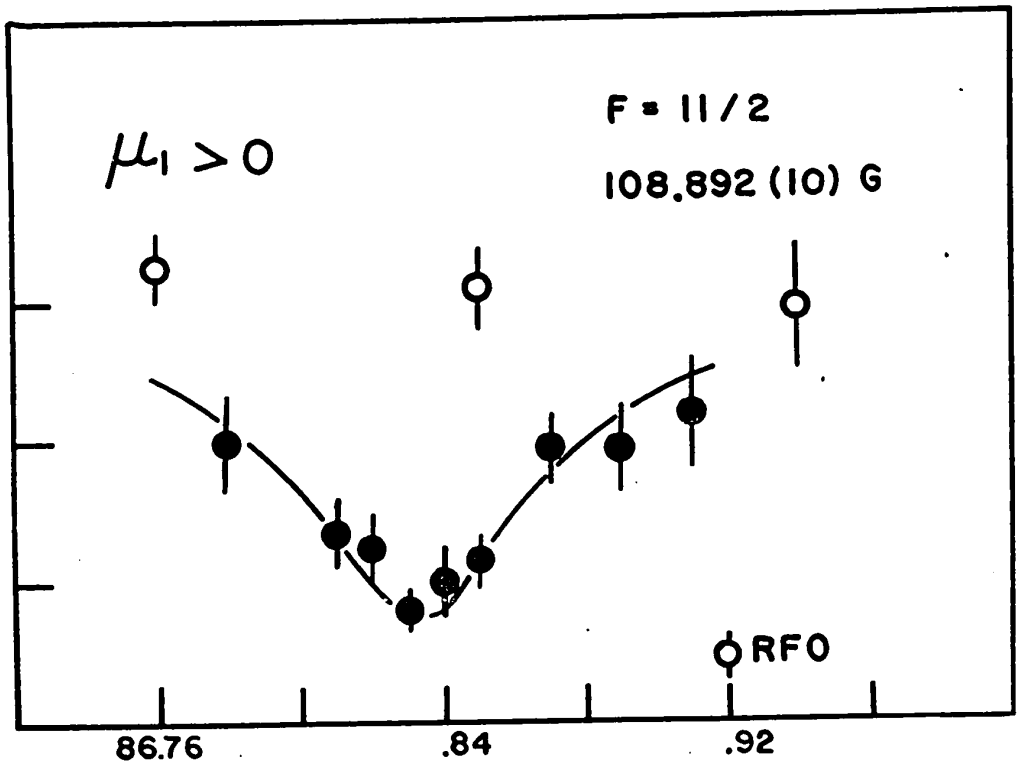
$\mu_1 > 0$
F = 11/2
108.892 (10) G
RFO
86.76
.84
.92

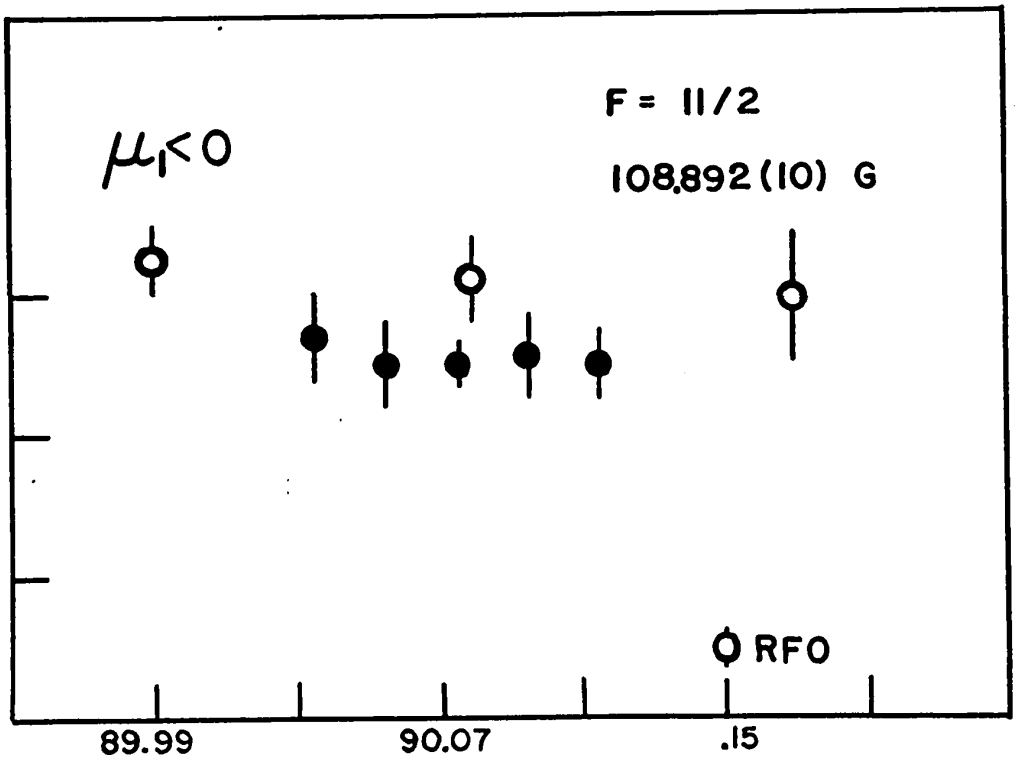
$\mu_1 < 0$
F = 11/2
108.892 (10) G
RFO
89.99
90.07
.15

"flop-out", and therefore, the sign of the magnetic dipole moment is determined to be positive.

5.3 Interpretation of Magnetic Moments

The magnetic moment of a state, whose wave function is given by equation 2.1, may be easily arrived at:

$$\mu_I = \alpha_i^2 \langle \pi 2d_{5/2}{}^{\nu} 2f_{7/2} : I | \tilde{\mu} | \pi 2d_{5/2}{}^{\nu} 2f_{7/2} : I \rangle + (1-\alpha_i^2) \langle \pi 1g_{7/2}{}^{\nu} 2f_{7/2} : I | \tilde{\mu} | \pi 1g_{7/2}{}^{\nu} 2f_{7/2} : I \rangle$$

where $\tilde{\mu}$ denotes the magnetic moment operator. In the above expression no cross-terms appear since the magnetic moment operator is diagonal in the orbital quantum number, ℓ. The magnetic moments of the pure configurations are:

$$\langle J_p J_n : I | \tilde{\mu} | J_p J_n : I \rangle = \frac{1}{2}\left(\frac{\mu_p}{J_p} + \frac{\mu_n}{J_n}\right) I + \frac{1}{2}\left(\frac{\mu_p}{J_p} - \frac{\mu_n}{J_n}\right) \frac{J_p(J_p+1) - J_n(J_n+1)}{I+1} . \quad (5.1)$$

It should be pointed out that in deriving equation 5.1, it has been assumed that both the neutron and proton orbits contain at the most one unpaired nucleon; the rest couple to a spin zero. This is the so-called "seniority one" arrangement. Configurations of the type $\left[(\pi g_{7/2}^4)_2 \, \pi d_{5/2}\right]_{J_p} (\nu f_{7/2})_{J_n}$ are, therefore, not included. When the experimentally measured magnetic moments from the neighbouring odd-A nuclei are used, the formula generally gives magnetic moments for odd-odd nuclei within 0.1 n.m. of observed values. Accordingly, if the magnetic moment of a $g_{7/2}$ proton is +2.8 n.m. (as found in ^{137}Cs and ^{139}La) and that of a $f_{7/2}$ neutron is -1.1 n.m. (as in ^{141}Ce and ^{143}Nd), then

$$\langle \pi g_{7/2} \nu f_{7/2} | \tilde{\mu} | \pi g_{7/2} \nu f_{7/2} \rangle = +0.49, \; J=2$$
$$\langle \pi g_{7/2} \nu f_{7/2} | \tilde{\mu} | \pi g_{7/2} \nu f_{7/2} \rangle = +1.23, \; J=5 \; .$$

Also, using the value $\mu_p = 4.14$ n.m. for a $d_{5/2}$ proton as measured in ^{141}Pr,

$$\langle \pi d_{5/2} \nu f_{7/2} | \tilde{\mu} | \pi d_{5/2} \nu f_{7/2} \rangle = -0.94, \; J=2$$
$$\langle \pi d_{5/2} \nu f_{7/2} | \tilde{\mu} | \pi d_{5/2} \nu f_{7/2} \rangle = +2.21, \; J=5 \; .$$

The magnetic moments of the 2^- ground state and 5^- isomeric state of ^{142}Pr may then be expressed in terms of the mixing parameter α^2:

$$\mu(J=2) = (-0.94)\alpha^2 + (0.49)(1-\alpha^2)$$
$$\mu(J=5) = (2.21)\alpha^2 + (1.23)(1-\alpha^2)$$

In Fig. 5.11 the magnetic moments of both the ground state and the isomeric state have been plotted as a function of their mixing parameters, α^2. The experimental values are shown by horizontal lines. The error in the result for the ground state is negligible, while that for the isomeric state is represented by cross-hatched region. On the basis of the measured values of the magnetic moments, then

$$\alpha^2 = 0.20 \qquad I=2$$
$$\alpha^2 = 1.00(10), \; I=5$$

where the error corresponds to the uncertainty in the magnetic moment. Kern et al. (1968) have interpreted their (d,p) and (n,γ) results for the low-lying negative parity states on the basis of configuration mixing, and thus deduced their wave functions. In particular, the mixing amplitudes for the 2^-

Figure 5.11

Magnetic moments of J = 2 and J = 5 states in ^{142}Pr, plotted as a function of mixing parameter α^2. The arrows indicate the values predicted by Kern et al.

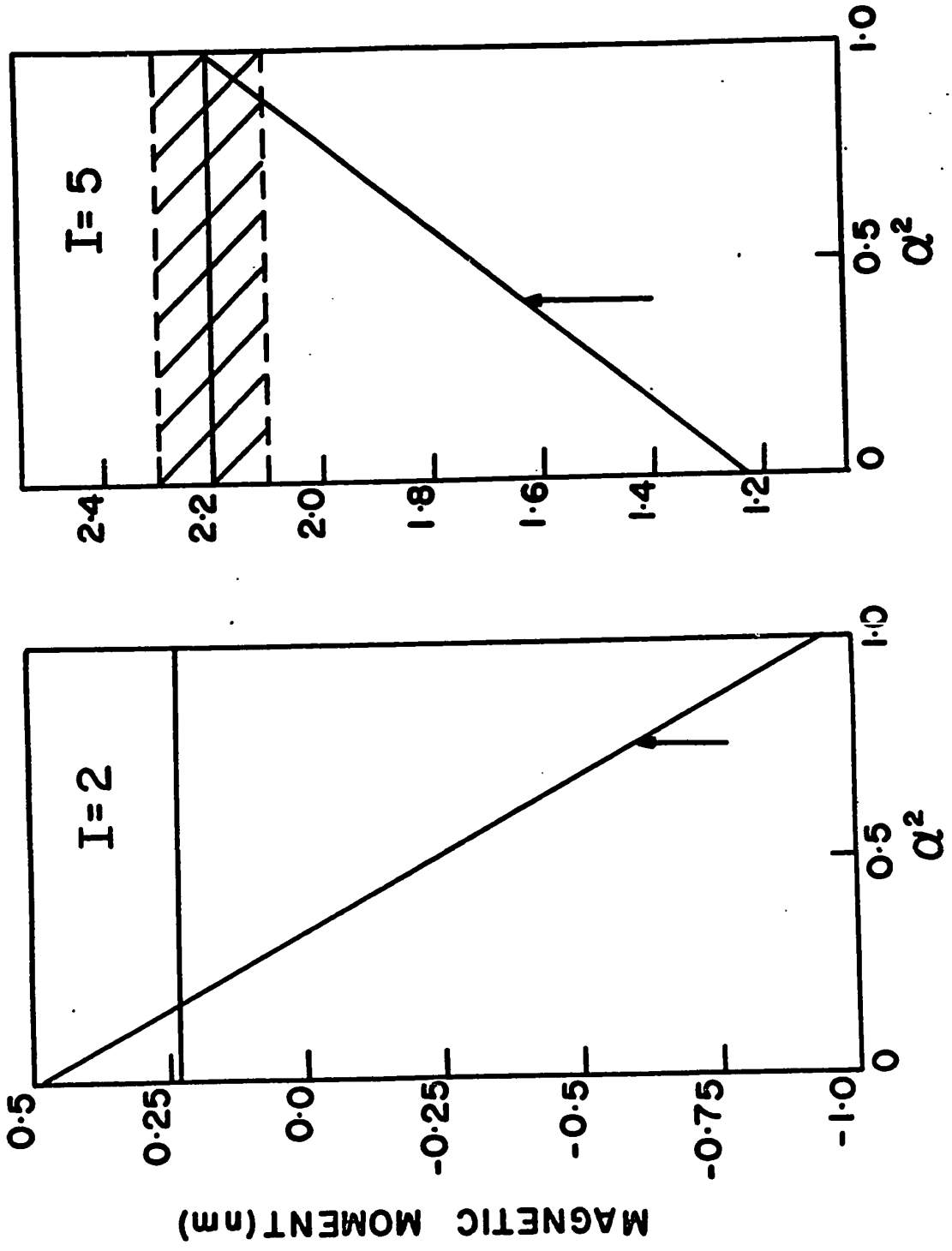
I=5
I=2
MAGNETIC MOMENT (nm)
α^2
0
0.5
1.0
2.4
2.2
2.0
1.8
1.6
1.4
1.2
0.5
0.25
0.0
-0.25
-0.5
-0.75
-1.0

ground state and the 5^- isomeric states are predicted to be 0.76 and 0.41, respectively. These results are in serious disagreement with those required to fit the magnetic moments. The next two chapters, therefore, deal mainly with an attempt to understand this discrepancy.

CHAPTER VI

FURTHER EXPERIMENTS AND ANALYSIS

6.1 The $^{141}Pr(d,p)^{142}Pr$ Experiment

The nuclear levels in ^{142}Pr have been previously studied in considerable detail by means of the (d,p) reaction and high- and low-energy (n,γ) spectroscopy (Kern et al., 1968). As outlined in Chapter II, the low-energy level scheme of ^{142}Pr should consist of fourteen states of negative parity arising from the mixing of two configurations:

$$\pi d_{5/2}\nu f_{7/2} : J^{\pi} = 1^-, 2^-, \ldots, 6^-$$
$$\pi g_{7/2}\nu f_{7/2} : J^{\pi} = 0^-, 1^-, \ldots, 7^-.$$

In the (d,p) experiment (at 10 MeV) performed by Kern et al. with an energy resolution of from 11.0 to 14.5 keV, eight of the twelve* levels were explicitly observed and resolved. Analysis of the intensities for the 6^- state (63.8 keV) and 1^- state (85.0 keV) indicated that the other two members of these spin-pairs would be populated only weakly. In addition, the presence and energies of two more states (5^- at 3.7 keV and 4^- at 72.3 keV) were deduced from the gamma ray results. Combining the

*The target nucleus, ^{141}Pr, has a ground state spin and parity $5/2^+$; states with spins 0^- and 7^- are, therefore, not populated in a (d,p) reaction.

(d,p) and the (n,γ) results, both the spins and the wave functions of ten low-lying negative parity states were obtained. As pointed out in the preceeding chapter, however, the resulting wave functions for the 2^- ground state and 5^- isomeric state at 3.7 keV are in serious disagreement with the measured magnetic moments of these states. Consequently, it was felt desirable to repeat the $^{141}Pr(d,p)^{142}Pr$ experiment, in the hope that better energy resolution might reveal the missing states in ^{142}Pr or otherwise resolve this discrepancy.

Two separate experimental runs were performed. The first experiment was designed to be a high-resolution one. It was, therefore, carried out at a deuteron beam energy of 10 MeV, using thin (10-30 μgm cm^{-2}) targets. The Enge split-pole magnetic spectrograph in which the emerging protons were momentum analyzed is, in principle, capable of yielding higher resolution than the simpler designs such as the single-gap Browne-Buechner type used by Kern et al. The aim of the second experiment was to locate any weakly populated states. In order to maximize the reaction yield, a higher (16 MeV) beam energy and thicker (∿ 100 μgm cm^{-2}) targets were used. The details of both these experiments are given below.

Targets were prepared by vacuum evaporation of 99.5% pure praseodymium metal from a small tantalum crucible onto 30 μgm cm^{-2} carbon foils. Because praseodymium reacts with water, it is necessary to first float off the carbon foils from

a glass slide onto aluminium frames, and then proceed with the evaporation.

One of the targets was then exposed to a 10 MeV deuteron beam from the McMaster F.N. Tandem Van de Graaff. The emerging protons were momentum analyzed in the split-pole Enge magnetic spectrograph, and detected using 5×25 cm, 50-μm nuclear emulsion plates (KODAK NTB-50) located in the focal plane of the spectrograph. In order to stop the elastically scattered deuterons the plates were covered with 0.02 in of aluminium. The proton tracks were then scanned in 1/4-mm strips under a microscope. In order to check the reproducibility of data and detect the presence of any light-mass impurities, exposures at three different angles were taken. The energy resolution obtained was between 7.5 to 10.5 keV. An energy spectrum taken at 60° and obtained with a beam exposure of $\sim$ 50,000 micro-Coulombs is shown in Fig. 6.1.

The spectra were analyzed using a computer programme SPECTR written by R.A. O'Neil. The line shape is taken as a standard Gaussian that has a high- or low-energy tail. The linewidth and the ratio of "tail-to-Gaussian" may be varied by a set of four parameters. In addition, the peak-height, peak-position and the background may also be varied. For a well-resolved sample peak known to be a singlet, the programme computes "best-fit" values for the parameters by successive iterations. The rest of the spectrum is then analyzed using these parameters to obtain the position and intensities (areas

Figure 6.1

Experimental proton spectrum from $^{141}Pr(d,p)^{142}Pr$ at E_d = 10 MeV. The horizontal scale is plate-position in cm. The peak labelled 1.7 KeV is an unresolved doublet.

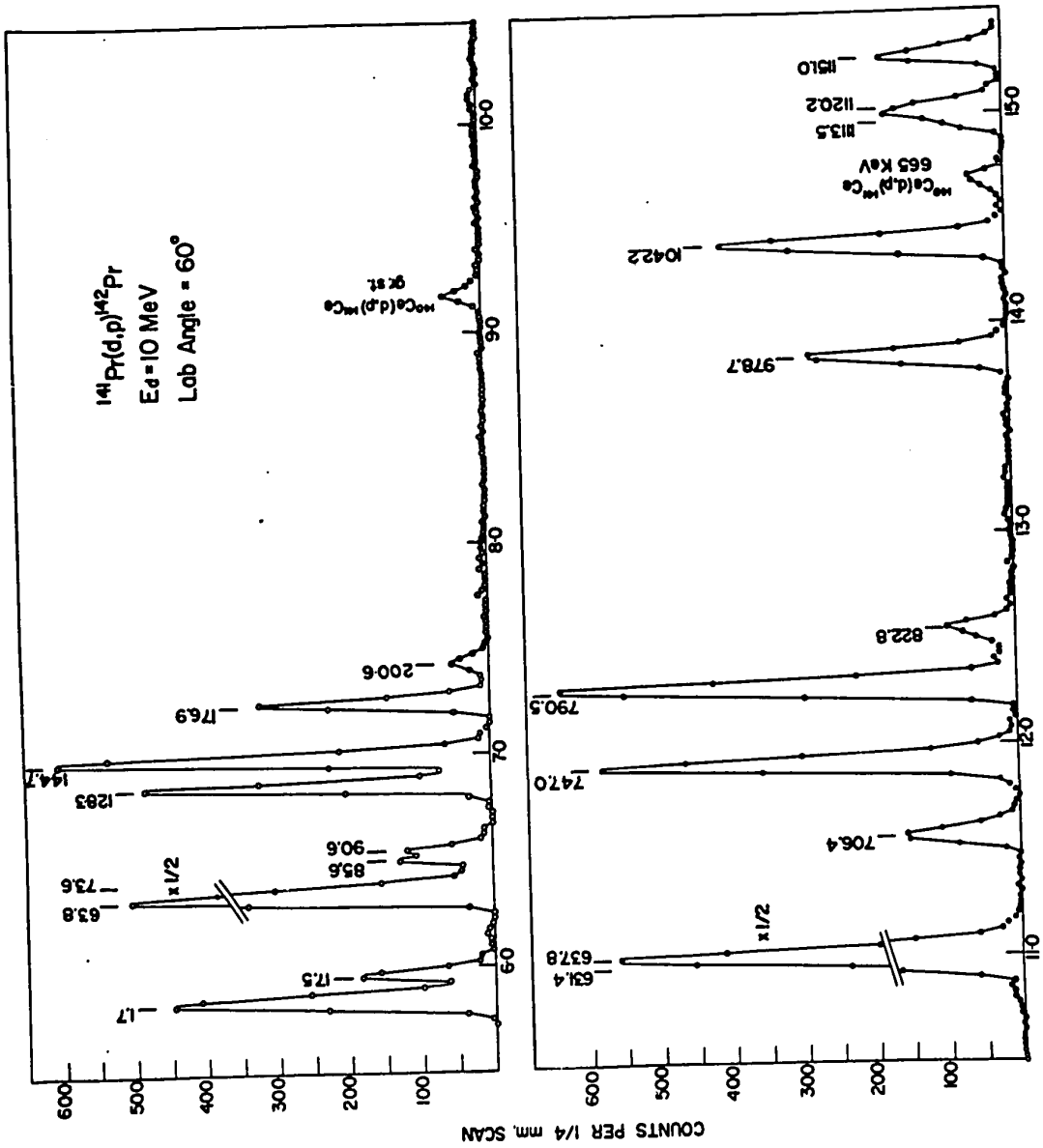
$^{141}Pr(d,p)^{142}Pr$
E_d = 10 MeV
Lab Angle = 60°
$^{140}Ce(d,p)^{141}Ce$ gr st
$^{140}Ce(d,p)^{141}Ce$ 665 KeV
COUNTS PER 1/4 mm. SCAN
x1/2
x1/2
17.7
17.5
63.8
73.6
85.6
90.6
128.3
144.7
176.9
200.6
63.4
63.78
706.4
747.0
790.5
822.8
978.7
1042.2
1113.5
1120.2
1151.0

under the peaks) of the other peaks. Knowing the beam energy and the ground state Q-value of the reaction, the excitation energies represented by the various peaks may then be computed.

6.1 a States up to 200 keV

A total of ten states with energies $\lesssim$ 200 keV are revealed in the present (d,p) experiment. Table 6.1 summarizes the experimental results and compares them with those obtained by Kern et al. The (d,p) intensities have been normalized such that the total intensity of the levels up to 200 keV equals 100 units.

The ground state group is assumed to be an unresolved doublet, the other member being the spin 5^- state at 3.68 keV as revealed through the (n,γ) results of Kern et al. These authors report that when their (d,p) level energies were shifted upwards by 1.6 keV an excellent agreement is obtained with the high-energy (n,γ) data. Under the assumption that the two components of the doublet are approximately equally intense, its separation was estimated as twice the energy shift, that is 3.2±1.5 keV. The resulting level energies as reported by Kern et al. are shown in column 2 of Table 6.1. In the present analysis, the energies of the states (shown in column 1) have been obtained by setting the strong (singlet) state at 176.9 keV, the energy of this state being taken from the (n,γ) results. The centroid of the ground state doublet is then found to be at 1.7±0.8 keV.

The state at 73.6 keV has not been previously resolved

Table 6.1

A summary of $^{141}Pr(d,p)^{142}Pr$ results for states up to 1150 KeV.

Energy (KeV)			Normalized intensity	
This work	Kern et al.		This work	Kern et al.
(d,p)	(d,p)	(n,γ)		
1.7(8)	0.0 (15)	0.0	16.9(4)	16.7(8)
	3.2	3.683(4)		
17.5(5)	17.8(6)	17.740(4)	5.2(4)	5.0(5)
63.8(3)	63.7(2)	63.746(4)	29.8(10)	30.5(15)
73.6(14)	--	72.294(4)	1.5(3)	
85.6(10)	86.2(7)	84.998(3)	2.7(8)	5.5(3)
90.6(12)	--	--	2.3(8)	
128.3(2)	128.0(4)	128.251(5)	12.8(3)	12.8(6)
144.7(3)	144.6(6)	144.587(4)	18.2(4)	17.4(9)
176.9	176.8(3)	176.863(3)	9.2(3)	9.9(5)
200.6(5)	200.8(5)	200.525(4)	1.5(1)	2.3(2)
631.4(7)	--	--	5.7(12)	45.8(6)
637.8(2)	637.2(5)	637.2(1)	39.1(14)	
706.4(4)	705.8(4)	703.6(3)	7.0(3)	6.4(2)
747.0(3)	748.2(6)	747.0(1)	23.7(8)	22.9(4)
790.5(3)	792.1(6)	790.4(1)	24.5(9)	24.6(2)
822.8(5)	823.5(7)	823.2(1)	3.5(1)	3.4(3)
978.7(4)	981.3(7)	978.2(1)	10.8(3)	11.7(2)
1042.2(4)	1045.2(7)	1041.9(1)	17.4(5)	17.9(4)
1113.5(15)	1115.4(12)	--	3.7(6)	--
1120.2(9)	1127.2(18)	1119.8(3)	4.5(7)	--
1151.0(3)	1154.4(9)	1150.9(1)	5.4(2)	--

in the (d,p) experiment. However, its presence is inferred from the high-energy (n,γ) data, and it has been consistently placed in the decay scheme on the basis of low-energy γ-ray fit. In the present (d,p) data, the strongly populated 64 keV state is noticeably broader than the single peaks, and the fitting programme SPECTR resolves the two states at all three angles in a consistent manner. Also, the previously reported state at 86.2 keV is found to be a doublet. Both the energies and intensities of the two members of this doublet are well reproduced at all three angles, and the sum of their intensities matches the intensity attributed to the 86.2 keV states by Kern et al. The energies of the two states are found to be 85.6 and 90.6 keV. Kern et al. have established that all their peaks followed an $\ell_n = 3$ angular distribution. Since the newly resolved state (90.6 keV) maintains a constant ratio with that at 85.6 keV, one can conclude that all the states below 200 keV involve the $2f_{7/2}$-neutron transfer.

6.1 b Higher Excited States

The scope of the present work concerns itself primarily with the low-lying states in ^{142}Pr. For completeness, however, the (d,p) results for levels up to 1150 keV will be presented and compared with those of Kern et al.

Beyond the low-lying group of states ($\lesssim$ 200 keV), the next level observed in the (d,p) reaction lies at $\sim$ 630 keV. Table 6.1 gives the excitation energies and normalized inten-

sities for states up to 1150 keV. It will be seen that, in general, the agreement between the two sets of (d,p) level energies, for the states between 630-1150 keV, is not as good as that for the low-lying group ($\lesssim$ 200 keV). On the other hand, except for the state at 706 keV, the present (d,p) results are in a better agreement with the (n,γ) results of Kern et al. The only impurity lines identified in the spectra correspond to the ground and first-excited states of ^{141}Ce. The states at 665, 682 and 767 keV reported by Kern et al. and designated as doubtful levels have not been observed.

There are two additional features in the present (d,p) results which are worth mentioning. The proton group at $\sim$ 635 keV is analyzed as a doublet, the lower member of which lies at 631.4 keV. In addition, the levels at 1113 and 1120 keV are also resolved, and it is concluded that the latter, in fact, corresponds to the 1120 keV state observed in the (n,γ) experiment of Kern et al.

An intensive search to locate any weakly populated states in the energy gap between 200 and 630 keV was carried out by bombarding a $\sim$ 100 μgm cm^{-2} ^{141}Pr target with 16 MeV deuterons. A proton spectrum taken at 30° with a beam exposure of $\sim$ 20,000 micro-Coulombs indicated that the reaction yield for the ground state group had increased (compared to that obtained in the 10 MeV run) by a factor of ten. However, it failed to reveal any peaks in the energy region of 200-630 keV

that could be assigned to the level scheme of ^{142}Pr. The experimental resolution was $\sim$ 20 keV, so that no further analysis of the data seemed worthwhile.

6.2 The Low-lying Level Scheme of ^{142}Pr

It is only fair to state at the very outset of this section that the experiments reported here were not carried out as part of the project outlined in this thesis. Rather, the results of other workers (the appropriate references have been cited) are merely presented and analyzed, in conjunction with the (d,p) results, in order to deduce two new states in the low-lying level scheme of ^{142}Pr (Fig. 6.2).

6.2 a $^{142}Ce(p,n\gamma)^{142}Pr$ and $^{139}La(\alpha,n\gamma\gamma)^{142}Pr$ Experiments

In an attempt to locate the missing states and verify the decay scheme proposed by Kern et al., a series of gamma-ray singles and coincidence experiments have been initiated at McMaster. In a preliminary $^{139}La(\alpha,n\gamma\gamma)^{142}Pr$ experiment at a beam energy of 15 MeV (Macphail, 1970), using two 50 c.c. Ge(Li) detectors, the strongest cascade observed involved the 85 and 268 keV γ-rays. Kern et al. report a close doublet of 84.998(3) and 86.056(3) keV γ-rays; the former has been assigned as a ground state transition. The same authors also report a 268.34(10) keV γ-ray, but this has not been incorporated in their decay scheme. On the basis of these and the (d,p) results, two new states at 89.7 and 358.1 keV are proposed. These are shown in Fig. 6.2. For consistency, the

Figure 6.2

The low-lying levels in ^{142}Pr

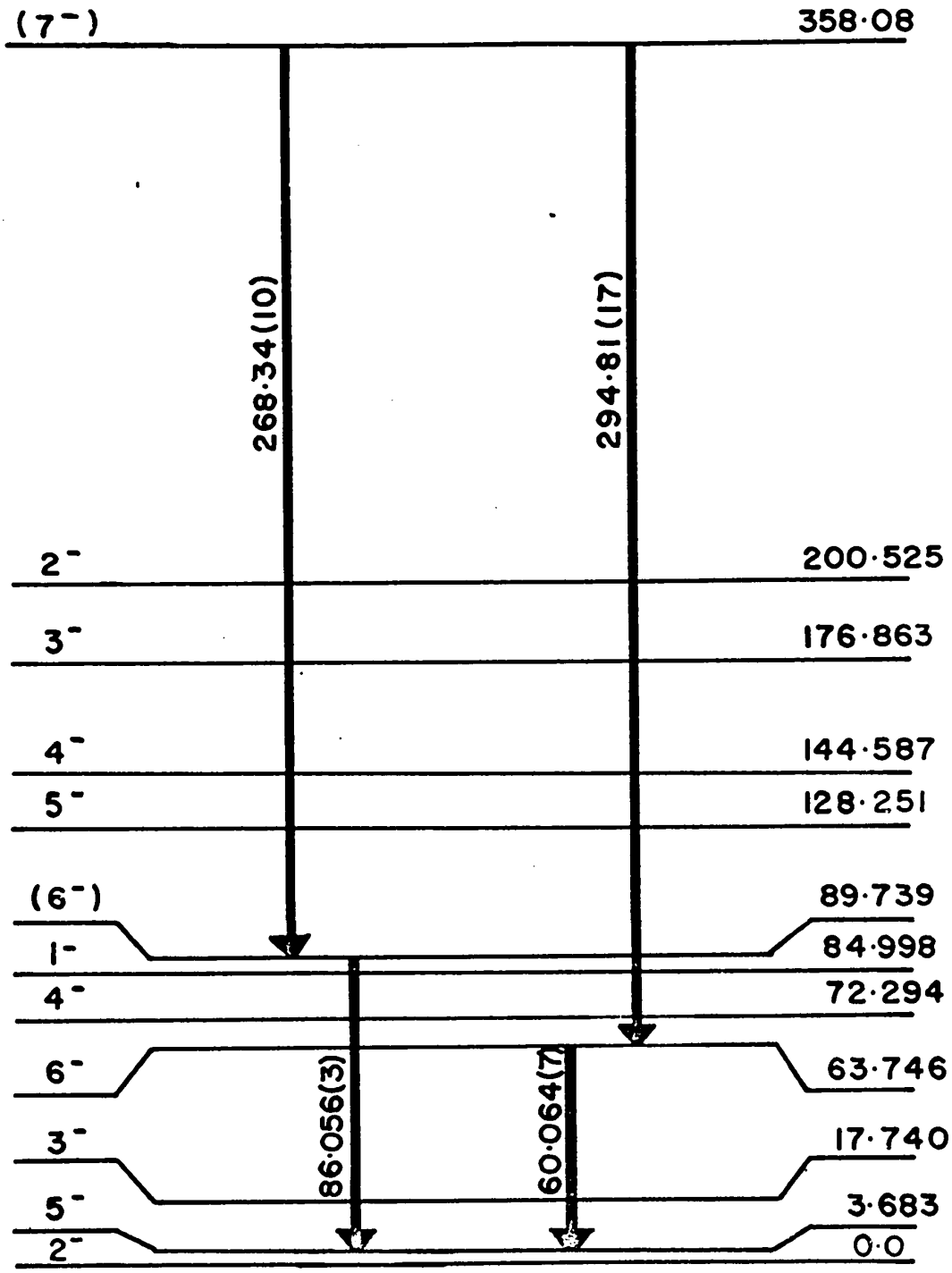
(7⁻)
358·08
268·34(10)
294·81(17)
2⁻
200·525
3⁻
176·863
4⁻
144·587
5⁻
128·251
(6⁻)
89·739
1⁻
84·998
4⁻
72·294
6⁻
63·746
3⁻
17·740
5⁻
3·683
2⁻
0·0
86·056(3)
60·064(7)

$^{142}_{59}Pr_{83}$

γ-ray energies shown are those given by Kern et al., although all the transitions have also been observed (but not with the precision of the bent crystal work) in the $(\alpha,n\gamma)$ reaction. The level-energies of the two (previously not known) states at 89.7 and 358.1 keV have been obtained on the basis of the coincidence data. The 294.8 keV γ-ray has been assigned as a 1041.9→747.0 keV transition by Kern et al.; however, it can also be consistently placed in the decay scheme shown. The state at 358.1 keV is not populated in the (d,p) reaction, suggesting that it is either the 0^- or 7^- member of the $|\pi g_{7/2}\nu f_{7/2} : J^\pi = 0^-,.....7^-\rangle$ multiplet. A series of high-resolution coincidence experiments at McMaster are still in progress (Aniol, 1972); however, there is no doubt that the 268 keV transition is, indeed, in coincidence with the 86 keV (rather than the 85 keV) member of the doublet. The states at 358.1 and 89.7 keV are, therefore, assigned spins 7^- and 6^- respectively. Further support for the spin 6^- assignment is provided by the intensity ratios of the 85 and 86 keV transitions as observed in $(p,n\gamma)$ and $(\alpha,n\gamma)$ spectra. In the $^{142}Ce(p,n\gamma)^{142}Pr$ reaction, the ground state spin of the target nucleus is 0, whereas the ground state spin of ^{139}La is 7/2. Furthermore, the α-particle can carry more orbital angular momentum than the proton. Hence, one would expect that the $^{139}La(\alpha,n)^{142}Pr$ reaction will have a higher probability of

populating the high-spin states in ^{142}Pr than the $^{142}Ce(p,n)^{142}Pr$ reaction. This is, indeed, what is observed experimentally. In particular, while the intensities of the 85 and 86 keV transitions are comparable in the (p,n) reaction the 86 keV transition dominates by a factor of $\sim$ 10 in the (α,n) reaction. This indicates that the levels from which the two transitions ensue have very different spins.

6.2 b The $^{144}Nd(d,\alpha)^{142}Pr$ Reaction

It has been mentioned earlier that the (d,p) reaction cannot populate the spins 0^- and 7^- states in ^{142}Pr. A feasible reaction which may establish the particle levels corresponding to these spins is $^{144}Nd(d,\alpha)^{142}Pr$. This reaction has been briefly studied by Macphail (1970), using Nd_2O_3 targets (enriched to 97.5% in ^{144}Nd) on 50 µgm cm^{-2} carbon backings. The emerging alpha particles were detected with a 5 cm × 1.4 cm Nuclear Diodes position sensitive counter, 240 µm thick, located in the focal plane of the Enge. In the first experiment carried out at a deuteron beam energy of 14 MeV, the alpha particles were observed at a laboratory angle of 40°; this permitted the states in ^{142}Pr up to an excitation energy of 800 keV to be examined. In a subsequent run at 16 MeV, the laboratory angle was changed to 20°, and states between 300-1100 keV were investigated. Although the extremely small cross sections did not warrant a thorough investigation, the observed α-particle spectrum was consistent with the known levels in ^{142}Pr obtained

from (d,p) studies. A result, relevant to the present discussion, is a particle level at 358(8) keV. This may be identified with the spin 7^- state deduced from the coincidence data.

6.2 c A Study of Nuclear Level Spins of ^{142}Pr

Mellema et al. (1970) have studied the nuclear level spins of ^{142}Pr by measuring the anisotropies of directional distributions of high- and low-energy gamma rays emitted after thermal neutron capture in oriented ^{141}Pr nuclei. Their conclusions yield spin restrictions for several excited states; in particular, definite spin values, 3 and 4, are obtained for the levels at 17.7 and 144.6 keV, respectively. The resulting spin assignments are given below and compared to those of Kern et al.

Level Energy (keV)	Spin Assignment	
	Mellema et al.	Kern et al.
17.7	3	3
63.7	3,4,5,6,7	6
72.3	3,4	4
85.0	1,2,3	1
128.3	3,4,5,6	5
144.6	4	4
176.9	2,3	3
200.5	2,3,4	2
703.6	2,3,4	3,4
1150.9	2,3	Not assigned

CHAPTER VII

DISCUSSION

7.1 Magnetic Moments and (d,p) Spectroscopic Factors

In view of the inconsistency between the measured magnetic moments and the (d,p) spectroscopic factors for the 2^- ground state and the 5^- isomeric state, one is led to conclude the following. If the simple, two-configuration model outlined in Chapter II is adequate in explaining the structure of the low-lying states in ^{142}Pr, including the magnetic moments, then the analysis of Kern et al. leading to their spin assignments and wave functions will have to be revised. In what follows, therefore, the (d,p) results will be reanalyzed to obtain spectroscopic factors consistent with the magnetic moment results and also to accomodate the spin 6^- state at 89.7 keV.

The nuclear spins of the ground state and the isomeric state have been measured by atomic beam method: the results are 2^- and 5^- respectively. The two states are unresolved in the (d,p) experiment, but the intensity of the doublet has been measured to be 16.9(4) units. Using the (2J+1) rule, the total intensity of the two states may, therefore, be expressed in terms of their mixing parameters:

$$16.9(4) = 2.08[5\alpha_2^2 + 11\alpha_5^2]$$

where the subscripts refer to the spins 2 and 5 respectively, and 2.08 is a normalization factor. The two mixing parameters are thus constrained (see Fig. 7.1) to give the observed intensity of the doublet. The values of the mixing parameters required to fit the observed magnetic moments and those obtained by Kern et al. from their analysis of (d,p) intensities are also indicated in Fig. 7.1. It can be seen that there is serious disagreement between the two sets of values. In particular, the magnetic moment for the spin 5^- state requires $\alpha_5^2 \gtrsim 0.9$ yielding a (d,p) intensity for this state of 20.6 units; this, in itself, is higher than the total observed intensity for the ground state doublet. It is possible to adjust α^2 for the two states such that the resulting magnetic moments are 'closest' to the observed values, at the same time reproducing the total observed (d,p) intensity for the doublet. For example, choosing $\alpha_2^2 = 0.25$ (and, therefore, $\alpha_5^2 = 0.63$), the magnetic moments are predicted to be:

$$\mu_{J=2} = 0.13(1) \text{ n.m.}$$
$$\mu_{J=5} = 1.85(2) \text{ n.m.}$$

where the errors indicated arise from the uncertainty in the measured (d,p) intensity for the doublet. The agreement with the experimental results is still inadequate. A second, and an equally important, consequence of the above reanalysis is the following.

Figure 7.1

The relationship between the mixing parameters α_2^2 (J=2) and α_5^2 (J=5) as determined by the total observed (d,p) intensity of the ground state doublet. The width of the line represents the uncertainty in the measured intensity. The values of α^2 required to fit the measured magnetic moments are indicated by arrows. Also shown are the values determined by Kern et al. from their analysis of (d,p) intensities.

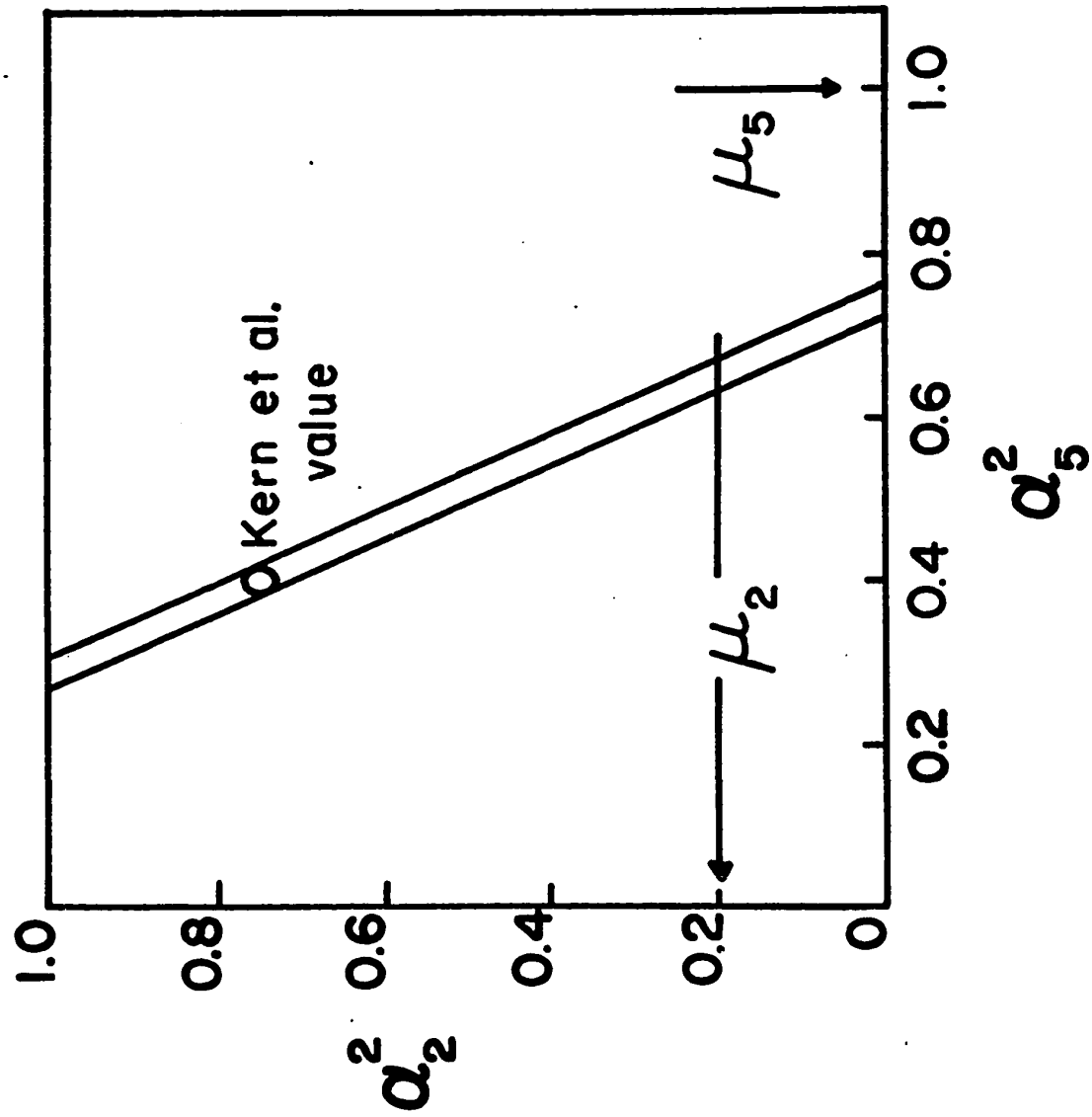
Kern et al.
value
μ_5
μ_2
α_2^2
α_5^2
0
0.2
0.4
0.6
0.8
1.0

Having chosen α^2 for the 2^- ground state and 5^- isomeric state to yield the observed magnetic moments, the mixing amplitudes for the corresponding orthogonal states with spins 2^- and 5^- are also determined. If the spin assignments of Kern et al. are retained, the state at 200.5 keV ($J^\pi = 2^-$) will, therefore, have a mixing amplitude given by

$$\beta^2_{J=5} = [1 - \alpha^2_{J=2}] = 0.75.$$

Similarly, the state at 128.3 keV has a spin 5^-, and therefore,

$$\beta^2_{J=5} = [1 - \alpha^2_{J=5}] = 0.37.$$

In Table 7.1, the results of such an analysis for all the low-lying states is presented and compared with those of Kern et al. It should be emphasized that in obtaining the mixing amplitudes, shown in column 3, it was demanded that these reproduce the measured magnetic moments for the lowest spins 2 and 5 states. It can be seen that, as a consequence of this, the experimental (d,p) intensity for the state at 200 keV is then no longer consistent with a spin 2^- assignment for this state. Also, the spin 1^- state (which was previously unresolved from the 89.7 keV state and, therefore, believed to be essentially pure) carries only 2.7(8) units of the total (6.3 units) spectroscopic strength for the 1^- pair. In fact, the missing strength is more consistent with the observed (d,p) intensity of the 200 keV state, and almost suggests a spin 1^- assignment for this state. This, however, would imply that the 182.8 keV transition to the spin 3^- state (reported by Kern et al.)

Table 7.1

(d,p) spectroscopic factors for states up to 200 KeV

Level energies (KeV)	J^{π}	This work			Kern et al.		
		α^2	(d,p) intensities calc.	(d,p) intensities expt.	α^2	(d,p) intensities calc.	(d,p) intensities expt.
0.0	2^-	0.25	2.6	16.9(4)	0.76	7.9	16.7(8)
3.683	5^-	0.63	14.4		0.41	9.4	
17.740	3^-	0.36	5.2	5.2(4)	0.35	4.9	5.0(5)
63.746	6^-	0.94	25.5	29.8(10)	1.00	27.1	30.5(15)
72.294	4^-	0.10	1.9	1.5(3)	0.12	2.2	
84.998	1^-	0.56	3.5	2.7(8)	0.87	5.5	5.5(3)
89.739	6^-	0.06	1.5	2.3(8)			
128.251	5^-	0.37	8.5	12.8(3)	0.59	13.5	12.8(6)
144.587	4^-	0.90	16.8	18.2(4)	0.88	16.5	17.4(9)
176.863	3^-	0.64	9.3	9.2(3)	0.65	9.7	9.9(5)
200.525	2^-	0.75	7.8	1.5(1)	0.24	2.5	2.3(2)

would be E2 rather than M1.

7.1a. Mixing of Higher Configurations

Whether or not the analysis outlined above represents a real state of affairs will have to be determined on the basis of further experiments. On the other hand, the discrepancy may be interpreted as an indication of possible mixing of higher configurations. From the energy-level systematics of adjoining odd-A nuclei, the next higher neutron orbital, $3p_{3/2}$, occurs at an excitation of $\sim$ 700 keV. The coupling of a $p_{3/2}$ neutron with $d_{5/2}$ and $g_{7/2}$ protons should then give rise to the following eight negative parity states:

$$\pi 2d_{5/2}\nu 3p_{3/2} : J^{\pi} = 1^-, 2^-, 3^-, 4^-$$

$$\pi 1g_{7/2}\nu 3p_{3/2} : J^{\pi} = 2^-, 3^-, 4^-, 5^-.$$

Apart from the pure 1^- and 5^- states, the states with spins 2, 3 and 4 may be close enough in energy so that they can be appreciably mixed. Indeed, a group of states between 600 and 1150 keV with an angular distribution of $\ell=1$, observed in the (d,p) experiment, may be assigned the above configurations. More relevant to the present discussion, however, is the fact that these states may, to some extent, mix in with the low-lying ground state group. The amount of mixing may be small enough to go undetected in the (d,p) angular distributions, but adequate to explain the observed magnetic moments. For example, using the Schmidt value for the g-factor of a $p_{3/2}$ neutron, the contribution to the ground state magnetic moment from $|\pi d_{5/2}\nu p_{3/2}>$

component in the wave function is:

$$\langle \pi d_{5/2} \nu p_{3/2} | \tilde{\mu} | \pi d_{5/2} \nu p_{3/2} \rangle = +2.8 \text{ n.m.}$$

The result is quite insensitive to the g-factor, so that the above estimate is a realistic one. Similarly,

$$\langle \pi g_{7/2} \nu p_{3/2} | \tilde{\mu} | \pi g_{7/2} \nu p_{3/2} \rangle = +3.4 \text{ n.m.}$$

It can be seen that, in view of the measured value of the ground state magnetic moment ($\mu_{J=2} = 0.234(1)$ n.m.), a small admixture of the $p_{3/2}$ neutron orbital can appreciably change the magnetic moment.

Having cited this possibility, however, it is important to realize that it becomes very complex to analyse these states in terms of such an extended configuration space. Moreover, it is no longer possible to utilize simple relationships such as the (2J+1) rule to deduce the nature of the low-lying states. There is so much freedom within such a model that until all the spins are definitely determined little meaningful analysis can be carried out. Thus, though this suggestion has to remain as a possible explanation of the discrepancies it cannot be followed up at this time.

7.2 Shell Model Calculations

During the past few years, a considerable amount of experimental data for odd-odd nuclei with 83 neutrons has been accumulated to warrant theoretical calculations for these nuclei. The two-configuration model, outlined in Chapter

II, has been successfully applied in deducing spins and parities, (d,p) spectroscopic factors and M1 transition rates for the low-lying states both in ^{140}La and ^{142}Pr. The measured ground state magnetic moments of ^{138}Cs and ^{140}La can also be understood in terms of configuration mixing between $\pi g_{7/2}\nu f_{7/2}$ and $\pi d_{5/2}\nu f_{7/2}$. Although these results indicate that these two configurations are undoubtedly the major ones to be considered, the real test of the model has to be its success or failure in predicting the observed energy levels in these nuclei. The ordering of the levels will be a function of the energy of the first excited states in the parent odd-A nuclei (the extent of configuration mixing), the nature of the residual n-p interaction, and of the number of unpaired protons. Struble (1967) has carried out an elaborate quasi-particle configuration mixing calculation for ^{140}La, using a finite range force. Although the agreement between the calculated and experimental branching ratios and (d,p) spectroscopic factors was satisfactory, the calculation failed to predict the observed ground state spin of 3. (The spin 6 was calculated to lie lowest in energy.)

More recently, Wildenthal (1969) has reported an extensive shell model calculation for N=82 nuclei. The model was based upon the assumption that, as far as the energy levels in the first 2 to 3 MeV excitations are concerned, the Z=50, N=82 closed shells can be considered inert. The model space was made up of all $1g_{7/2}^{-2}d_{5/2}$ configurations plus all

configurations formed by exciting one proton from the "g-d" subspace to either the $2d_{3/2}$ or $3s_{1/2}$ orbit. The two-body part of the Hamiltonian was parametrized in terms of the modified surface δ-interaction (Arvieu et al., 1966; Glaudemans et al., 1967). The Hamiltonian is, thus, determined by six adjustable parameters: a strength A of SDI, a strength B of extra (modifying) monopole term and the single-particle energies for the $1g_{7/2}$, $2d_{5/2}$, $2d_{3/2}$ and $3s_{1/2}$ orbits. The strength A and the three single-particle energy splittings were adjusted to give a least-squares fit to 40 excitation energies of levels of known J^{π} in N=82 nuclei from A=136 to A=145. The strength B and the absolute value of the $1g_{7/2}$ single-particle energy were adjusted to give a best fit to the known binding energies of N=82 ground states. The values of the parameters thus obtained are: A = 0.383 MeV, B = 0.597 MeV, $E_{7/2}$ = -10.14 MeV, $E_{5/2}$ = -9.62 MeV, $E_{3/2}$ = -7.02 MeV, and $E_{1/2}$ = -7.19 MeV. Using these parameters, the level energies and wave functions for ten of the N=82 nuclei were calculated. Even with this somewhat limited space, the dimensions of the shell model matrices may be as high as 300×300. The authors note that for the eight-particle states (which correspond to states in ^{140}Ce), the wave functions had from 100 to 300 components. The results of the calculations are very encouraging. In particular, the model succeeeds remarkably in predicting the observed ordering of low-lying states in the odd-A proton nuclei: ^{137}Cs

to ^{145}Eu. In addition, the model wave functions yield spectroscopic factors that are in good agreement with those obtained experimentally. These results definitely merit a similar calculation for the case of odd-odd nuclei with 83 neutrons. In what follows, therefore, an attempt will be made to carry out an approximate version of such a calculation for ^{142}Pr.

In the model space considered, the nine active protons beyond the doubly-magic (inert) core of $^{132}_{50}Sn_{82}$ were allowed to occupy the $1g_{7/2}$ and $2d_{5/2}$ orbits (only), to form configurations of the type:

$$(g_{7/2})^{4+2x}_{o} \quad (d_{5/2})^{5-2x}_{5/2} \quad \text{and} \quad (d_{5/2})^{6-2x}_{o} \quad (g_{7/2})^{3+2x}_{7/2}$$

where x is a suitable integer. Configurations such as

$$\{(g_{7/2})^{6}_{2}(d5_{5/2})^{3}_{5/2}\}_{J_p}$$

are, therefore, not included. The basis states for ^{142}Pr are, then, constructed by coupling either a $2f_{7/2}$ or a $3\ p_{3/2}$ neutron to these proton configurations.

The only parameters which affect the energy-level spectrum are the strength A of SDI and the single-particle splittings. The modifying monopole term, introduced by Wildenthal to obtain the correct ground state binding energies is, therefore, not included in the present calculations. For the single-particle splitting between the $g_{7/2}$ and $d_{5/2}$ proton states, the value 0.520 MeV obtained by Wildenthal is used, while that for the $f_{7/2}$-$p_{3/2}$ splitting

is taken to be 0.7 MeV. (The $p_{3/2}$ neutron state occurs at $\sim$ 660 keV in ^{141}Ce and $\sim$ 740 keV in ^{143}Nd.) The strength A of SDI may not necessarily be the same for both the proton-proton and proton-neutron interactions. While the former (A_0) is fixed at 0.383 MeV as determined by Wildenthal, the latter (A_2) was treated as a free parameter. In this respect, therefore, the calculation has only one parameter which is adjusted to obtain a fit to the experimentally observed energy-levels in ^{142}Pr. In the parameter search for A_2, the initial value was set equal to A_0. The spin 2^- state (observed as the ground state) was then predicted at 600 keV, and the first fourteen states were spread over an energy range of $\sim$ 2 MeV. As A_2 is increased, the whole spectrum gets compressed in energy, very rapidly at first (A_2 = 0.38-0.42 MeV). Both the excitation energies relative to the predicted ground state (always the spin 1^- state) and the energy-spacings between pairs of states (of same J^π) get smaller. Moreover, the rate of change with respect to A_2 is not equal for different spin states, so that it is possible to change the level ordering. For $A_2 \gtrsim 0.42$ MeV, the predicted spectrum is no longer very sensitive to a change in A_2, and the level ordering remains unaltered. The energy spectrum obtained, using the value 0.44 MeV for the proton-neutron strength of SDI, is shown in Fig. 7.2. The resulting wave functions are listed in Table 7.2, where the column headings indicate the appropriate configurations; for example,

Figure 7.2

Comparison of experimental spectrum for ^{142}Pr with the mixed-configuration shell model calculation (MCSMC) using Surface Delta Interaction.

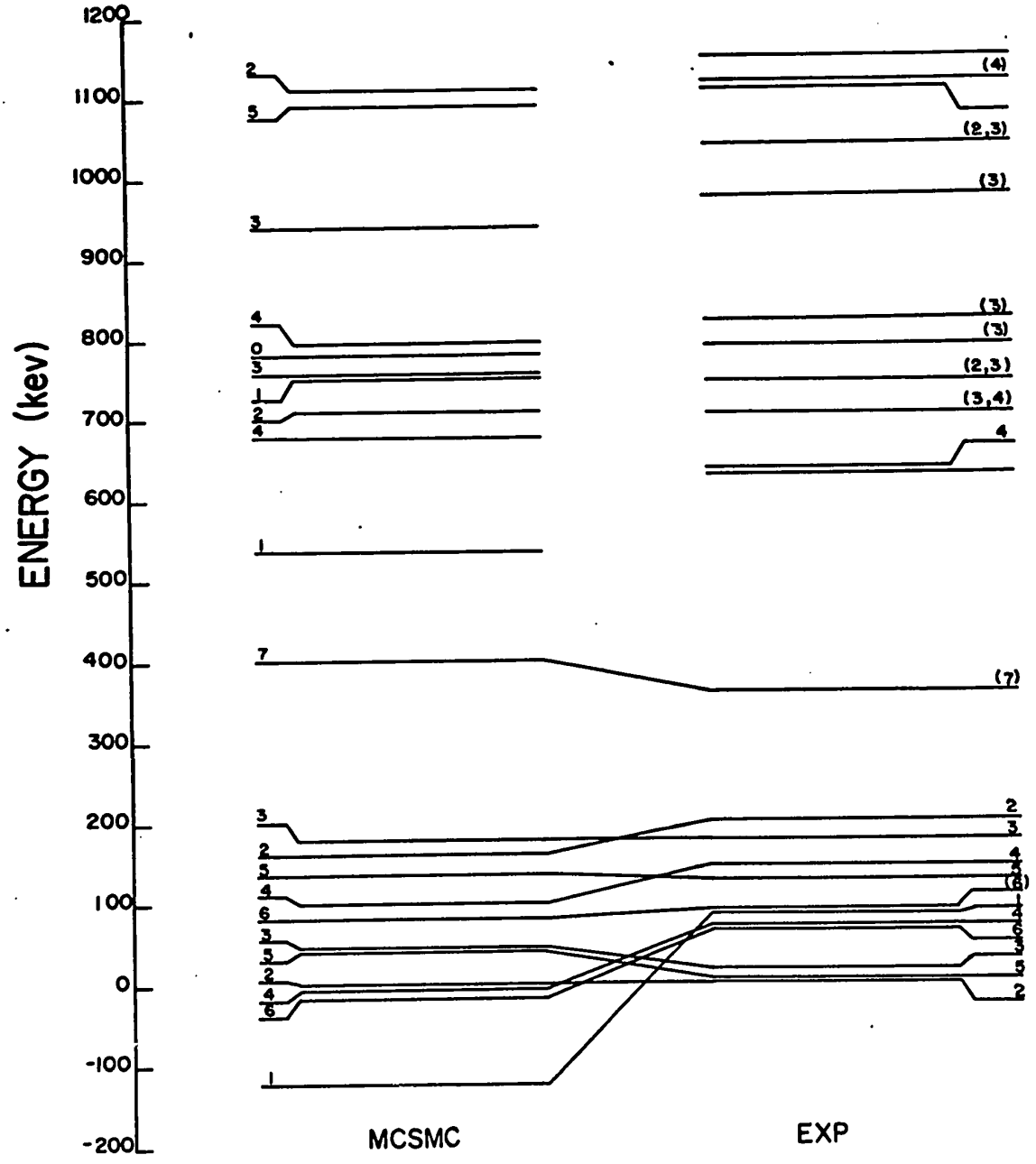
ENERGY (kev)
1200
1100
1000
900
800
700
600
500
400
300
200
100
0
-100
-200
MCSMC
EXP
(4)
(2,3)
(3)
(3)
(3)
(2,3)
(3,4)
4
(7)

^{142}Pr

Table 7.2

Calculated energies and wave functions in ^{142}Pr

Energies (KeV)	J^{π}	1810	3610	5410	2710	4510	6310	1801	3601	5401	2701	4501	6301
- 123	1^-	-0.556	0.657	-0.261	-0.212	-0.340	0.160	-0.010	-0.061	0.045	0.	0.	0.
- 17	6^-	-0.380	0.555	-0.269	0.464	0.480	-0.172	0.	0.	0.	0.	0.	0.
- 7	4^-	-0.400	0.649	-0.357	0.342	0.368	-0.136	-0.116	0.057	0.028	-0.039	-0.023	0.003
0	2^-	-0.443	0.710	-0.382	0.225	0.255	-0.097	-0.097	0.041	0.034	-0.078	-0.092	0.036
42	5^-	-0.363	0.725	-0.452	-0.229	-0.266	0.109	0.	0.	0.	0.049	0.003	0.019
44	3^-	-0.384	0.704	-0.410	-0.262	-0.315	0.130	-0.017	-0.015	0.034	0.045	-0.002	0.018
79	6^-	0.331	-0.535	0.281	0.513	0.485	-0.161	0.	0.	0.	0.	0.	0.
98	4^-	0.214	-0.412	0.252	0.579	0.572	-0.198	-0.008	0.048	-0.048	-0.096	-0.077	0.021
135	5^-	-0.130	0.279	-0.184	0.604	0.605	-0.213	0.	0.	0.	-0.229	-0.200	0.061
157	2^-	0.141	-0.298	0.188	0.606	0.623	-0.226	-0.030	0.060	-0.044	-0.166	-0.121	0.025
176	3^-	-0.157	0.324	-0.207	0.584	0.590	-0.208	0.006	-0.031	0.030	-0.224	-0.198	0.062
400	7^-	0.	0.	0.	0.618	0.729	-0.294	0.	0.	0.	0.	0.	0.
534	1^-	-0.228	0.313	-0.169	0.526	0.623	-0.249	-0.215	0.214	-0.060	0.	0.	0.
677	4^-	-0.116	-0.056	0.139	-0.068	-0.014	-0.009	-0.452	0.700	-0.380	0.232	0.243	-0.089
711	2^-	-0.117	-0.039	0.126	-0.094	-0.068	0.018	-0.440	0.753	-0.439	-0.009	-0.036	0.019
753	1^-	-0.119	-0.131	0.142	-0.242	-0.168	0.025	-0.477	0.709	-0.362	0.	0.	0.
755	3^-	-0.065	0.007	0.053	-0.010	-0.041	0.023	-0.387	0.752	-0.467	-0.154	-0.172	0.066
781	0^-	0.	0.	0.	0.484	0.772	-0.411	0.	0.	0.	0.	0.	0.
795	4^-	0.049	-0.006	-0.031	0.090	0.119	-0.050	0.153	-0.257	0.149	0.635	0.638	-0.225
938	3^-	-0.017	0.093	-0.083	0.130	0.234	-0.115	-0.093	0.192	-0.119	0.607	0.643	-0.239
1092	5^-	0.012	0.066	-0.090	0.114	0.259	-0.140	0.	0.	0.	0.593	0.680	-0.273
1108	2^-	0.013	0.039	-0.040	0.067	0.212	-0.127	-0.017	0.059	-0.037	0.589	0.703	-0.293

"5410" and "5401" denote $\pi d^5_{5/2}\pi g^4_{7/2}\nu f_{7/2}$ and $\pi d^5_{5/2}\pi g^4_{7/2}\nu p_{3/2}$ respectively.

7.2a Spectroscopic Factors

As a test for the model wave functions, in this section the (d,p) spectroscopic factors will be calculated and compared with those obtained experimentally. This may be done using equation (1.13). That is,

$$S_{\ell j} = [\sum_{p,q} a_p b_q]^2.$$

a_p and b_q are the mixing amplitudes in the initial and final states respectively, so that it is also essential to calculate the wave function of the target ground state. A shell model calculation for the odd-A ^{141}Pr was, therefore, carried out, using the SDI parameters obtained by Wildenthal. In the model space considered, the "active" protons were allowed to occupy the $2d_{5/2}$ and $1g_{7/2}$ orbits only. Furthermore, of all possible configurations only those that had at most one unpaired proton were included. The spin $7/2^+$ first-excited state is then predicted to lie 166 keV above the $5/2^+$ ground state. (The observed $5/2^+$ - $7/2^+$ separation is 145 keV). The resulting wave function for the ground state is:

$$|^{141}\text{Pr}, J^\pi=5/2^+\rangle = -0.455|d_{5/2}g^8_{7/2}\rangle_{5/2} + 0.78|d^3_{5/2}g^6_{7/2}\rangle_{5/2} - 0.43|d^5_{5/2}g^4_{7/2}\rangle_{5/}$$

The calculated spectroscopic factors for ℓ=3 ($f_{7/2}$ neutron transfer) and ℓ=1 ($p_{3/2}$-neutron transfer), using the wave functions of ^{142}Pr listed in Table 7.2, are shown in Table 7.3. The

Table 7.3

Energy levels of ^{142}Pr and spectroscopic factors in $^{141}Pr(d,p)^{142}Pr$, predicted by the shell model calculation using SDI. The resulting (d,p) intensities for $\ell_n=3$ are compared with those observed experimentally.

J^π	Energy (KeV)		Spectroscopic factors		(d,p) intensity	
	calc.	expt.	$S_{\ell=1}$	$S_{\ell=3}$	calc*	expt.
2^-	0	0.	0.004	0.846	8.8	16.9(4)
5^-	42	3.7	0.	0.856	14.6	
3^-	44	17.7	0.	0.810	11.8	5.2(4)
6^-	-17	63.8	0.	0.521	14.1	29.8(10)
4^-	- 7	72.3	0.007	0.709	13.3	1.5(3)
1^-	-123	85.0	0.004	0.770	4.9	2.7(8)
6^-	79	89.7	0.	0.474	12.9	2.3(8)
5^-	135	128.3	0.	0.127	2.9	12.8(3)
4^-	98	144.6	0.004	0.278	5.2	18.2(4)
3^-	176	176.9	0.002	0.171	2.5	9.2(3)
2^-	157	200.5	0.006	0.143	1.5	1.5(1)
7^-	400	358.1	0.	0.	0.	--
1^-	534	--	0.084	0.177	1.1	--
0^-	781	--	0.	0.	0.	--

* Comparison between the calculated and experimental (d,p) intensities for spins 3^- and 4^- states suggests that the predicted levels at 44, -7, 98 and 176 KeV should be identified with the observed states at 176.9, 144.6, 72.3 and 17.7 KeV respectively.

corresponding (d,p) intensities for the $f_{7/2}$-neutron transfer have been compared with the experimental intensities. As will be noticed, with the exception of the spin 1^- state at 534 keV, the contribution due to $\nu p_{3/2}$-transfer in the low-lying states is negligible. This is consistent with what is observed experimentally.

7.2b Remarks on Shell Model Results

An obvious failure of the shell model calculation described is that it does not reproduce the observed spin 2^- state as the ground state of ^{142}Pr. The calculation does, however, reveal the essential gross features of the observed spectrum, including the $\sim$ 400 keV energy gap (between the lower group of levels and those arising from a $p_{3/2}$ neutron) which characterises the ^{142}Pr level scheme. In order to indicate the merits (or failure) of SDI, therefore, the calculated spectrum for ^{140}La is also shown in Fig. 7.3, and the results are compared with the experimental energy levels and the quasi-particle calculation of Struble (1967). It will be seen that, on the whole, the results of the two calculations are comparable; in particular, both calculations fail to predict the observed spin 3^- as the ground state.

The resulting wave functions cannot be regarded as very realistic, in view of the calculated spectroscopic factors. The most probable reason for the 2^- state being the ground state is configuration interaction due to neutron-proton force. The calculated wave functions indicate that the two-body force

Figure 7.3

Comparison of experimental spectrum for ^{140}La with the mixed-configuration shell model calculation (MCSMC) using Surface Delta Interaction, and the quasi-particle calculation of Struble (1967).

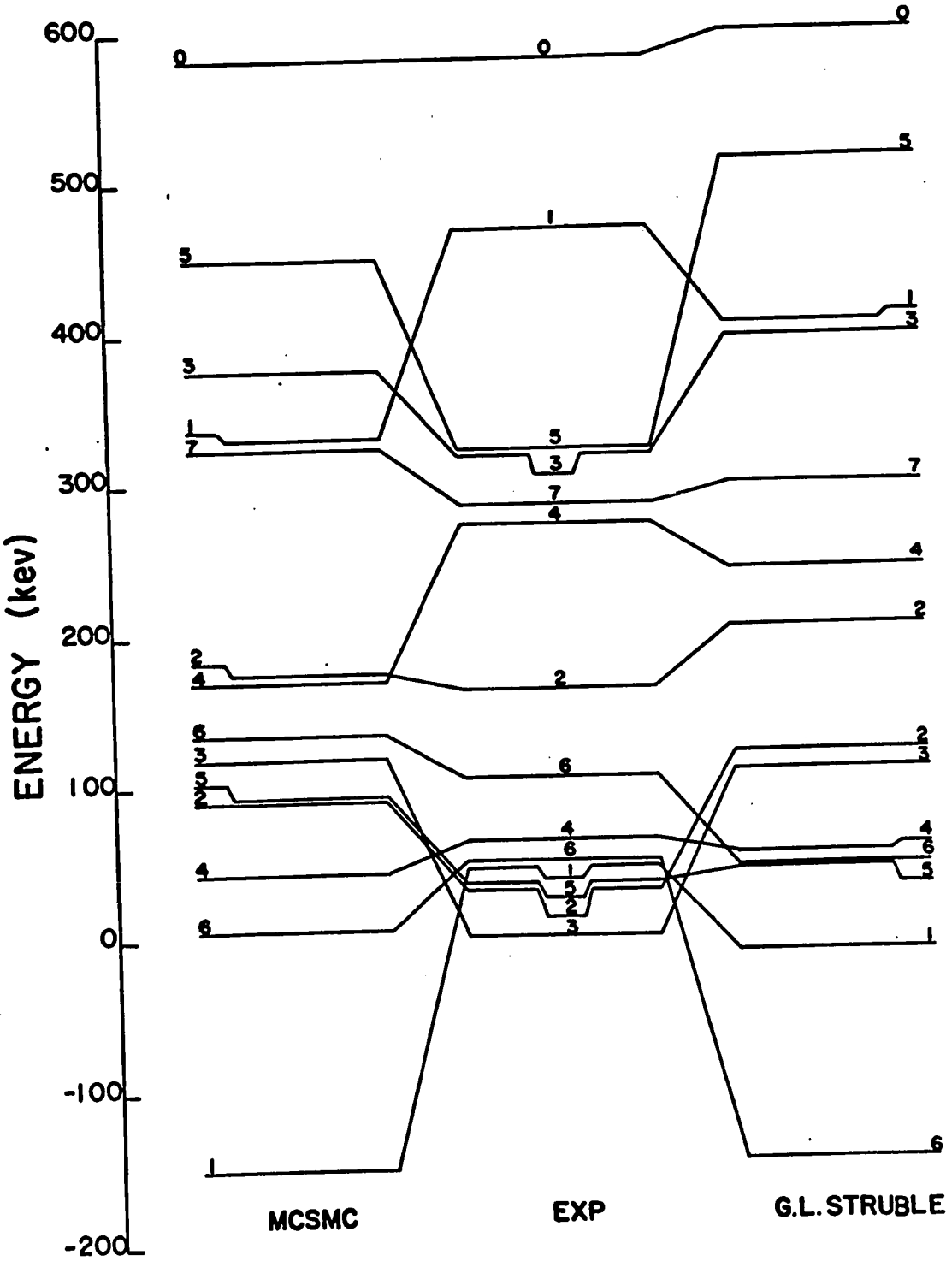
600
500
400
300
200
100
0
-100
-200
ENERGY (kev)
MCSMC
EXP
G.L. STRUBLE

^{140}La

used does not produce the "correct" amount of mixing between a pair of states with same J. In other words, the off-diagonal matrix elements are unrealistic. For example, the spin 2^- state is predicted to be rather pure; a higher admixture would not only be more consistent with what is obtained experimentally, but it would also spread the two 2^- states apart thus depressing the lower-lying member. On the other hand, the two 6^- states are predicted to be highly admixed which causes the lower member of this pair to be pushed down in energy. A smaller amount of mixing for $J = 6^-$, as indicated by the (d,p) intensities, would improve the fit between the calculated and observed energies for these states.

Considering the fact that the present calculation has been carried out in the most restricted configuration space, it would be unfair to conclude, just yet, that the surface δ-interaction cannot serve as a reasonable, effective two-body force for N=83 odd-odd nuclei. The final test must involve a much more general calculation in an extended shell model basis. Jones et al. (1971) have pointed out that in order to predict the 2^+ (first-excited) state at 1.6 MeV in ^{140}Ce, it is essential to consider proton excitations into the $2d_{3/2}$ and $3s_{1/2}$ orbits. The same authors also find that, in the N=82 odd-A parent nuclei, the $d_{3/2}$ and $s_{1/2}$ states (corresponding to a single proton in these orbits) are strongly mixed with seniority 3 states in the $d_{5/2}$-$g_{7/2}$ doublet. In an extended calculation for odd-odd nuclei, therefore, these two types of configurations

must be considered on an equal footing. Such a calculation, however, requires improved computer techniques, and is certainly beyond the scope of present work.

CONCLUDING REMARKS AND SUMMARY

In summary, then, the nuclear spin and magnetic moment of the 14.6 min isomeric state in ^{142}Pr have been measured by the method of atomic beam magnetic resonance. In addition, using two radiofrequency loops in a "flop-out on flop-in" atomic beam experiment the sign of the ground state magnetic moment has been determined to be positive.This technique of sign determination should prove useful for other radioactive isotopes whose magnetic moments are too small to permit a feasible direct measurement.

The low-lying negative parity states in ^{142}Pr have been interpreted in terms of mixing between the two configurations: $\pi 2d_{5/2}\nu 2f_{7/2}$ and $\pi 1g_{7/2}\nu 2f_{7/2}$. Although the measured spin of the isomeric state confirms the spin assignment of Kern et al., the mixing amplitudes for both the ground state and isomeric state, as predicted by their magnetic moments, are in serious disagreement with their results. The latter part of the research project has, therefore, dealt with an attempt to understand this discrepancy.

The $^{141}Pr(d,p)^{142}Pr$ experiment has been repeated at McMaster at a higher resolution. The results, taken together with the analysis of presently available γ-ray singles and coincidence data, have revealed two new states at 89.7 and 358.1 keV. Tentative spin assignments for these states have also been made. It has been found that the spin 1^- state at 85 keV (previously believed to be essentially pure) is highly

mixed. Further, the observed (d,p) intensity of the level at 200 keV almost suggests a spin 1^- assignment for this state. This, however, requires the 182.8 keV transition to the spin 3^- state to be E2 rather than M1. It would be worthwhile, therefore, to measure electron conversion rates and angular distributions of gamma rays following $^{142}Ce(p,n)^{142}Pr$ reaction in order to reveal the multipolarity of the low-energy transitions.

Of the fourteen negative parity states in ^{142}Pr, expected from the coupling of a $f_{7/2}$ neutron to the $d_{5/2}$ and $g_{7/2}$ proton states, the spins 0^- and 1^- states still remain to be located. The latter should be populated in a (d,p) reaction. However, the failure to observe this state in the $^{141}Pr(d,p)^{142}Pr$ experiment indicates that it probably lies at an energy $\gtrsim$ 630 keV, where a high density of strong ℓ_n=1 states would make it difficult to identify. A single proton pick-up reaction, $^{143}Nd(d,^3He)^{142}Pr$, offers a suitable alternative to locate both the missing states. The ground state of ^{143}Nd (Z=60, N=83) is $7/2^-$, so that a $d_{5/2}$ or $g_{7/2}$ proton pick-up will populate all the fourteen negative parity states. In particular, the spin 0^- (and 7^-) should have a pure ℓ_p=4 angular distribution. The Q-value for this reaction is -1.98 MeV so that a deuteron beam energy of $\gtrsim$ 20 MeV is necessary. With the recent upgrading of the terminal voltage of the McMaster Tandem Van de Graaff, the experiment is now feasible and should certainly be attempted.

It has also been suggested that the possibility of an admixture from higher configurations into the low-lying states cannot be ruled out. More specifically, it has been demonstrated that a small admixture ($\sim$ 10%) from the next $3p_{3/2}$ neutron orbital can drastically alter the magnetic moment predictions. This is especially so for the ground state whose measured magnetic moment is only $\sim$ 0.2 nuclear magnetons.

Finally, using a surface delta interaction, a shell model calculation in a highly truncated model space has been carried out. It is emphasized that the calculation involved only one free parameter. Although the results reproduce the gross features of the observed energy-spectrum, it does not yield the observed level ordering. A full calculation in an extended shell model basis should help decide whether the surface δ-interaction can be considered as a reasonable effective neutron-proton force in N=83 odd-odd nuclei. Meanwhile, the growing amount of experimental data for these nuclei (^{138}Cs, ^{140}La, ^{142}Pr, ^{144}Pm and ^{146}Eu) certainly warrants an alternative approach at obtaining the effective interaction: the two-body matrix elements can be treated as free parameters, these being determined by obtaining a best fit to the observed energy-levels.

It is hoped that the experimental work reported here will generate further interest in a theoretical understanding of these nuclei.

REFERENCES

Aniol, K. 1972. Private Communication.

Arvieu, R. and Moszkowski, S.A. 1966. Phys. Rev. 145, 830.

Bassell, R.H. 1966. Phys. Rev. 149, 791.

Brennan, M.H. and Bernstein, A.M. 1960. Phys. Rev. 120, 927.

Cabezas, A.Y., Lindgren, I.P.K., Marrus, R. and Nierenberg, W.A. 1962. Phys. Rev. 126, 1004.

Cameron, J.A., King, H.J., Eastwood, H.K. and Summers-Gill, R.G. 1962. Can. J. Phys. 40, 931.

Childs, W.J., Goodman, L.S. and Kieffer, L.J. 1960. Phys. Rev. 120, 2138.

Elliott, J.P. and Lane, A.M. 1957. Handbuch Der Physik, 39, 241.

Fink, R.W., Jopson, R.C., Mark, H. and Swift, C.D. 1966. Rev. Mod. Phys. 38, 513.

French, J.B., Halbert, E.C., McGrory, J.B. and Wong, S.S.M. 1969. Advances in Nucle. Phys. 3, 193.

Glaudemans, P.W.M., Brussard, P.J. and Wildenthal, B.H. 1967. Nucl. Phys. A102, 593.

Goeppert Mayer, M. 1948. Phys. Rev. 74, 235.

_____ 1949. Phys. Rev. 75, 1969.

Haxel, O., Jensen, J.H.D. and Suess, H.E. 1948. Naturwiss, 35, 375.

_____ 1949. Phys. Rev. 75, 1766.

Jones, W.P., Borgmann, L.W., Hecht, K.T., Bardwick, J. and Parkinson, W.C. 1971. Phys. Rev. C4, 580.

Jurney, E.T., Sheline, R.K. and Shera, E.B. 1970. Phys. Rev. C2, 2323.

Judd, B.R. and Lindgren, I.P.K. 1961. Phys. Rev. 122, 1802.

Karttunen, E., Freund, H.U. and Fink, R.W. 1971. Phys. Rev. 4, 1695.

Kern, J., Struble, G.L. and Sheline, R.K. 1967. Phys. Rev. 153, 1331.

Kern, J., Mauron, G. and Michaud, B. 1967. Phys. Lett. 24B, 400.

Kern, J., Struble, G.L., Sheline, R.K., Jurney, E.T., Koch, H.R., Maier, B.P.K., Gruber, U. and Schult, O.W.B. 1968. Phys. Rev. 173, 1133.

King, H.J. 1960. Ph.D. Thesis, McMaster University.

King, J.G. and Jaccarino, V. 1954. Phys. Rev. 94, 1610.

Kopfermann, H. 1958. Nuclear Moments (trans. E.E. Schneider, Academic Press, New York).

Lew, H. 1953, Phys. Rev. 91, 619.

——— 1970. Physics in Canada, 26, 65.

Macphail, M.R. 1970. Private Communication.

McGuire, E.J. 1972. Phys. Rev. A6, 1043.

Mellema, J., Reddingius, E.R. and Postma, H. 1970. Nucl. Phys. A157,577

Pierce, A.R. 1966. M.Sc. Thesis, McMaster University.

Quaranta, A.A., Bertin, A., Matone, G., Palmonari, F. and Placci, A. 1967. Nucl. Instr. and Meth. 55, 273.

Robertson, R.G.H. 1970. Private Communication.

Satchler, G.R. 1964. Nucl. Phys. 55, 1.

———— 1965. Lectures in Theoretical Physics. Vol. IIIC, ed. Kunz, P.D., Lind, D.A. and Brittin, W.E.

Stinson, G.M., Archer, N.P., Waddington, J.C. and Summers-Gill, R.G. 1967. Can. J. Phys. 45, 3393.

Struble, G.L. 1967. Phys. Rev. 153, 1347.

Wildenthal, B.H. 1969. Phys. Rev. Lett. 22, 118.

———— 1969. Phys. Lett. 29B, 274.